UNIVERSITAT DE BARCELONA

Mechanics of boundary formation in epithelial monolayers by Eph-ephrin interactions

Pilar Rodríguez Franco

Tesi doctoral

Mechanics of boundary formation in epithelial monolayers by Eph-ephrin interactions

Memòria presentada per optar al grau de Doctora

dins el programa de Biomedicina

Barcelona, novembre de 2016

Institut de Bioenginyeria de Catalunya (IBEC)

Presentada per Pilar Rodríguez Franco

Dirigida pel Dr. Xavier Trepat i Guixer

UNIVERSITAT DE BARCELONA

El Dr. Xavier Trepat i Guixer, del departament de Ciències Fisiològiques I de la Universitat de Barcelona

CERTIFICA

Que aquest treball, titulat "Mechanics of boundary formation in epithelial monolayers by Eph-ephrin interactions", presentat per la Pilar Rodríguez Franco per optar al grau de Doctora en Biomedicina, ha estat realitzat sota la seva direcció.

Dr. Xavier Trepat i Guixer

Professor Visitant

Departament de Ciències Fisiològiques I

Universitat de Barcelona

Group Leader / ICREA Research Professor

Integrative cell and tissue dynamics

Institut de Bioenginyeria de Catalunya (IBEC)

Barcelona, novembre de 2016

Als pares, i a l'avi, i al Juan.

ABSTRACT

For an organism to develop and maintain homeostasis, cell types with distinct functions must often be separated by physical boundaries. The formation and maintenance of such boundaries is commonly attributed to local mechanisms restricted to the cells lining the boundary. Here we show that, besides these local subcellular mechanisms, the formation and maintenance of tissue boundaries involves long-lived, long-ranged mechanical patterns. We analyzed the formation of repulsive epithelial boundaries between two epithelial monolayers, one expressing the receptor tyrosine kinase EphB2 and one expressing its ligand ephrinB1. Upon contact, both monolayers exhibited oscillatory patterns of traction forces and intercellular stresses that spanned several cell rows and tended to pull cell-matrix adhesions away from the boundary. With time, monolayers jammed and supracellular mechanical patterns became long-lived, thereby permanently contributing to sustain tissue segregation. Jamming was paralleled by the emergence of soliton-like deformation waves that propagated away from the boundary. This phenomenon was not specific to EphB2-ephrinB1 repulsion but was also present during the formation of boundaries with an inert interface. Our findings thus unveil a global physical mechanism that sustains tissue separation independently of the biochemical and mechanical features of the local tissue boundary.

ACKNOWLEDGEMENTS

In producing this dissertation, a special acknowledgement goes to Agustí Brugués. He provided inspiration and lively discussion at all times. I am also thankful for his contribution to the experimental section at the last stage of the project. Agu, you are a charm, aside from one of the most talented scientists that I am to meet.

I would like to express thanks to Vito Conte and Raimon Sunyer, for their support with the computational part and the 3D printing respectively. They helped me get familiar with many technicalities of the work. You two are amazing guys!

I also wanted to thank my PhD commission. They kept track of my work and gave me invaluable insights on the direction the project should take. Specially, thanks to Pere Roca-Cusachs, who shares lab with us. He contributed to the final discussions on the project.

Many thanks to Carlos Perez and Elsa Bazellieres, for helping me with the understanding of the biological side of my project. Sharing discussions with you has been very enlightening. Sorry for the silly questions, though… I cannot pay you enough awful-vending-machine-coffees to compensate for that.

I wanted to thank Natalia Castro for her constant assistance during the development of my experiments. She was always helpful with all these little details that we all underestimate but that make the experiments work. Thanks Natalia for your devotion!

I cannot forget to thank Science Communication people from IBEC, Pilar Jiménez and Carolina Llorente. Thanks for trusting me and giving me the chance to bring science to young students. It has been an amazing experience. Also thanks to Laura Casares, who worked with me on our workshops for kids about 'cells exerting forces'. Terrific experience!

The same applies to Jesús Purroy, Miriam Martínez and Carla Vázquez. Thanks for giving me the chance to develop a workshop from scratch and for giving me the tools to do so. It has been utterly satisfying. Giving a new perspective of math and physics to teens helps them see science as something much more appealing. I appreciate that you shared mi view on that. Thanks you to Marina Uroz as well, who helped me develop my idea into compelling contents. Not forgetting Ernest, who will carry on the workshop in the near future and is already engaged in the activity lively.

Thanks as well to the JIPI community, which taught me that union makes force. Maybe one PhD student couldn't handle the organization of a conference, but with a well-organized team of amazingly energetic PhD students, everything is possible. Seriously, working with you was great inspiration.

A general thank you goes to all my lab-mates and colleagues during these years; for all the small things that don't fit a sheet of paper, thanks.

I also take the opportunity to thank my supervisor, Xavier Trepat, for his invaluable guidance and assistance during my Thesis. Being part of your Lab has been a life-changing, eye-opening experience - in many ways. Thanks for giving me the chance to be part of your team. You helped me become a wiser person during these years.

Finally, I am grateful to Mauricio Moreno and Albert Romano, from my previous lab. Thanks for giving me the chance to start a career in science. Thank you also for your generosity at all times.

Also thanks to Eva Baldrich, from CNM (at the time). Maybe you are not aware enough, but you made me want to become a scientist with all that passion of yours. I will never forget the long afternoons of experiments together, watching the screen, waiting for the results, enjoying the beauty of science.

Bé, no sóc gaire amiga d'escriure dedicatòries a les persones que estimo. Els que em coneixeu, sabeu que sóc més de dedicar paraules d'amor en persona.

Per aquest motiu, em desmarco de fer una llista d'agraïments sentits – que hauria de ser interminable – i simplement, us dic a tots vosaltres, amics meus i família, que heu estat el meu motor. Que sense vosaltres hagués estat impossible assolir aquesta empresa. I sobretot, que sense la vostra ajuda incansable, ara no seria la persona en que m'he convertit.

Per tot això i també per tot el que em deixo – música i farra inclosos –

GRÀCIES DE TOT COR.

CONTENTS

1 INTRODUCTION

1.1 Biomechanics of cell

Virtually all cells and organisms across the evolutionary spectrum, from the most primitive to the most complex, are mechanosensitive (Galizia, 2013). This universal property allows cells to convert mechanical stimuli from their physical surroundings or from within the organism to electrochemical or biochemical signals, which then regulate a wide repertoire of physiological responses (Jaalouk, 2009).

In contrast to the level of understanding of how specific chemicals trigger and transduce signals within cells, studies of how cells sense force and how they respond to different levels, durations, and directions of force are much less common, but have recently attracted increasing attention from biologists and bioengineers. Defining specific structures and mechanisms by which forces are sensed by cells and how this stimulus leads to specific responses is likely to help explain the complex functions of cells and to design better materials for cell and tissue engineering and other applications in vivo (Janmey, 2007).

A particularly relevant and poorly understood phenomenon in mechanobiology is the formation of boundaries between epithelial tissues. Dynamics of tissue segregation involves multiscale cellular movements, deformations, rearrangements and forces. Current understanding emphasizes that these mechanical variables and their mutual relationships can be understood on the basis of energy minimization principles in thermodynamic equilibrium; cells within tissues explore ergodically their configuration space so as to reach a state of minimum free energy in which a boundary emerges and settles (Steinberg, 1963). Despite the predictive success of this equilibrium view in embryo explants (Foty, 1996), its generality in non-equilibrium tissues is unclear. This is particularly relevant in epithelial monolayers, in which jamming and collective migration might

impair reaching an equilibrium state (Angelini, 2011; Nnetu, 2012; Pawlizak, 2015; Tambe, 2015; Park, 2015; Garcia, 2015).

In this chapter I will describe the main cellular elements responsible for generating, transmitting, sensing, and responding to mechanical stimuli in the context of boundary formation. These include the structural machinery building the cell cytoskeleton and also the structures used to interact with the environment and to create stable barriers. I will cover some of the main methods used for interrogating the mechanical properties of adherent cells and epithelium. Furthermore, I will describe the process of cell mechanotransduction and its regulation during the Eph-ephrin boundary buildup.

1.1.1 Cytoskeleton

The cytoskeleton is the principal machinery responsible for cell shape and mechanics. It is fundamental to cell migration, division and intracellular transport of organelles. It is commonly studied in terms of distinct functional subsystems: actin filaments (AFs), microtubules (MTs) and intermediate filaments (IFs).

1.1.1.1 Actin filaments

Actin filaments are two helicoid polymers of actin protein. They are flexible structures, with a diameter of 5-9 nm, organized in 2D and 3D bundles. AFs have an average persistence length (PL) of about 10 μm.

Although AFs are spread in the cytoplasm, they concentrate at the cell cortex, below the plasma membrane. AFs determine the shape of cell surface and are essential to cell locomotion (Figure 1-1).

AFs are organized and crosslinked making higher order structures:

- Stress fibers are long and straight filaments. They are highly contractile and exert forces.
- Lamellipodia are broad, sheet like projections of the membrane at the leading edge of a migrating cell. Their Arp2/3 mediated actin branching pushes the membrane forward.
- Filopodia are thin projections of the plasma membrane that let the cell explore the environment.
- Cell cortex, at the inner face of the plasma membrane. It plays a central role in cell shape control.

Actin is the main force generator during cell adhesion, spreading and migration. This force is generated by two main mechanisms:

- By actin polymerization, as in lamellipodia.
- By coupling to the motor protein myosin, as in stress fibers.

1.1.1.2 Intermediate filaments

IFs are rope like structures, with a 10 nm diameter in average. At the single filament level, IFs are the most flexible, with a PL in the 1 μm length. They extend throughout the cytoplasm, providing the cell with strength and resistance to mechanical stress. In epithelial cells, IFs anchor to the cell-cell desmosomes, and to the cell-matrix hemi desmosomes (Figure 1-1).

1.1.1.3 Microtubules

They are long and hollow cylinders made out of the tubulin protein. With an external diameter of 2 nm, they are far less flexible than AFs. They have a PL in the range of 1 mm. In general, they are bound to a centrosome at one end. MTs direct intracellular transport (Figure 1-1).

1.1.1.4 Cytoskeletal crosstalk

Aside from the individual properties of each of the three networks, many others arise from the interplay between them by means of motors, cross-linkers and steric interactions in charge of coupling their behaviour. Together, they provide the cell with a wide cast of linear and non-linear responses to stimuli, which would not be achieved by the sum of the individual parts.

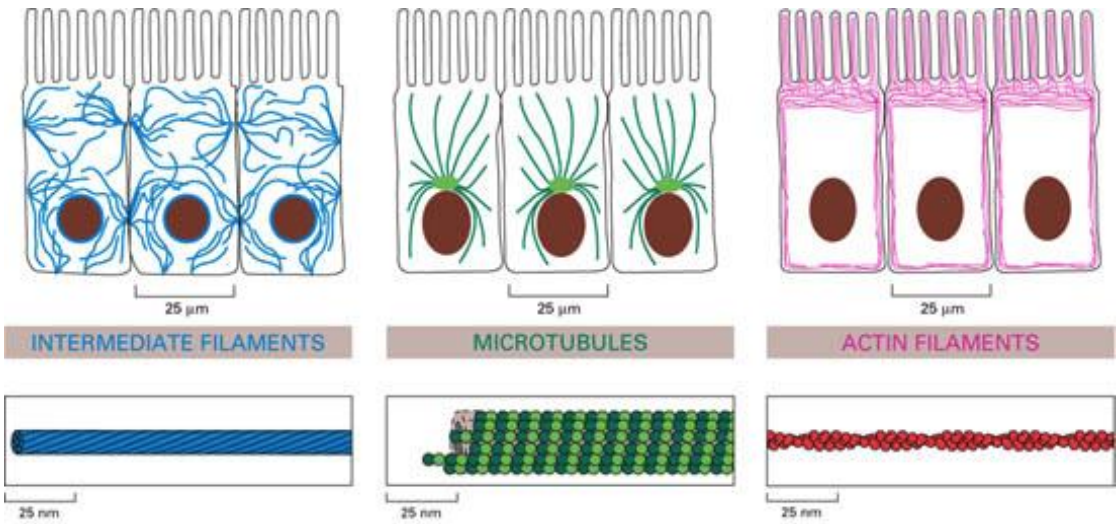

Figure 1-1| Major components of the cytoskeleton. Distribution in the cell (top) and structure (bottom) of intermediate filaments, microtubules and actin filaments (Alberts, 2002).

1.1.1.5 Actin supracellular structures

Actin fibers are often found in bundles within the cell cytoskeleton. When cells are connected, a mesh of actin fibers creates a complex network among them (Lodish, 2000; Millán, 2010). A migrating epithelium connects its cells through cell-cell junctions, which are anchored to the actin cytoskeleton by a number of specialized proteins (Vasioukhin, 2000).

Further specializations of junctional actin structures are supracellular arrangements that appear to stretch over many cell diameters. Such actin cables have been shown to serve several important functions, in processes such as wound healing (Brugués, 2014), epithelial morphogenesis (Kiehart, 2000) and maintenance of compartment identities during development (Fagotto, 2013).

Particularly in development and homeostasis, some structural features of epithelia must be preserved. It is the case for boundaries and patterns (Dahmann, 2011), which must keep regions of cells separated and overcome the local and timely tissue reorganization (neighbour exchange, cell translocation, cell extrusion) and cell division. The staples of these structures are mainly ordered actin fibers that cover supracellular distances (Reffay, 2014; Ravasio, 2015) (Figure 1-2).

Static actin cables are present at several boundaries, i.e. the parasegment boundary (Drosophila), the wing disk DV boundary (Drosophila) and the rhombomeres (chick, mouse) (Röper, 2013). In Xenopus, the boundary between ectoderm-mesoderm (Rohani, 2011) and the subsequent partition of dorsal mesoderm into notochord and the paraxial-mesoderm (Reintsch, 2005) display enriched actomyosin regions between niches of populations.

Actomyosin supracellular cables might therefore provide a general mechanism to restrict cells into defined compartments during development

(Figure 1-2), although upstream signals will differ depending on the context (Röper, 2013).

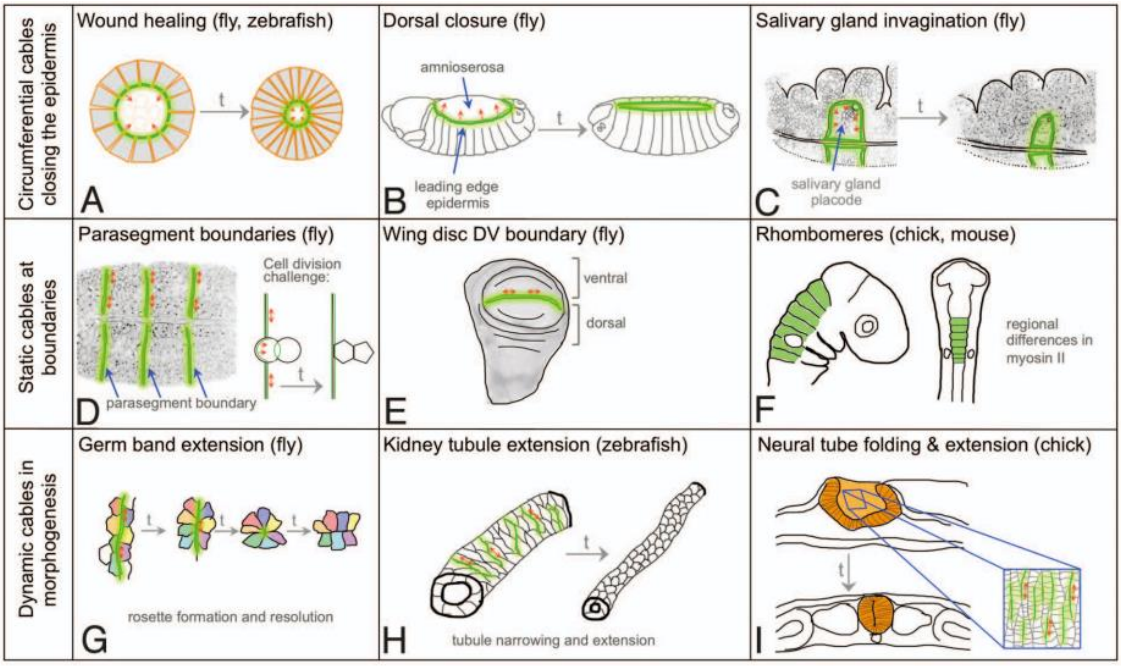

Table 1. Upstream signals and molecular anisotropies leading to actomyosin cable formation

Tissue/process	Upstream signal	Molecular asymmetry/anisotropy
wound healing (*Drosophila*)	H_2O_2/loss of contact	bazooka, Cadherin ?, Crumbs?, Echinoid?
dorsal closure (*Drosophila*)	Dpp, JNK, Wg, Notch signaling	Echinoid, Flamingo, Frizzled, Canoe, Dlg, Crumbs?
salivary gland tubulogenesis (*Drosophila*)	hairy, hkb, fkh activated transcription	Crumbs, aPKC, Rok
Parasagment boundaries (*Drosophila*)	Wg, Hh signaling	unknown
wing disc DV boundary (*Drosophila*)	Notch, Wg signaling	Baz
rhombomere/ventricle formation (chick)	unknown	unknown
germ band extension (*Drosophila*)	pair rule gene expression/ A-P patterning	Rok, Baz, Cadherin, Arm
tracheal pit invagination (*Drosophila*)	EGF signaling	p-ERK
kidney tubule extension (zebrafish)	PCP: Wnt signaling	unknown
neural plate extension/folding (chick)	PCP: ?	Celsr1/Flamingo, DAAM, ROCK1

Figure 1-2| Actomyosin cables during development. Supracellular actomyosin cables tend to fall into three categories: circumferential cables (A–C), static cables at boundaries (D–F) and dynamic cables during morphogenesis (G–I) (Röper, 2013).

1.1.2 Cell adhesion

Unicellular organisms, like bacteria and unicellular fungi, interact with different kind of structures and environments to perform their function. In multicellular organisms, though, cells need to interact both with their environment and with other cells. The specialized structures that cells use to that purpose are called cell adhesions (Gumbiner, 1996). These can be distinguished as 1) cell adhesions to the extracellular matrix (ECM) and 2) cell-cell adhesions.

1.1.2.1 Cell adhesion to the extracellular matrix (ECM)

Complex organisms are formed by many types of tissues, in which cells are assembled and bound together in different ways. In both animals and plants, however, an essential part is played in most tissues by the ECM. This complex network of secreted extracellular macromolecules has many functions, but first and foremost it forms a supporting framework. It helps hold cells and tissues together, and, in animals, it provides an organized environment within which migratory cells can move and interact with one another in orderly ways (Alberts, 2002).

Cells attach to the extracellular matrix through hemidesmosomes and focal adhesions. Focal adhesions link the extracellular matrix to the actin cytoskeleton of the cell, whereas hemidesmosomes link it to intermediate filaments (keratin mainly) (Lodish, 2000). Both are made of integrins, a family of hetero-dimeric transmembrane proteins formed by different types of alpha and beta subunits.

In focal adhesions integrins cluster into oval structures. These provide anchoring points for the actin filaments, which generate the cellular forces used for attachment, spreading or migration (Partridge, 2006). Focal adhesions are able to adapt to their specific extracellular matrix through integrin signalling: integrins transmit mechanochemical information about the extracellular composition via outside-in signalling; reversely, intracellular signals induce changes in integrin conformation and attachment to the ECM, via inside-out signalling (Harburger, 2009) (Figure 1-3, left).

In connective tissue, the ECM is plentiful, and cells are sparsely distributed within it. The matrix is rich in fibrous polymers, especially collagen. Direct attachments between one cell and another are relatively rare. In epithelial tissue, by contrast, cells are tightly bound together into sheets called epithelium. The ECM consists mainly of a thin mat called the basal lamina, which underlies the epithelium. The cells are attached to each other by cell-cell adhesions, which bear most of the mechanical stresses (Alberts, 2002).

1.1.2.2 Cell-cell adhesion

Epithelial cell sheets line all the cavities and free surfaces of the body. The specialized junctions between the cells enable epithelia to form barriers that control the movement of water, solutes, and cells from one body compartment to another. What is more, tissue must maintain its integrity for cells to migrate as a cohesive group when needed. To this purpose, strong intracellular protein filaments (components of the cytoskeleton) cross the cytoplasm of each epithelial cell and attach to specialized junctions in the plasma membrane. Junctions, in turn, tie the

surfaces of adjacent cells to each other (Alberts, 2002). There are four main types of cell-cell adhesion complexes: tight junctions, adherens junctions, desmosomes and gap junctions (Figure 1-3, right). The first three types provide structural support and allow mechanical coupling between cells (Gumbiner 1996; Getsios, 2004). Gap junctions, by contrast, are channels that connect the cytoplasm of adjacent cells to homogenize their biochemical conditions (Mese, 2007), but they are also likely to play a mechanical role (Bazellieres, 2015).

Aside from providing structural support, epithelial cells must be able to change shape or intercalate as tissues deform. To achieve this goal the cell-cell multiprotein complexes must be highly dynamic. Indeed, the source of epithelial plasticity and fluid behaviour resides in the ability to actively remodel cell-cell junctions (Takeichi, 2014). Tissue fluidity emerges from local active stresses acting at cell interfaces and allows maintenance of epithelial organization during morphogenesis and tissue renewal (Guillot, 2013).

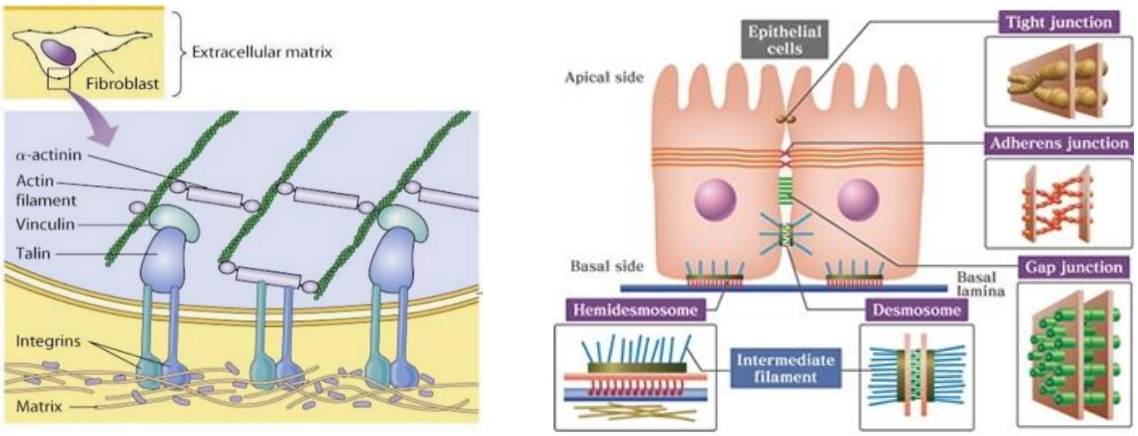

Figure 1-3| Left: distribution of cell-ECM junction. Focal adhesions can join a cell to the ECM, primarily through fibronectin receptors. Right: Distribution of the main cell-cell junctions in epithelial cells: tight junctions, adherent junctions, desmosomes and gap junctions (Tokyo University, 2010).

1.1.2.3 Adherens junctions: the cadherins family

Cadherins are transmembrane proteins that form the building blocks of adherens junctions. They are linked to the cytoskeleton by accessory proteins, such as alpha catenin, beta catenin or p120-catenin (Figure 1-4). Cadherins carry two main functions in tissue morphogenesis and homeostasis: 1) the decrease in interfacial tension at the forming cell-cell contact, thereby promoting contact expansion; 2) the stabilization of contacts by resisting mechanical forces that pull on the contact (Maître & Heisenberg, 2013).

In epithelia, adherens junctions give rise to a continuous adhesion belt. This network is fundamental to coordinate collective processes such as collective cell migration, epithelial wound healing or epithelial folding (Alberts, 2002).

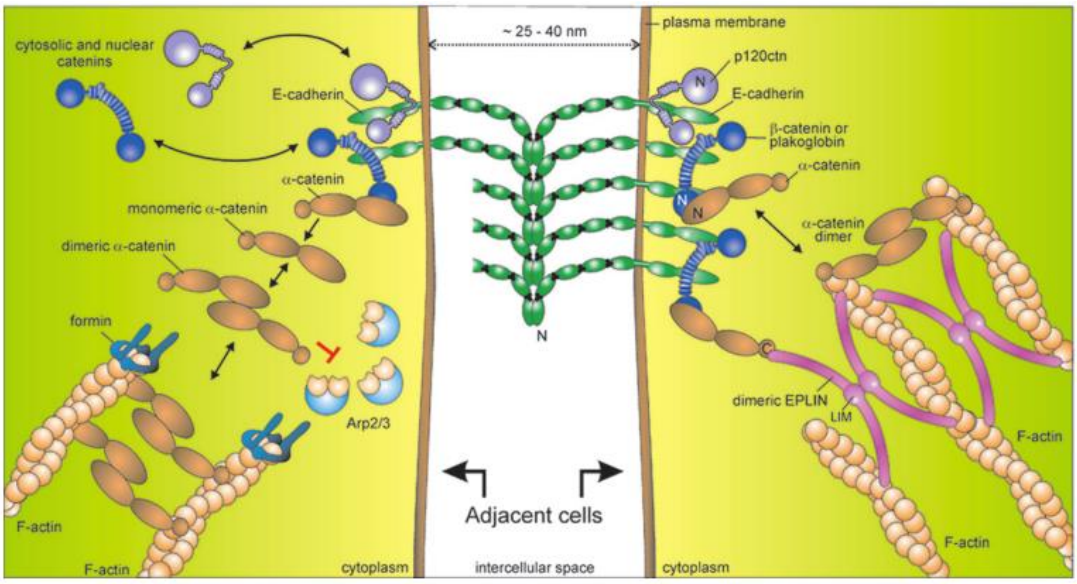

Figure 1-4| Detailed description of adherent junction (Van Roy & Berx, 2008).

1.1.3 Mechanotransduction

Mechanical forces are controlled by cells and are integrated into tissues to produce the final form of an organism through processes of mechanotransduction that affect cell shape, proliferation, migration and apoptosis (Iskratsch, 2014).

Mechanotransduction converts mechanical stimuli into chemical signals to regulate cell behaviour and function. Examples are substrate rigidity (through contractile units or mature integrin adhesions), stretching (through cell-cell contacts or integrin adhesions) or shear stress. Typically, the pathway involves receptors at focal adhesions or cell-cell contacts (integrins and cadherins), mechanosensors (stretchable proteins such as talin and P130Cas) and nuclear signalling factors to change gene and protein expression profiles (DuFort, 2011). Nuclear deformation can also lead to changes in gene expression patterns. The timescale of these events ranges from milliseconds to seconds for the stretching of mechanosensors, hours for altered gene expression, days for changes in cell behaviour and function, and weeks for tissue development (Iskratsch, 2014) (Figure 1-5).

Ultimately, cells respond to the sensed mechanical stimuli by migrating, adhering, de-adhering, differentiating or dividing, for instance. It has been shown that the response can be driven by cell elements and pathways that need not to be different than the well-established biochemical pathways (Vogel & Sheetz, 2006).

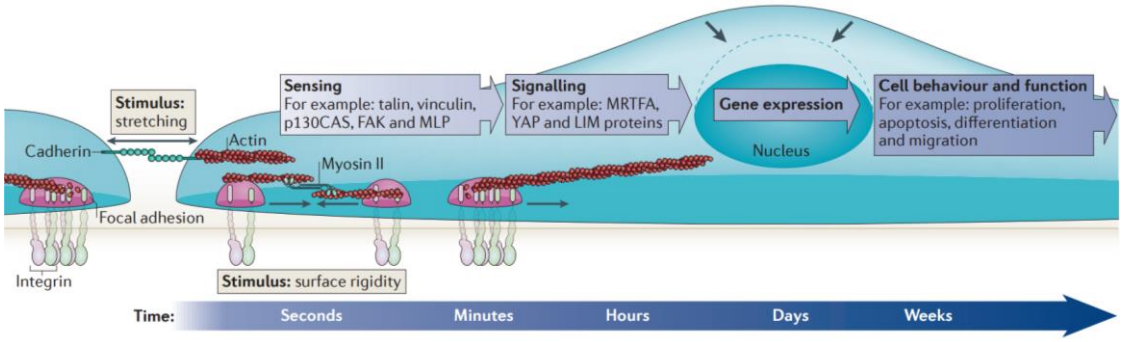

Figure 1-5| Mechanotransduction stages and their timings (Voguel & Sheetz, 2006).

1.1.3.1 YAP signalling

Recently YAP (Yes-associated protein) has been pointed out as the nuclear downstream effector of mechanical signals exerted by ECM rigidity and cell shape (Dupont, 2011) (Figure 1-5). This regulation requires Rho GTPase activity and tension of the actomyosin cytoskeleton. Strikingly, expression of activated YAP overcomes physical constraints in dictating cell behaviour. These findings identify YAP/TAZ as sensors and mediators of mechanical cues instructed by the cellular microenvironment. It is remarkable that the capacity of YAP and TAZ to feel the force has proven to be a universal feature in mammalian cells (Kaminski, 2014).

1.1.4 Cell migration and traction forces

In vivo, cells generate traction forces to drive processes like migration, morphogenesis, and extracellular matrix remodeling (Friedl, 2009). Cells generate tractions by anchoring themselves to neighbouring objects and contracting. Anchoring occurs on protein networks in the extracellular environment (extracellular matrix), and on neighbouring cells via membrane-spanning protein complexes (Style, 2014). Contraction in

eukaryotic cells is typically driven by networks of actin filaments and myosin motors. In highly-contractile cells, contraction is usually produced by stress fibres – ordered bundles of actin filaments resembling muscle fibres. However, other types of cytoskeletal architectures can also generate contraction (Haeger, 2015). Traction forces can be observed in isolated cells on flexible substrates coated with adhesion-stimulating proteins. The magnitude and spatial distribution of these tractions vary widely with cell type. Cells typically pull on the substrate near their edges, with contraction indicated by inwardly-directed traction forces. In migrating cells, traction forces are often polarized according to the direction of motion (Style, 2014).

1.1.5 Experimental tools in mechanobiology

In the last years, many techniques have arisen that allow the study of mechanical properties at the level of tissue, single cell and single molecule.

1.1.5.1 Microfabricated post array detectors

Microfabricated post array detectors (mPADs) have provided the first quantitative measurement of cellular forces at the sub cellular level. Cells are seeded to attach and spread across multiple posts of an array of closely spaced vertical posts of silicone elastomer (Trichet, 2012). The posts are bent like vertical cantilevers as the cells probe the surface. For small deflections, the posts behave like simple springs such that the deflection is directly proportional to the force applied by the attached cell at each post (Figure 1-6). mPADs provide a strategy to independently manipulate

mechanical compliance and surface chemistry (Kim, 2009), to control the spatial presentation of these properties across a surface with micrometer resolution (Lemmon, 2005) and to measure traction forces generated by cells at multiple locations (Tan, 2003).

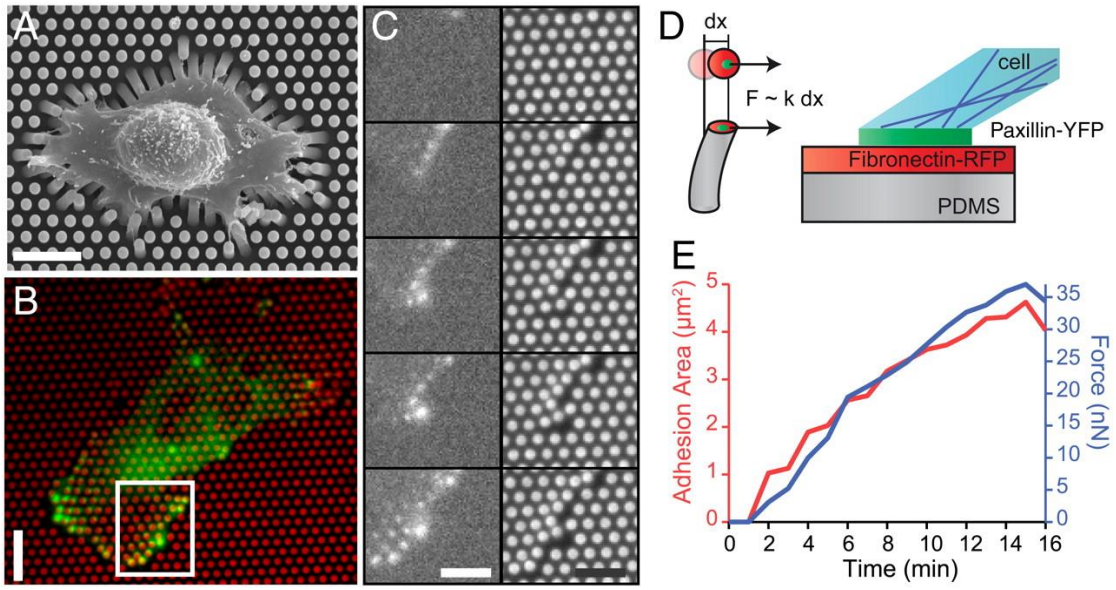

Figure 1-6| Cell adhesion and traction forces developed by REF52 fibroblasts expressing YFP-paxillin on micropillar substrates. (a) Scanning electron micrograph image of a typical REF52 cell on a micropillar substrate (Scale bar, 15 µm). (b) Epifluorescent image of a single cell deforming the micropillar substrate (here of spring constant k=34 nN/µm). Micropillars are labelled by Cy3-fibronectin (red), and YFP-paxillin-rich patches are in green (scale bar, 15 µm). (c) Sequential images of the insert area of b showing the dynamics of focal adhesions growth and micropillar displacements (scale bar, 10 µm). (d) Schematic representation of the experimental setup showing the formation of focal adhesions on the top of a PDMS micropillar. (e) Typical example of the formation of a focal adhesion area (red) and the buildup of force (blue) as a function of time (on a substrate of 34 nN/µm) (Trichet, 2012).

1.1.5.2 Traction Force Microscopy

Traction force microscopy allows the measurement of cell traction forces on a continuum substrate. The measurement of the forces is achieved in three steps (Figure 1-7, right): (1) Cells are seeded on a soft, elastic transparent substrate filled with fluorescent markers. (2) As cells migrate, they deform the gel. These deformations can be tracked by quantifying the displacement of the beads. To do so, the image of beads at every time point is compared with a reference image of the beads, which corresponds to the

image of the gel without cells. This reference image is obtained at the end of the experiment by applying a trypsin treatment. (3) Finally the traction forces are obtained from the gel deformations, or displacements, produced by the cells (Wang & Lin, 2007) (Figure 1-7, right).

Polyacrylamide (PA) gels are the most suitable substrate used for traction force microscopy. They convey several advantages: they are elastic, transparent and stable. Their stiffness can be tuned by changing the proportion of acrylamide and bis-acrylamide monomers. In addition, they are easy to prepare and to handle. Usually gels used in TFM have thicknesses in the range of 50 to 100 μm. Polyacrylamide gels must be coated with an extra-cellular matrix protein prior to cell seeding (Kandow, 2007). Recently, it has been possible to create gels made of soft PDMS (Bergert, 2015; Style, 2014). Aside from being elastic, they are also non porous, which may be an interesting property to study cell permeability (Casares, 2015). Furthermore, PA gels cannot be easily micro-patterned with protein because of their aqueous nature, whereas soft PDMS can be dried and stamped with ease.

TFM was originally developed to measure single-cell traction forces. Cells are typically of the order of 10-100 μm in diameter, and their reported stresses range from 10 Pa in neuronal growth cones to 1 kPa for platelets (Style, 2014). This makes cell-associated stresses among the smallest reported in the TFM literature (Figure 1-7, left). Cellular TFM has given a detailed understanding of cell tractions and the intra- and inter-cellular structures contributing to force generation (Trepat, 2009). Cells on planar substrates usually spread out to become very thin. Therefore, cellular tractions are predominantly inplane. However, recent studies have suggested that cortical tension, nuclear compression, and focal-adhesion rotation can cause significant out-of-plane forces on the substrate (Legant, 2013).

Multicellular systems are inherently more complicated than single-cell systems because of intercellular adhesion and all of its downstream signalling. Recently TFM has begun to be applied to multicellular systems, advancing understanding of cooperative phenomena in cell mechanics. One of the first multicellular applications of TFM measured intercellular forces and showed how cells move at the edge of advancing epithelial-cell sheets. This study showed that collective motion is not driven by leader cells at the sheet edge, but by cells distributed throughout the sheet (Trepat, 2009). The authors also introduced a key force-balance concept for calculating cell–cell forces with TFM, and with a tug-of-war analogue. For simple geometries, the intercellular tension is given by the integral of the traction forces from the edge of the cell colony. This technique has been extended to generate 2-dimensional maps of intercellular stresses in large sheets of cells (Tambe, 2011).

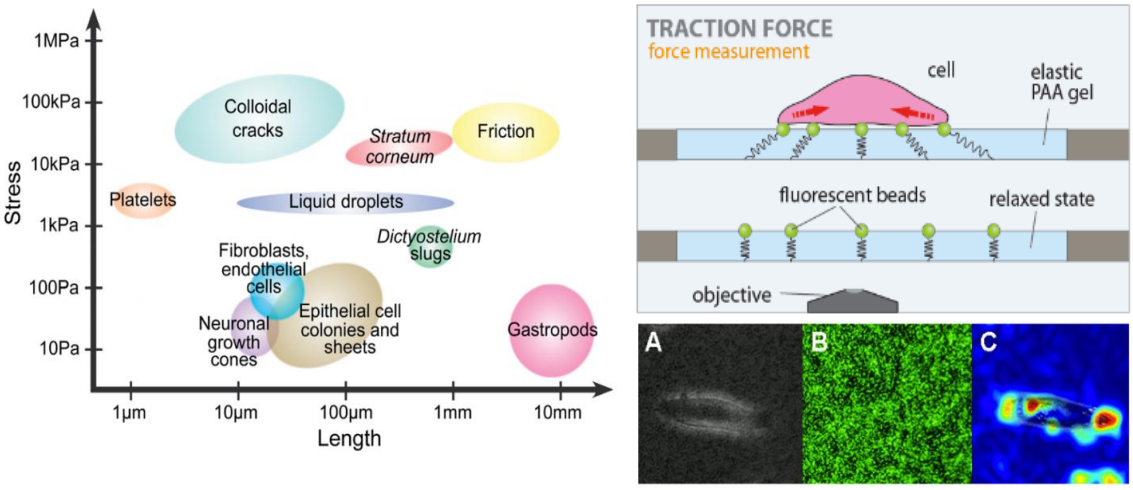

Figure 1-7| Left: Traction force microscopy across scales for different tissues and mechanical events (Style, 2014). Right: Top, a schematic view of TFM principle. Bottom, an illustration of a TFM readout: A bright field image (A) accompanied by a fluorescent image of the beads (B) within the gel underneath the cell. The direct outcome from the beads is the displacements field (C) (Fabry Lab, 2013).

1.1.5.3 Monolayer Stress Microscopy (MSM)

MSM is a young technique that provides the local state of stress within a monolayer (Tambe, 2011). Prior to that, mechanical stresses exerted at cell–cell junctions had not been accessible experimentally. The stress is inferred from the measured traction forces that cells exert on the substrate. Finally, from these traction forces measured directly at the interface between the cell and its substrate, a two-dimensional balance of forces is used to obtain the distribution of the mechanical line forces everywhere within the cell sheet (Figure 1-8); for convenience, these measured line forces (in units of force per unit length) are converted to stresses (force per unit area) using the average monolayer height, h.

Work of Tambe et. al. based on MSM shows that neighbouring cells transmit forces within a sealed monolayer through cell-cell junctions. What is more, cells proved to migrate following the local orientation of the maximal principal stress, describing a novel mechanism of collective cell guidance: plithotaxis.

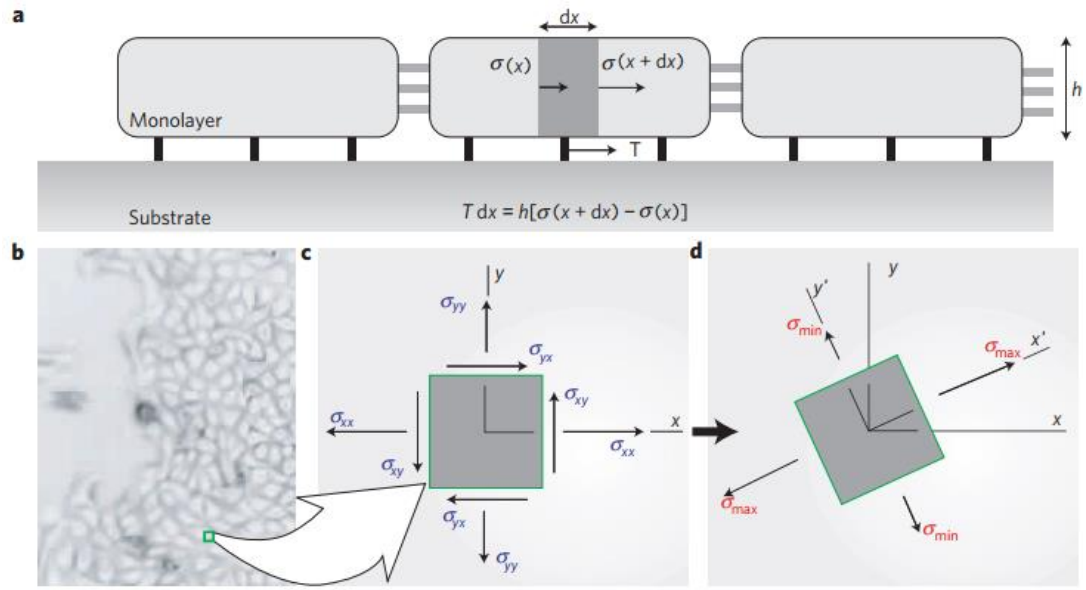

Figure 1-8| Monolayer stress microscopy. (a) Simplified representation of the physical relationship between cell-substrate tractions, T, and intercellular stresses, σ. Intercellular stresses arise from the accumulation of unbalanced cell–substrate tractions. At any point within the monolayer (b), the intercellular stresses, defined in laboratory frame (x,y), (c), have shear (σ_{xy}, and σ_{yx}) and normal (σ_{xx}, and

σ_{vv}) components. This frame can be rotated locally to obtain the principal frame (x_0 ,y_0), (d), where shear stresses vanish and the resulting normal stresses are called principal stresses (σ_{max} and σ_{min}). The corresponding axes are called maximum, aligned with x_0, and minimum, aligned with y_0, principal orientations (Tambe, 2011).

1.1.5.4 Laser ablation and FRET

One of the main limitations of TFM and MSM is their inability to measure forces in vivo. To overcome this drawback several techniques have sprung, mainly Laser ablation and FRET.

Laser ablation allows perturbing the mechanical state of living tissues and provides an estimation of the magnitude of forces that were held prior to the perturbance (Rauzi, 2015). A short wavelength laser is used to cut force-bearing structures within the cell (such as actin fibers or cell-cell junctions). After cutting the structure, the retraction dynamics can be observed, providing a qualitative estimation of the tensional state of the probe (Fink, 2011). Also from PIV analysis of the retraction and using an appropriate physical model, a quantitative estimate of the forces involved can be provided (Colombelli, 2009) (Figure 1-9).

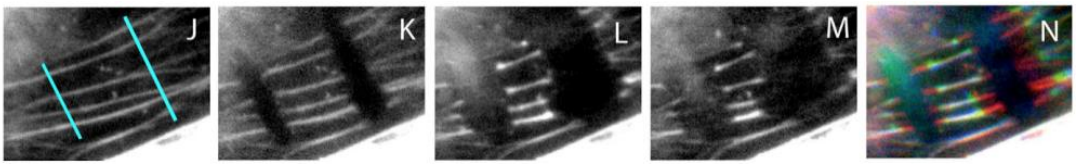

Figure 1-9| (J-N) Stress fibers dissected simultaneously in two locations. The retraction occurs from both locations and is shown 2 seconds, 10 seconds and 60 seconds after cut in K, L and M, respectively. (N) Overlap of the three time points with red (K), green (L) and blue (M) shows no lateral movement of the fiber fragments as they retract along their original axis (Colombelli, 2009).

In order to unravel molecular mechanisms responsible for force transmission within sub-cellular structures, the FRET technique has been developed.

FRET is a process in which energy is transferred nonradiatively from an electronically excited donor (D) chromophore to a nearby acceptor (A).

The FRET efficiency E, defined as the proportion of donor molecules that transfer excitation energy to the acceptor, is highly dependent on the D-A separation distance r and characterized by the Förster distance R_0 (Souza, 2014). Based on that same principle, a tension sensor module domain can be inserted between two fluorophores that undergo efficient FRET (Grashoff, 2010). Since FRET is highly sensitive to the distance between the fluorophores, FRET efficiency should decrease under tension. This construct can be transfected to cells in order to screen the force transmission through the selected molecule of study.

In their work, Grashoff et. al. describe the development of a calibrated biosensor that measures forces across specific proteins in cells with piconewton (pN) sensitivity. They apply the method to vinculin, a protein that connects integrins to actin filaments and whose recruitment to focal adhesions (FAs) is force dependent. They show that tension across vinculin in stable FAs is 2.5 pN and that vinculin recruitment to FAs is force-dependent.

To fully harness the power of FRET-based biosensors, suitable microscopy techniques and data analysis algorithms are critical. For this purpose, a number of approaches to determine FRET in cells are available. One of the most frequently used methods is based on intensity measurements, in which the donor fluorophore is excited and the emission intensities of donor and acceptor fluorophore are used to calculate a FRET ratio. This estimate of relative FRET can be measured with any appropriately equipped widefield or confocal microscope (Cost, 2015).

1.1.5.5 Other methods: photoactivation of GTPases

Light-activated proteins have recently become a way to control the function of a protein. The ability to fuse a light-sensitive domain onto other functional domains can be used to control many cellular functions. One example is Hahn's Lab work on light-based systems using the LOV (light, oxygen, voltage) domain of the oat photoreceptor phototropin, which can serve as a photactivatable protein switch (Wu, 2011). When the protein is exposed to blue light, a helix in this domain unwinds. This movement is used to block key sites in another protein. The LOV domain has been successfully attached to GTPases that control components of the cytoskeleton, like Rac1, Rho and Cdc42 (Wu, 2009; Wang, 2010). In the dark, the helix from the LOV domain is held tight against the GTPase, blocking the protein from interacting with its downstream targets. In the light, the helix relaxes, allowing GTPases partner to bind and activate the enzyme (Figure 1-10). In the dark, the LOV domain closes again over about 20 seconds. In cells containing photoactivatable Rac1, ruffles and protrusions appear in the spots illuminated by blue light, causing cells to crawl in that direction (Baker, 2012).

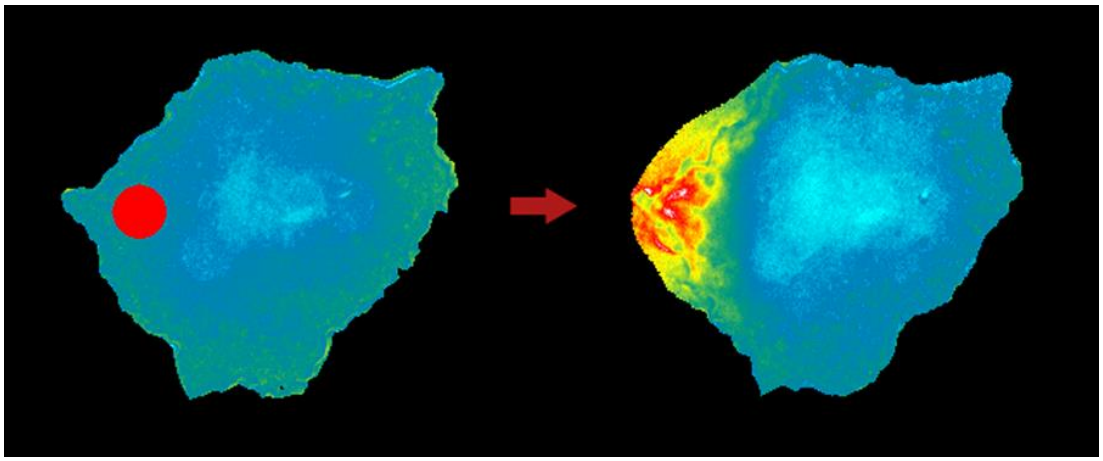

Figure 1-10| Example of Hela cell transfected with PA-Rac1, photoactivated at the right spot (left). Localized irradiation of photoactivatable Rac1 triggers activation of RhoA (Wu, 2010).

1.2 Creation and maintenance of boundaries in epithelia

The generation of a complex organism requires the formation and maintenance of a precise organization of different tissues and of distinct cell types within tissues. Such spatial compartmentalization is achieved in part through localized cell-to-cell signalling that induces specific tissues, regional domains, or cell types to form at the appropriate location. However, these compartments are initially imprecise and undergo refinement. Furthermore, the emerging compartments can potentially become scrambled owing to cell intercalation during proliferation (Monier, 2010) or convergence-extension movements (McMillen & Holley, 2015 (Current Opinion in Genetics & Development)). The control of cell movements to generate and maintain the precision of tissue organization is thus of central importance in embryogenesis, as well as in tissue homeostasis in the adult organism. A failure to maintain the correct localization of cells underlies clinically relevant disorders such as the metastatic spreading of tumors. There is consequently much interest in identifying the underlying cellular and molecular mechanisms of patterning and segregation (Batlle, 2012).

In this section, I will cover the main mechanisms in charge of boundary maintenance known to date. Further, I will give a closer look to the Eph-ephrin mechanism, being it the object of study of this dissertation.

1.2.1 Mechanisms of boundary formation and maintenance

Several mechanisms have been proposed to allow the formation of sharp boundaries. They can be summarized in four subgroups: Firstly, the *Differential Adhesion Hypothesis*; from that view, cells can be confined

within a domain due to preferential adhesion, for example by homophilic adhesion via cadherins (Foty & Steinberg, 2004). Secondly, recent studies have proposed a role of *Differential Mechanical Tension* in border sharpening (Brodland, 2002; Landsberg, 2009). A third mechanism involves *Contact Repulsion*; it is based on the mutual inhibition of cell invasion via bidirectional activation of Eph receptors and ephrins at the interface of domains (Mellitzer, 1999; Xu, 1999). Last, *jamming* or *cell proliferation* as a segregation building block (Pawlizak, 2015). A glassy phase transition of the epithelial tissue is proposed to be behind the stabilization and maintenance of boundaries (Pegoraro, 2016).

1.2.1.1 Differential cell adhesion

The concept that cells along boundaries do not mix due to differences in the adhesion or affinity between cells in neighbouring compartments is at the core of the differential cell adhesion hypothesis of Malcom Steinberg.

Steinberg proposed that different adhesive properties underlie the clustering of dissociated embryonic cells representative of their layer of origin (Steinberg, 1963), and that this sorting is driven by thermodynamic principles similar to those that induce the separation of two immiscible liquids (Duguay, 2003) (Figure 1-11, left).

Work in tissue culture has shown that artificially intermingled populations expressing cadherins will segregate from each other (Nose, 1988). This sorting is driven either by the preferential adhesion of cells expressing the same adhesion molecules i. e. in mixtures of cells expressing different cadherin molecules, or by differences in the expression level of an adhesion molecule between populations (Foty & Steinberg, 2004; Nnetu, 2012).

However, the strength of interaction between cadherins is not sufficient to fully account for cell sorting (Niessen & Gumbiner, 2002).

Although sorting of completely intermingled populations is likely to be of limited relevance *in vivo*, adhesion molecules are likely to play a role in preventing intermingling of previously segregated populations at interfaces. Indeed, cadherins could play a role in maintaining the segregation of adjacent populations during development. As an example, Redies et. al. show that cadherins have spatially restricted expression patterns in the vertebrate central nervous system (Redies & Takeichi, 1996). Recent studies have shown that cell sorting is not solely a result of differential adhesion, but rather incorporates dynamic cytoskeletal tension and extracellular matrix assembly (McMillen & Holley, 2015 (c. op. in cell biol.)).

1.2.1.2 Differential interfacial tension

The importance of cortical tension - rather than solely adhesion - in the process of sorting supports an alternative model to the DAH, called the Differential Interfacial Tension Hypothesis (DITH). DITH postulates that cells sort in order to minimize the interfacial tension of the system (Brodland, 2002). The DITH does not treat cells as liquid molecules, but rather proposes that cells generate mechanical tension at their cell-to-cell and cell-to-medium interfaces (interfacial tension), which depends largely on cell contraction and adhesion (Figure 1-11, right). The membrane and the underlying cortical cytoskeletal components are thought to generate contractile forces (F_{mem} and F_{cc}, respectively), which reduce the contact area, while cell adhesion creates adhesive force (F_{adh}), which acts in the opposite direction and thus increases the contact area. Consequently, the

interfacial tension of cell A at the cell-to-medium interface can be expressed as $\gamma^{A} = F_{mem}{}^{A} + F_{cc}{}^{A} - F_{adh}{}^{AM} + F_{other}{}^{AM}$, where F_{other} is the force resulting from the contraction of non-cortical elements and viscous properties of the cell and its constituent organelles, reducing the interfacial area (Figure 1-12).

The interfacial tension at the interface between cells A and B can be expressed as $\gamma^{AB} = F_{mem}{}^{A} + F_{mem}{}^{B} + F_{cc}{}^{A} + F_{cc}{}^{B} - F_{adh}{}^{AB} + F_{other}{}^{AB}$. In a heterotypic aggregate, cells of type B tend to envelop cells of type A when $\gamma^{AM} > \gamma^{BM}$, and fully engulf the latter when $\gamma^{AM} > \gamma^{AB} + \gamma^{BM}$.

The DITH differs from the DAH theory by combining cell contraction and adhesion and taking into account the possibility of additional properties of the cell (e.g. cytoplasm viscosity, density of the cell content), which are likely to influence interfacial tensions and, consequently, drive cell sorting.

Mechanical tension has been shown to play a role in the maintenance of sharp boundaries. Actomyosin filaments provide compartments with a physical barrier through which cells cannot cross. In drosophila embryos, cell divisions have been shown unable to challenge the boundary integrity. Reversely, when Myosin II activity was locally reduced by chromophore-assisted laser inactivation (CALI), cell division caused the boundary to become irregular (Monier, 2010).

Modelling has addressed whether an increase in mechanical tension is sufficient to maintain compartment boundaries. Simulation of straight interfaces between two populations shows how cell proliferation promotes fuzziness, whereas an increase in mechanical tension along the interface causes the interface to become straighter (Landsberg, 2009). This modelling suggests that an increase in mechanical tension is sufficient to maintain straight interfaces between compartments, i.e. in Drosophila

(Dahmann, 2011). Cortical tension has also been shown to play a role in cell segregation between germ layers in zebrafish (Krieg, 2008).

The DITH effectively describes cell sorting in vitro (Green, 2008; Amack, 2012). However, cell sorting in vitro does not necessarily recapitulate cell sorting in embryos, as zebrafish ectodermal cells sort internally in aggregates and externally in embryos (McMillen & Holley, 2015 (c. op. in cell biol.); Krieg, 2008). It is clear that the in vivo context influences patterns and rates of cell sorting. Computer simulations suggest that both extra-embryonic tissues and the interface between cells and interstitial fluid impact cell sorting. For example, cell–ECM interactions play an important role in embryonic morphogenesis (Kleinman, 2003). Dimensionality and physical context strongly influence cell–ECM interactions and may be very different in cell aggregates compared to an embryo (McMillen & Holley, 2015 (c. op. in cell biol.))

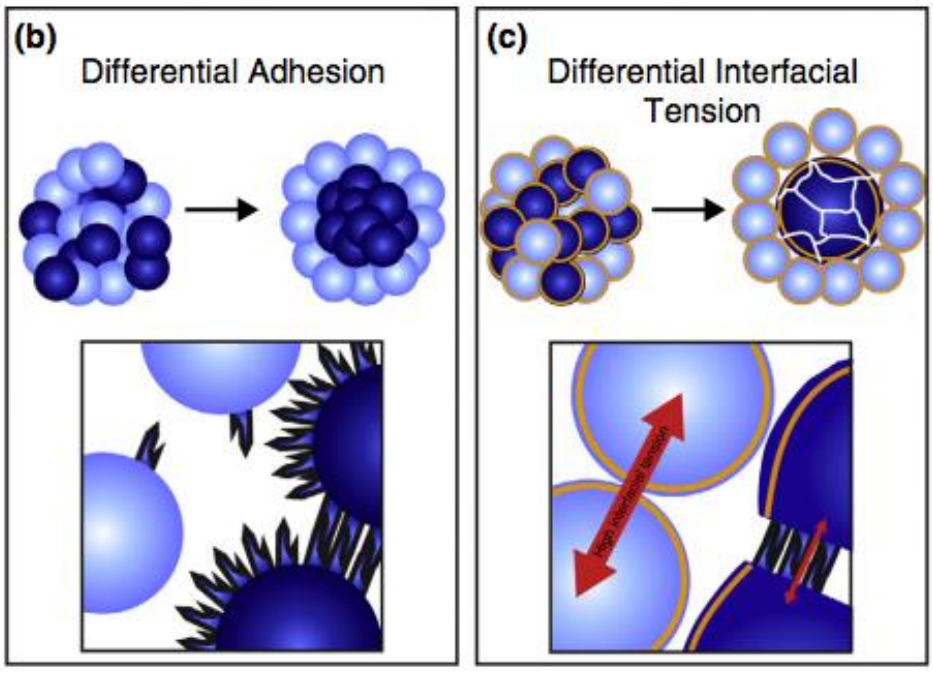

Figure 1-11| Models for cell sorting: (b) The DAH accurately predicts that cells expressing different levels of the same cadherin will effectively sort. (c) The DITH predicts that changes in cortical tension largely mediated by the cytoskeleton drive cell sorting. Cadherins affect sorting by both reducing cytoskeletal tension and by mediating cell-cell adhesion (McMillen & Holley, 2015 (c. op. in cell biol.)).

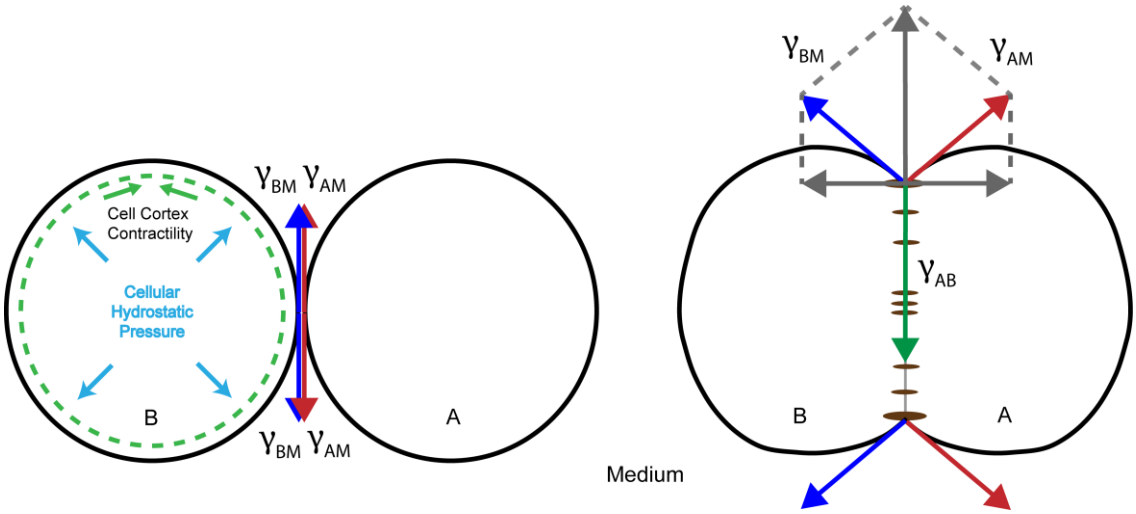

Figure 1-12| Cell surface tension, adhesion and interfacial tension from the DITH perspective. Forces exerted on adhering cells are classically modeled using the concept of cellular surface tension, by analogy with the surface tension of liquids. For single cells, the surface tension (blue and red arrows) is dictated by the cortical contractility, which tends to minimize the cell surface area (cell rounding). In a system with two or more cells, cell-cell adhesion produces an opposing force that increases cell-cell contact. Interfacial tension results from the balance of these two forces.

1.2.1.3 Eph-ephrin mediated contact repulsion

Eph receptors and ephrins are cell surface proteins that mediate local cell-to-cell communication. Typically, upon cell-cell contact, Eph receptors and ephrins expressed on neighbouring cells interact with each other, thus triggering a signalling cascade. The best-characterized biological outcome of Eph-ephrin signalling is the regulation of cell adhesion, either positively or negatively, depending on the cellular context (Pasquale, 2008) (Figure 1-13).

The localised activation of Eph receptors and ephrin ligands at the interface of complementary expression domains underlies a mutual repulsion that prevents intermingling across boundaries. Eph-ephrin interactions could contribute to the sharpening of segments by regulating both repulsion at interfaces (Marston, 2003) and adhesion of cells (Mellitzer, 1999). As an example, it has been observed that cadherin clustering is specifically inhibited at the vertebrate notochord-presomitic mesoderm boundary,

preventing formation of adhesive bonds between cells of the two different types (Fagotto, 2013). This local regulation depends on differentially expressed ephrins and Eph receptors, which increase cell contractility and generate a membrane blebbing-like behavior along the boundary.

Eph-ephrin juxtacrine signalling pathway in particular is notable for regulating both cadherins and integrins, and for its importance during a number of early morphogenic events (Arvanitis, 2008). In Xenopus, Eph-ephrin signalling drives paraxial mesoderm/notochord boundary formation by destabilizing cadherin–cadherin interactions (Batlle, 2012). In zebrafish, Eph-ephrin and integrin signalling jointly control extracellular matrix assembly along tissue boundaries (Jülich, 2009). Eph-ephrin also induces somite boundary formation by activating integrins and thereby establishing fibronectin matrix (Dahmann, 2011).

Eph-ephrin signalling has also been extensively studied in the context of the developing mammalian nervous system, where it has been involved in topographic mapping, axon guidance, neuronal migration and synapse formation among others (Laussu, 2014).

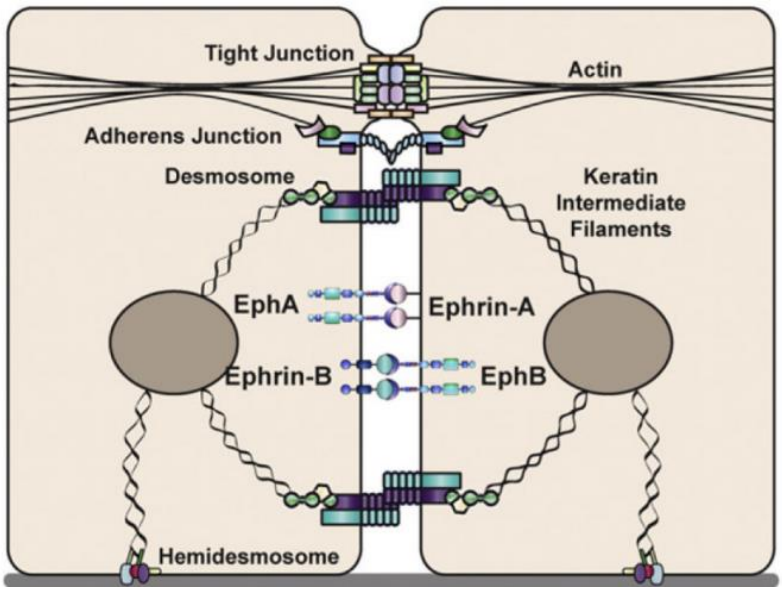

Figure 1-13| A scheme of two polarized epithelial cells joined together by adherens junctions, desmosomes and tight junctions. Eph receptors and ephrin ligands are functionally integrated with intercellular adhesion complexes (Lin, 2012).

1.2.1.4 Jamming in epithelial sorting

It is commonly accepted that cell affinities alone do not fully capture cell sorting. Thus, cell affinity must act in cooperation with other mechanisms that contribute to cell-sorting behavior. More often cell motility and contractility are pointed out, but patterned cell proliferation may also play a major role in segregation (Tepass, 2002). It is well known that many epithelial tissues pack cells into a honeycomb pattern to support their structural and functional integrity (Gibson, 2006). Developmental changes in cell packing have been shown to be regulated by both mechanical and biochemical interactions between cells (Lecuit & Lenne, 2007). At the single cell level, geometry is regulated by forces acting along the plane of the adherent junctions, such as tension, which shortens the cell contact surface, and pressure, which counteracts tension to maintain the size of a cell (Sugimura, 2013).

In the context of cell sorting, jamming may be a mechanism that helps to stabilize and maintain segregation between cell populations. While DAH makes the strong assumption that cells behave as immiscible Newtonian fluids, it has become increasingly obvious that this paradigm is unable to explain the experimental observations in several in vivo models (Ninomiya, 2011). Alternatively, if cells are nearly jammed, then cells cannot freely explore the landscape for the minimal free energy of the system, and it is possible for the segregated tissue to undergo a different process than free energy minimization. Pawlizak et. al. studied the boundary formation among different lines of cancer cells that exhibit a shift in E-, N- and P-cadherin levels, characteristic of an epithelial−mesenchymal transition associated with processes such as metastasis. In their study, extended DAH was unable to predict the final sorted state for their experiments. Their observations showed that the surface of sorted droplets of cells were more

reminiscent of dense colloidal clusters or complex yield-stress fluids than of fluid-like droplets (Pawlizak, 2015).

Further, in the context of repulsive boundary formation, ephrinB1 forward signalling has been shown to regulate craniofacial morphogenesis by controlling cell proliferation across Eph-ephrin boundaries (Bush, 2010).

These observations suggest a paradigm-shifting hypothesis that cell jamming, regulated by material properties, could be a key determinant in boundary formation.

1.3 Receptor tyrosine kinases (RTKs): The Eph-ephrin family

Eph receptors and their ephrin ligands constitute the largest subfamily of receptor tyrosine kinases and are components of the cell signalling pathways involved during development.

Receptor tyrosine kinases (RTKs) are transmembrane glycoproteins that act as key regulators of cell growth, differentiation and motility. In addition, abnormal RTK expression activity is characteristic of most human cancers (Herath, 2010). The 16 vertebrate Eph receptors form the largest subfamily of RTKs.

Ephs and ephrins are both divided into two subclasses – A and B – based on their affinities for each other and on sequence conservation. In general, the nine different EphA RTKs (EphA1–EphA9) bind promiscuously to, and are activated by, six A-ephrins (ephrinA1–ephrinA6), and the EphB subclass receptors (EphB1–EphB6) interact with three different B-ephrins (ephrinB1-ephrinB3) (Himanen, 2007).

1.3.1 Eph receptors

Eph receptors are divided into EphA (EphA1-10), and EphB kinases (EphB1-EphB6) according to sequence homology and binding specificity to their membrane bound ligands, ephrins. The A-type Ephs preferentially bind the GPI linked A ephrins, whereas the B Ephs preferentially bind type-B transmembrane ephrins. However, this does not preclude crossclass interactions as has been shown for EphA3, EphA4 and EphB2, which bind to ephrinB2 and ephrinB3 respectively (Herath, 2010) (Figure 1-14).

The first Eph receptor was cloned from a human erythropoietin-producing hepatocellular cell line. Subsequently, other Eph receptors were isolated from various cDNA libraries (Herath, 2010; Hirai, 1987; Arvanitis, 2008).

1.3.2 Ephrin ligands

Ephrins are ligands attached to the plasma membrane. They are characterized by the presence of a unique N-terminal receptor-binding domain (RBD), which is separated from the membrane via a linker of approximately 40 aminoacids. A-ephrins are attached to the cell via a glycosylphosphatidylinositol (GPI) linkage. B-ephrins possess a transmembrane region and short, but highly conserved, 80 aminoacid cytoplasmic domain, which includes a C-terminal PDZ-binding motif (Himanen, 2003) (Figure 1-14). It has been shown that the intercellular domain of ephrinB is necessary for the completion of cell sorting (Adams, 2001).

The first ephrin ligand was identified from cancer cells (Arvanitis, 2008; Bartley, 1994; Beckmann, 1994; Cheng & Flanagan, 1994; Xi, 2012).

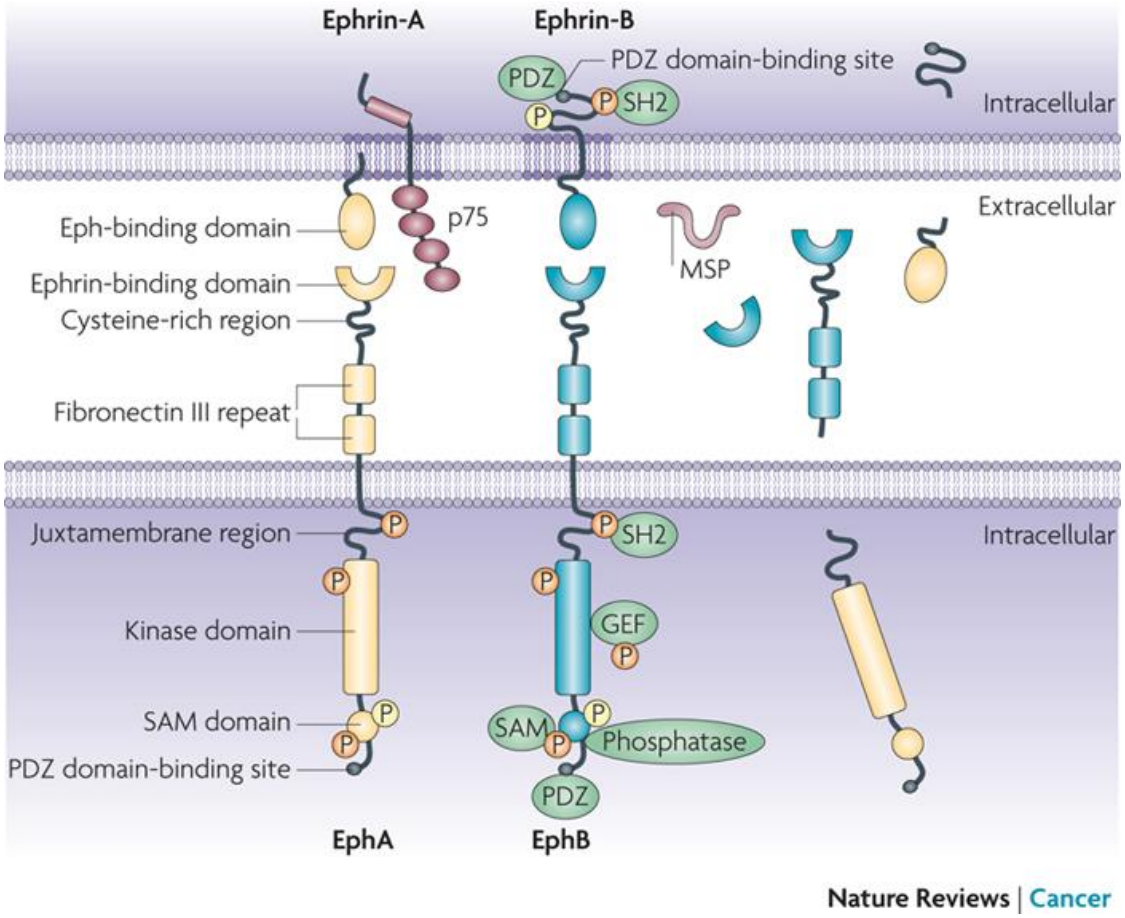

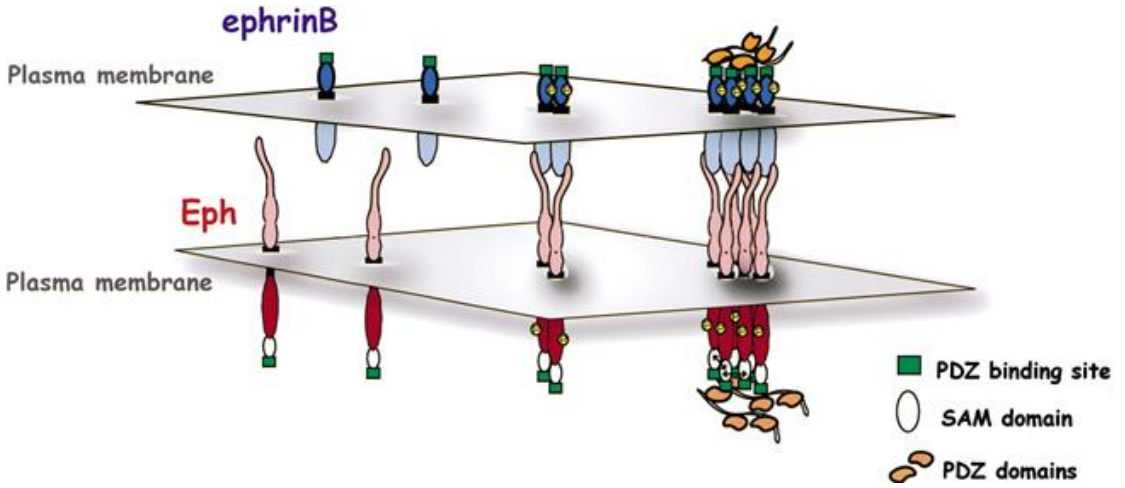

Figure 1-14| Top: scheme of the main building blocks of the Eph-ephrin complex (Pasquale, 2010). Bottom: usual Eph-ephrin complex structure at the cell-cell junction. Membrane attachment of both Ephs and ephrins provides a mechanism whereby interactions between receptors and ligands occur only at sites of cell–cell contact, leading to the multimerization of both molecules to distinct clusters in their respective plasma membranes (Palmer, 2003).

1.4 Eph-ephrin bidirectional signalling

Eph receptors and their ephrin ligands are important mediators of cell–cell communication regulating cell attachment, shape and mobility. Both Ephs and ephrins are membrane-bound and their interactions at sites of cell–cell contact initiate unique bidirectional signalling cascades, with information transduced in both the receptor expressing and the ligand-expressing cells (Himanen, 2003).

Ephrins bind Eph receptor tyrosine kinases (RTKs) and activate their tyrosine kinase catalytic domains. Concomitant with activation of Eph kinases and transduction of the typical forward signal into the receptor-bearing cell, the ligand–receptor interaction also leads to transduction of a reverse signal into the ephrin-bearing cell (Lisabeth, 2013). Eph receptor "forward" signalling depends on the tyrosine kinase domain, which mediates autophosphorylation as well as phosphorylation of other proteins, and on the associations of the receptor with various effector proteins. EphrinB "reverse" signalling also depends in part on tyrosine phosphorylation of the ephrin cytoplasmic region (mediated by Src family kinases and some receptor tyrosine kinases) and on associated proteins (Palmer, 2003).

Over the years, a wealth of publications has identified downstream effectors of Eph receptor tyrosine kinases, such as small GTPases, GAPs, GEFs, cytoplasmic kinases and phosphatases (Nievergall, 2011). On the contrary, the molecular characterization of reverse signalling has progressed at a slower pace, perhaps because the biological outputs of reverse signalling are in general less robust than those of forward signalling. The majority of molecular effectors of Eph-ephrin signalling identified to date relate to the adhesive function of the pathway and to local regulation of the cell cytoskeleton (Lisabeth, 2013).

A well-characterized effect of Eph forward signalling is retraction of the cell periphery following contact with ephrin expressing cells (Pasquale, 2005). This repulsive response is particularly important for axon guidance and sorting of Eph-expressing cells from ephrin-expressing cells during development. Three main mechanisms can explain how the initial adhesive contact evolves into cell separation:

(1) One is removal of the adhesive Eph-ephrin complexes from the cell surface by endocytosis of vesicles containing plasma membrane fragments derived from both cells (Egea & Klein, 2007). An implication of this unusual mechanism is that the two cells exchange Eph receptors or ephrins and possibly their associated proteins, which may continue to signal from intracellular compartments (Figure 1-15, bottom).

(2) Another way to convert cell adhesion into repulsion is proteolytic cleavage (Egea & Klein, 2007; Himanen, 2007). Studies have shown that metalloproteinases and other proteinases can cleave the extracellular portions of EphB receptors and ephrins. The remaining membrane-anchored fragments are further cleaved by γ-secretase, followed by proteasomal degradation (Figure 1-15, top). Furthermore, Solanas et. al. have shown that EphB receptors interact with E-cadherin and with the metalloproteinase ADAM10 at sites of adhesion. Downstream of their activation, E-cadherin shedding is induced by ADAM10 at interfaces with ephrinB1-expressing cells (Solanas, 2011).

(3) The third mechanism states that Eph-ephrin interaction at the boundary promotes a local increase in contractility along the boundary interface. This produces high interfacial tension between

the two cell populations independently of global tissue tension and adhesiveness (Dahmann, 2011; Landsberg, 2009; Fagotto, 2014).

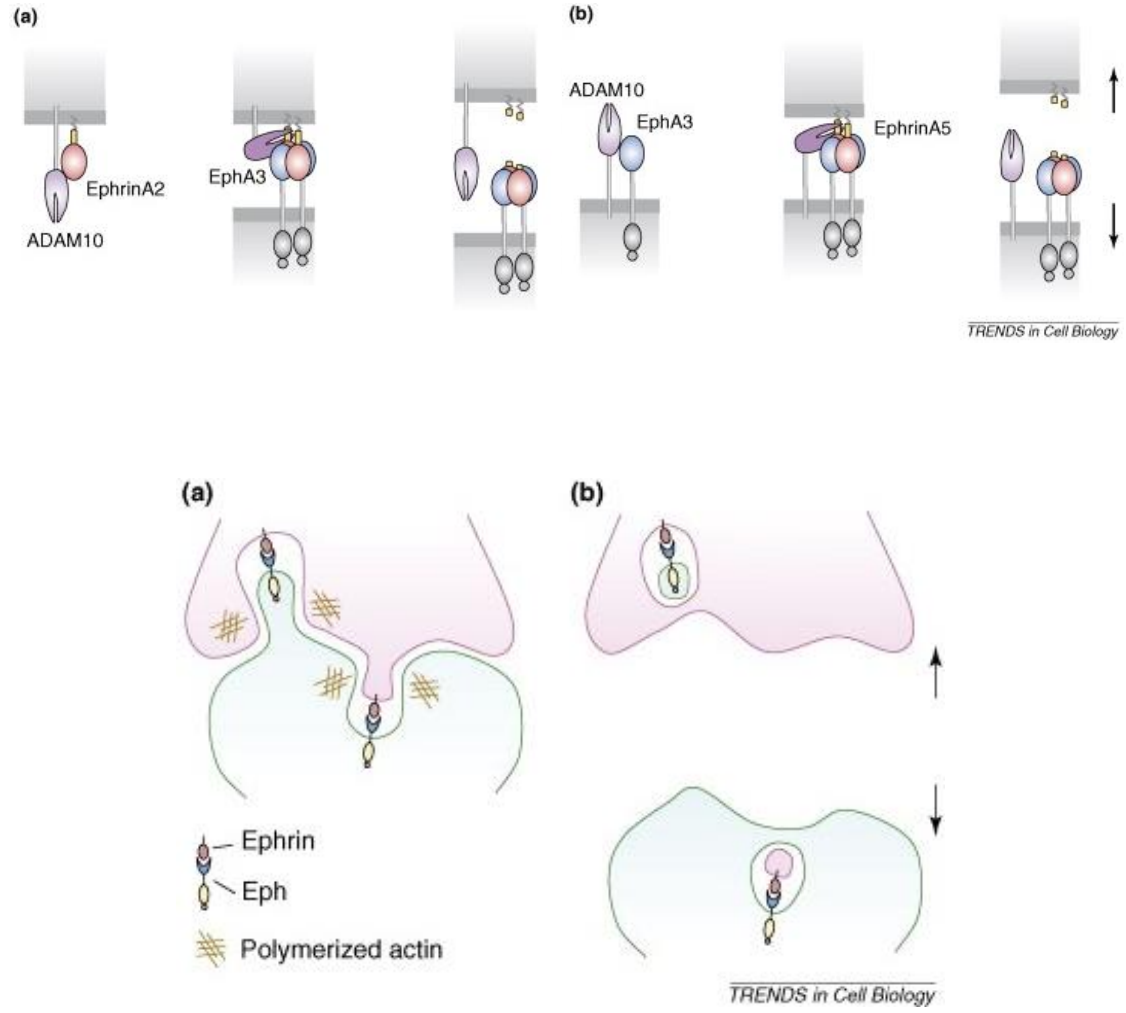

Figure 1-15| Top: Mechanisms of ephrin cleavage by metalloproteinases. (a) A cell co-expressing ephrin (red) and ADAM10 (purple) metalloproteinase encounters a second cell expressing Eph receptors. Interaction between ephrin and Eph leads to the formation of higher-order ligand–receptor clusters (shown here as heterodimers) and to *cis* cleavage of the ephrin stem region (yellow) by ADAM10. (b) A cell co-expressing Eph and ADAM10 encounters a second cell expressing ephrin (red). Interaction between ephrin and Eph results in the activation of ADAM10 and *trans* cleavage of ephrin. Bottom: Bidirectional trans-endocytosis of ephrin–Eph complexes. (a) The encounter of cells expressing ephrin with cells expressing Eph receptors can result in bidirectional endocytosis of the ligand–receptor complexes. (b) This mechanism, which involves *trans*-internalization of full-length proteins, can turn cell attraction into cell repulsion. EphrinB endocytosis into the EphB-expressing cell requires actin polymerization (Egea & Klein, 2007).

2 AIMS OF THE THESIS

2.1 General aim

The general aim of this thesis was to study the mechanics involved in the formation and maintenance of repulsive Eph-ephrin boundaries.

2.2 Specific aims

1. To develop an in vitro assay that allows the formation of boundaries whilst measuring traction forces and performing time-lapse microscopy.
    a. To design a master that allows further replication of PDMS stencils containing two independent seeding cavities separated by a controlled distance (300-400 microns).
    b. To produce stencils which are attachable to PA gels without leaking or damaging the gels during hours of seeding.
    c. To design an assay for epithelial migration against a barrier based on the same technology.

2. To measure traction forces, cell-cell stresses and cell morphology in the context of Eph-ephrin boundary formation.
    a. To perform high-resolution imaging to study morphological features of repulsive boundaries.
    b. To measure traction forces and velocities during the formation of a repulsive epithelial boundary.
    c. To implement monolayer stress microscopy in the context of an Eph-ephrin boundary buildup.

3. To provide an analysis of epithelial biomechanics and morphology during Eph-ephrin boundary formation.
    a. To study the morphological changes that cells undergo during repulsive boundary formation.
    b. To study the contribution of cell proliferation to Eph-ephrin boundary buildup.
    c. To study the effect of disrupting cell junctions and perturbing cell contractility during repulsive boundary formation.

4. To study the mechanics involved in migration against a barrier in comparison with boundary formation.

5. To study the mechanics involved in control Eph-Eph boundaries (wound healing assay) compared to boundary formation.

6. To identify the mechanisms behind the creation and maintenance of the different boundaries under study.

7. To foresee a theoretical framework able to predict the mechanical features of boundary formation and maintenance.

3 MATERIALS AND METHODS

3.1 Laboratory techniques

3.1.1 Cell generation and sorting

MDCK cells expressing either EphB or ephrinB ligands were kindly provided by E. Batlle. Generation of these cell lines was described elsewhere (Solanas, 2011). Briefly, MDCK cells were infected with lentivirus carrying EphB2 or ephrinB1 complementary DNAs. The canine E-cadherin–GFP fusion construct (gift from J.W. Nelson) was inserted downstream of the cytomegalovirus promoter into the FUW lentiviral vector backbone. The E-cadherin–Cherry fusion construct was derived from the E-cadherin–GFP FUW plasmid. Lentiviral particles containing those cDNAS were produced to infect the EphB-positive (E-cadherin–GFP) or ephrinB1-positive (E-cadherin–Cherry) populations.

MDCK cells expressing homogeneous levels of anti-EphB-mcherry (ab)/GFP (protein) or anti-ephrinB-GFP (ab)/Cherry (protein) were selected using an ARIA fluorescence-activated cell sorter (BD). An extended version of this procedure can be found at the appendix 7.4 (Cell sorting protocol).

3.1.2 Lifeact lentiviral transfection

MDCK Eph-ephrin expressing cells were infected with lentivirus carrying lifeact-mcherry or lifeact-CFP respectively (gift from J. de Rooij) and FAC sorted using an ARIA fluorescence-activated cell sorter (BD).

3.1.3 Cell culture

MDCK cells were cultured in minimum essential media (MEM) with Earle's Salts and l-glutamine (31095-029, Thermofisher) supplemented with 10% fetal bovine serum (FBS; 10270-106, Thermofisher), 100 units ml^{-1} penicillin, 100 µg ml^{-1} streptomycin and 292 µg ml^{-1} l-glutamine (10378-016, Thermofisher). Cells were maintained at 37^{o}C in a humidified atmosphere with 5% CO_2.

3.1.4 Design and 3D printing of masters

We used the open source software openSCAD to design the masters for the PDMS stencil replication and also to design the magnet holder. Sketches were exported to a stereolithography format file (STL), which is a standard file for 3D printing. An FDM 3D printer was used to print the prototype pieces using the open source software Slic3r (http://slic3r.org/) to obtain the gcode. The final masters were ordered through the 3D printing service of Shapeways (www.shapeways.com). The final designed pieces are a stencil, a single well stencil, a barrier and a magnet holder.

3.1.5 Magnetic PDMS stencil preparation

We prepared the magnetic PDMS by mixing thoroughly the base and cross-linker in a 10:1 proportion. Then added 50% (w/w) of magnetite (Inoxia) and mixed for 5 min. Air was removed by placing the mixture in a vacuum jar for 1 h. Afterwards, we filled the master with magnetic PDMS and cured it for 2 h at 60ºC.

3.1.6 Polyacrylamide gel preparation

3.1.6.1 Reagents

- Bind Silane (3-trimethoxysilyl popyl methacrylate) (M6514, Sigma-Aldrich)
- Acetic acid (A6283, Sigma-Aldrich)
- Ethanol (96%, Panreac)
- Hepes solution (10 mM) (H0887, Sigma-Aldrich)
- 40% Acrylamide solution (161-0140, BioRad)
- 2% Bisacrylamide solution (161-0142, BioRad)
- 200-nm-diameter dark red fluorescent carboxylate-modified beads (F8807, Thermofisher)
- Rat tail collagen type I (08-115, EMD Millipore)
- 10% Amonium Persulfate diluted in water (APS) (A3678-25G, Sigma-Aldrich)
- Sulfo-SANPAH (4822589, Culteck)
- N-N-N-N-Tetramethylethylenediamine (TEMED) (T-9281, Sigma-Aldrich)
- 6-well glass bottom plate (Mattek)
- GelBond PAG film (54723, Lonza)

3.1.6.2 Protocol

Polyacrylamide gel preparation was adapted from protocols described previously (Kandow, 2007). Glass-bottom dishes were activated by using a 1:1:14 solution of acetic acid/bind-silane/ethanol. The dishes were washed

twice with ethanol and air-dried for 10 min. For 15 kPa gels, a 500 µl stock solution containing 93.75 µl acrylamide, 45 µl bisacrylamide, 2.5 µl APS, 0.25 µl TEMED and 3.2 µl of 200-nm-diameter far red fluorescent carboxylate-modified beads was prepared. A drop of 15 µl was added to the centre of the glass-bottom dishes, and the solution was covered with 18-mm-diameter GelBond film coverslips custom cut by an electronic cutting tool (Silhouette Cameo). After 1 h of polymerization, 2 ml of MiliQ water were added and GelBond coverslips were removed with a pair of flat tip tweezers. Gels were functionalized with sulfo-sanpah and exposed to UV light for 5 minutes. Then, gels were washed with miliQ water for 5 minutes. Afterwards, gels were washed with PBS and incubated with 100 µl of a collagen I solution (0.1 mg ml^{-1}) overnight at 4ºC. Collagen was aspirated and gels were washed afterwards twice with PBS. Finally gels were incubated with cell culture media for 1 h.

3.1.7 Boundary buildup experiment

3.1.7.1 Reagents

- Pluronic acid F-127 (P2443, Sigma-Aldrich)
- Neodymium magnets (20x10 mm) (Calamit)
- Magnetic PDMS stencils (custom made)

3.1.7.2 Protocol

We autoclaved the magnetic PDMS stencils at 135ºC with a dry program. We passivated the stencils by incubating them for 1h in a solution of 2%

Pluronic in PBS. Afterwards, we washed the stencils twice in PBS and dried them with a N_2 flux gun. We then washed the polyacrylamide gels twice using PBS and aspirated the PBS. We dried the polyacrylamide gel surface with a N_2 flux. We placed the 6-well plate on a custom designed and 3D printed holder containing a neodymium magnet underneath each coverslip position. Afterwards, we placed the magnetic PDMS stencil on top of each gel, making sure there was a flat, homogenous contact between the PDMS and the gel. Finally, we added 150,000 Eph cells concentrated in 120 µl of media in the left hollow region defined by the PDMS membrane and 150,000 ephrin cells in the right hollow region. We waited 1 h for cell attachment. We washed the two hollow regions and added media. We then cultured the cells 4 h prior to experiment.

3.1.8 Physical barrier experiment

For the physical barrier experiments the surface of a glass bottom petri dish and the contact surface of the PDMS barrier were activated with corona. Immediately after, the PDMS barrier was put in contact with the glass and pressed for a few seconds ensuring that the two surfaces were making contact and the PDMS was properly attached (attachment can be improved using magnetic PDMS barriers and performing all the steps on top of a magnet). The barrier was passivated adding 2 ml of 2% pluronic for 1h. Prior to seeding, the petri dish was placed on top of a magnet and blow-dried with nitrogen. Then a single gasket made of magnetic PDMS was inserted to fit in with the barrier. 150,000 cells were seeded and let attach for 5 hours before removing the gasket.

3.1.9 Immunofluorescence staining

Immunofluorescence microscopy experiments were carried out by fixing the cells with 3% paraformaldehyde (Sigma-Aldrich) in PBS, permeabilizing with 0.5% Triton X-100 (Sigma-Aldrich) in PBS, and blocking with 10% FBS (Sigma-Aldrich) in PBS. Primary antibodies mouse anti-E-cadherin (610181, BD Biosciences) and rabbit anti-phMLCII (1673674S, Cell Signalling) diluted at 1:400 and 1:200, respectively, in 10% FBS in PBS were incubated for 3 h at room temperature, and were detected using secondary antibodies goat anti-mouse (A11029, Thermofisher) and donkey anti-rabbit (A21245, Thermofisher) diluted at 1:200 in 10% FBS in PBS. Hoechst 33342 (H3570, Thermofisher) and Phalloidin (A22287, Thermofisher) diluted at 1:5000 and 1:40, respectively, in 10% FBS in PBS were incubated during 1 h with the secondary antibodies.

3.2 Data processing techniques

3.2.1 Time lapse imaging

Multidimensional acquisition routines were performed on an automated inverted microscope (Nikon Eclipse Ti) equipped with thermal, CO_2 and humidity control, using MetaMorph (Universal Imaging) software. Time-lapse recording started approximately 30 min after removing the PDMS stencils. The interval between image acquisitions was 7.5 min and a typical experiment lasted for 18 h. Images were acquired at ×20 for every time point.

3.2.2 Spinning-Disk imaging

A spinning disk microscope (Nikon Andor) was used for high-resolution image acquisition of stained samples.

3.2.3 Traction microscopy

Traction forces were computed using Fourier transform based traction microscopy with a finite gel thickness. Gel displacements between any experimental time point and a reference image obtained after monolayer trypsinization were computed using home-made particle imaging velocimetry software (Trepat, 2009).

3.2.4 Monolayer stress microscopy

Monolayer stresses were computed using monolayer stress microscopy (Tambe, 2011). Monolayer stress microscopy uses traction forces and straightforward force balance demanded by Newton's laws to map the two-dimensional stress tensor σ in the monolayer.

By rotating these stress components at each point in the cell sheet, we computed the magnitude of the two principal stress components σ_{max} and σ_{min} and their corresponding, mutually perpendicular, principal orientations. For each point in the monolayer, we then computed the average normal stress within and between cells defined as $\sigma = (\sigma_{max} + \sigma_{min})/2$ and the maximum intercellular shear stress defined as $\mu = (\sigma_{max} - \sigma_{min})/2$.

3.2.5 Velocity measurements

Velocity fields were computed using custom-made particle image velocimetry software (PIV) on the phase-contrast images. The interrogation window was 96×96 pixels, and the time interval between consecutive analysed images was 7.5 min.

3.2.6 Kymography

Monolayer boundaries were drawn by hand using a home-made algorithm which overlaid traction maps on phase-contrast images to improve accuracy.

For each pixel of each side of the boundary, we computed the distance to its leading edge. Next we computed the median values of velocities, tractions, monolayer stresses and strain rates of all pixels located at a given distance from the boundary. To that aim, we performed a coordinate system change from Cartesian coordinates to Parallel and Perpendicular coordinates (with respect to the boundary). Median values of either Perpendicular or Parallel components were then represented on an unidimensional segment whose width was the mean width of the monolayers. This operation was repeated for each experimental time point.

3.2.7 Image segmentation

Single cell segmentation and analysis of boundary cells was performed with a semi-automatic method:

1) Phase contrast images were converted to RGB images.
2) Cells at the boundary were contoured with a red line in Fiji.
3) Custom made software in Matlab was developed to recognize the red contours and post-process the geometrical information therein.

Epithelial segmentation was performed by a custom method that allowed acquiring tractions and geometrical information at the same time for a selected number of time points:

1) A capture of the phase contrast and the fluorescent beads on the gel underneath was taken.
2) A trypsin treatment was applied. During the first minutes of the treatment, cells dissolve their junctions but retain their shape, allowing the light to travel through the cell-cell junctions. Phase

contrast captures taken at this moment allowed segmenting the cell shapes directly from phase contrast images afterwards.

3) After 10 minutes, all cells were detached from the gel. A final image of the relaxed gel was taken to get the corresponding tractions.
4) Phase-contrast images were pre-treated in FIJI to remove very small or large features by a spectral filter.
5) The treated images were processed with a Matlab custom-made software based on feature recognition.

4 RESULTS

4.1 Boundary formation assay

In this dissertation we aimed at examining epithelial mechanics during the formation and maintenance of repulsive unidimensional interfaces. To accomplish this, we developed a novel assay that enabled the formation of boundaries together with the measurement of traction forces exerted by cells and the imaging of the boundary buildup. Our design allows for the co-culture of different cell populations seeded in close vicinity (300-400 μm of interdistance). Our custom PDMS-based stencils can be attached to PA gels without damaging them during hours of incubation.

4.1.1 Design and optimization of the experimental setup

Our first approach was to use blocks of PDMS and cut out two cavities at a nearby distance by a biopunch (Figure 4-1, a-b). The main challenge was to have control over the interdistance, which had a variability of 300-500 μm. Further, the area in which cells collided in a pseudo-flat fashion was too short (Figure 4-1, c). Still, this approach allowed us to identify some experimental problems and to solve them by design:

1) Each cavity must have sufficient volume to allocate a drop of medium with cells. The height of the cavity had to be adjusted. If it was too low, the two independent drops of cells could have eventually mixed (Figure 4-2).

2) The intermediate distance had to be thick enough not to be broken.

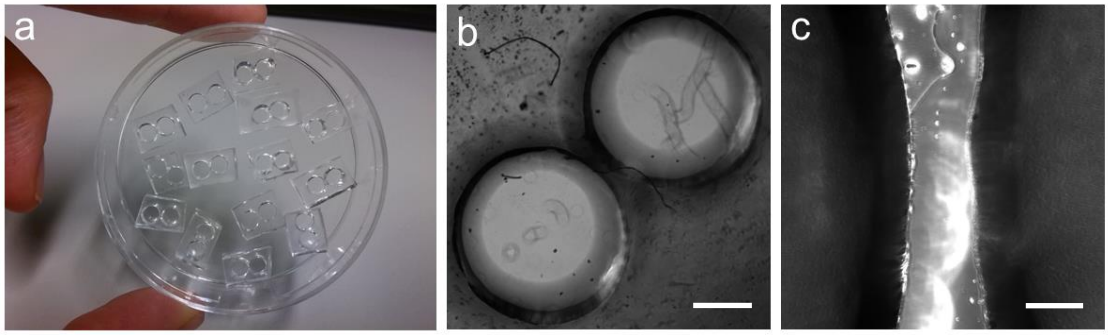

Figure 4-1 | a, Photography of PDMS stencils. b, Zoom of the two cavities cut by a biopunch (4x). Scale bar is 670 µm. c, Detail of the intermediate space of the PDMS stencil (10x). Scale bar is 120 µm.

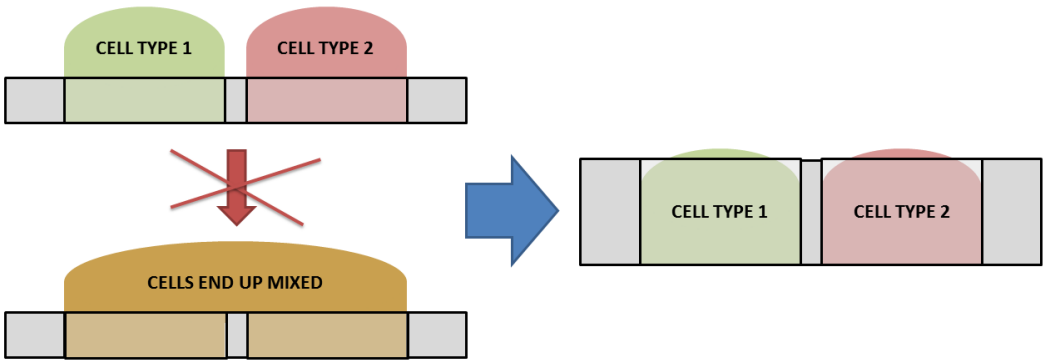

Figure 4-2| Schematic view illustrating the design limitation.

4.1.2 3D printer design

The previous technique implied too much variability, so we continued working to find a more reproducible method to create stencils with two cavities.

Advances in 3D printing allowed us to 3D-print a master that enabled stencil replication in PDMS over bench. In this way, we could overcome the usual clean room procedure to pattern the stencil by photolithography.

The stencils produced consist of one single element containing two rectangular cavities separated by a constant distance (300 µm) (Figure 4-3).

In order to make the intermediate wall less fragile, we made the wall thicker at its top than at the bottom (gel contact site). In this way, we could have cells seeded in close vicinity but having a robust wall between them (

Figure 4-4).

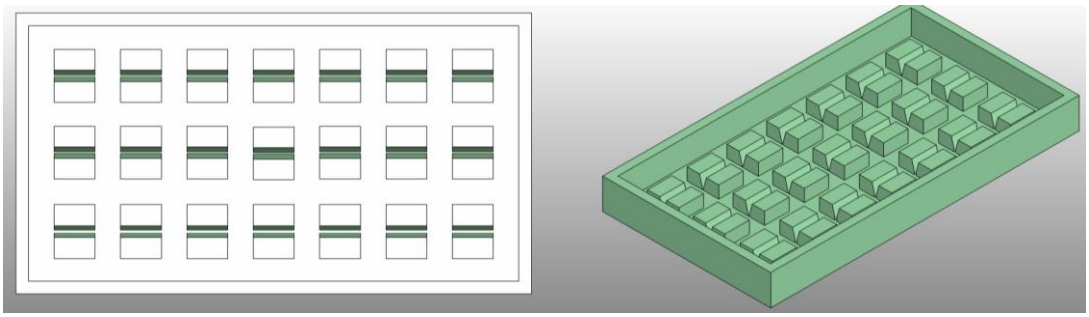

Figure 4-3| Top and perspective view of the master.

The stencils were cut out from the master by a blade and a pair of flat tip tweezers. They were autoclaved before use. PDMS stencils proved very resistant and could be reused up to 5 times each.

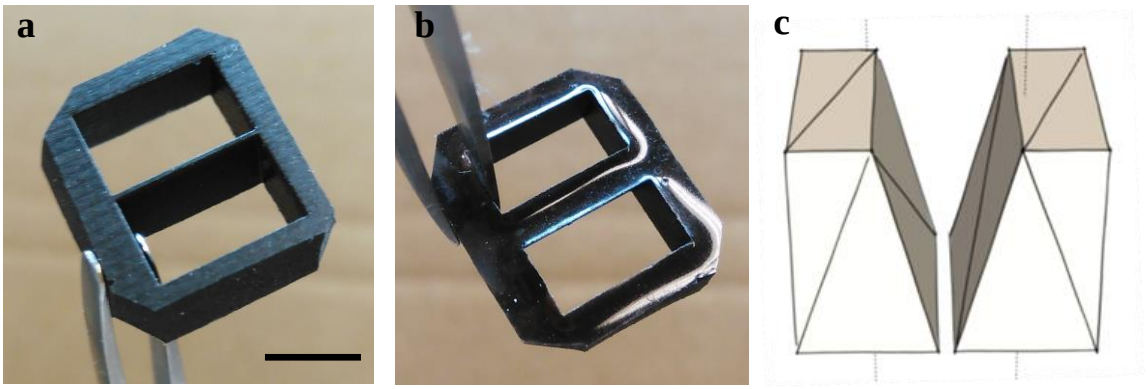

Figure 4-4| a, Bottom view of a fabricated PDMS stencil. Scale bar is 4 mm. b, Top view of a fabricated PDMS stencil. c, Detail of the shaped teeth in the master.

4.1.3 Magnetic PDMS

The created PDMS stencils could be attached to an elastic substrate that allowed interrogating traction forces. We chose PA gels to perform our experiments, as they can be tuned to provide physiological stiffnesses (Levental, 2007).

On a first approach, we passivated the PDMS stencils by a pluronic treatment and afterwards we attached them to the previously dried surface of the PA gels. Unfortunately the outcome produced frequent leakage between cell islands by the PDMS central fence.

As an alternative method, we confined cells in islands using the same design, but with magnetic PDMS instead. This technique consists on fabricating magnetically attachable stencils made of a mixture of PDMS and magnetite. A magnet underneath the sample secures the magnetic PDMS stencil on the wet polyacrylamide gel while preserving the gel protein coating (Serra-Picamal, 2015) (Figure 4-5, a-b).

With that design we managed to create long and even boundaries on PA gels (Figure 4-5, c). In order to increase the throughput of each experiment, we adapted the technique to be used with 6-well plates. The corresponding 6-well holder containing the magnets was also custom designed and 3D printed (Figure 4-6).

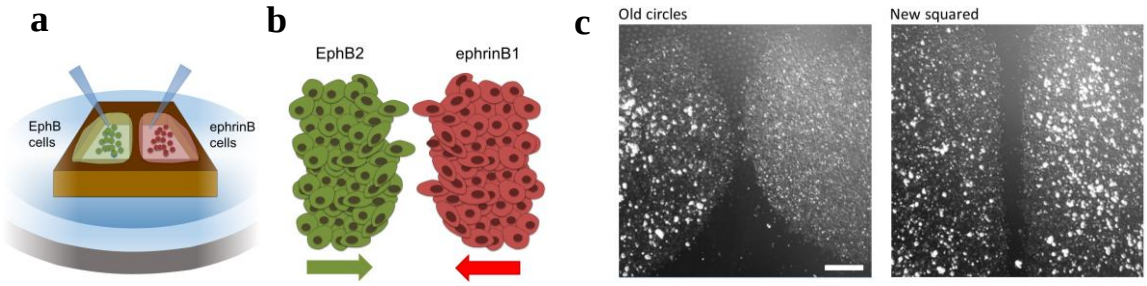

Figure 4-5| a, Principle of function of the magnetic attachment of the stencil to the PA gel. b, Top view of the cells seeded at each cavity. c, Comparison between the boundary achieved by the initial method and the 3D printing method. Scale bar is 500 µm.

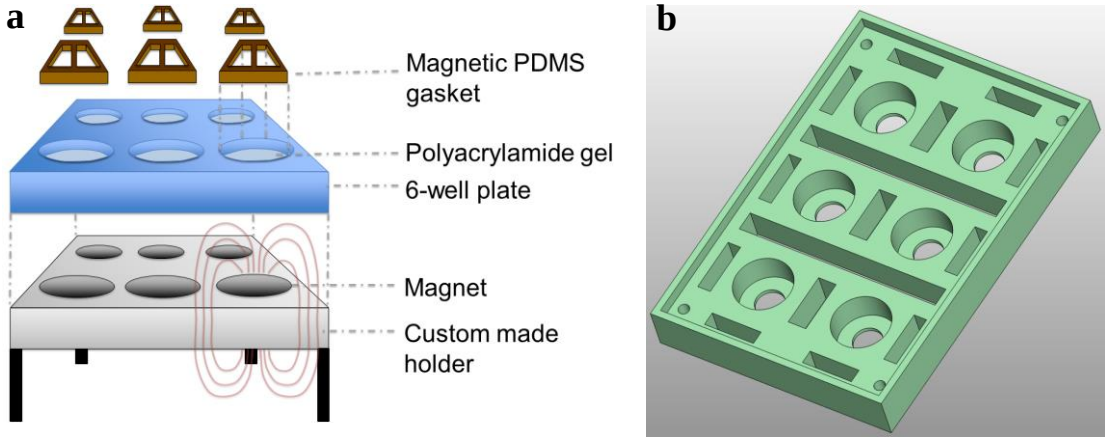

Figure 4-6| a, Scheme of the different elements of the high throughput setup. b, 3D design of the 6-well magnet holder.

4.2 Eph-ephrin repulsive boundary formation

In this section, we provide a study of the morphological changes that epithelial cells undergo during the process of Eph-ephrin boundary formation. We based our study on the novel assay introduced at the previous section.

4.2.1 Stages of boundary formation

In order to study epithelial mechanics during boundary formation, we used traction force microscopy and monolayer stress microscopy to compute the forces that cells exert on their substrate (tractions) and the forces transmitted through the cellular junctions (stresses).

To that aim, we seeded two populations of MDCK cells on PA gels using the stencils introduced in the previous section; one expressing the receptor EphB2 and the other ephrinB1, its ligand. We seeded cells for 5 hours on a collagen-I matrix. Once cells adhered to the substrate and formed a cohesive monolayer, the PDMS stencil was removed and monolayers migrated towards each other as extensively described in classical wound scratch assays (Liang, 2007) (Nnetu, 2012).

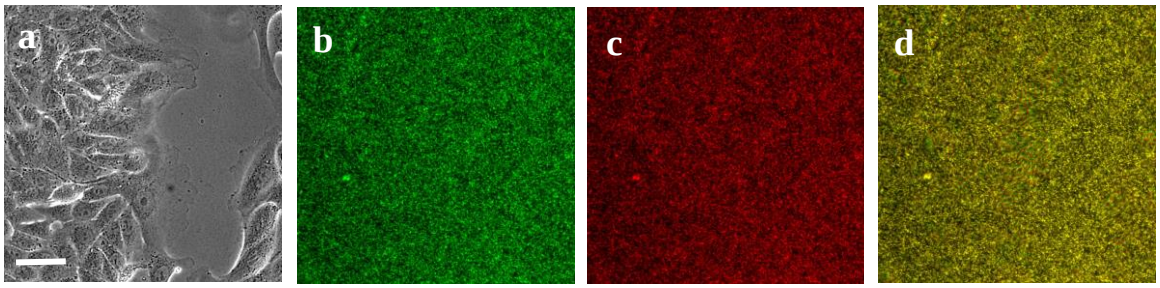

Figure 4-7| a, Phase contrast image of MDCK cells on top of a collagen-coated polyacrylamide gel. b, Beads displaced by the cells. c, Beads after cell trypsinization. d, Composite of fluorescent markers images taken with and without the cells. Yellow colour beads indicate no displacement between the two images. Scale bar is 75 µm.

During the experiment, we obtained phase contrast and fluorescent images of the cells and also fluorescence images of the microbeads in the gel for each timepoint. At the end of the experiment (15 to 20 hours), cells were trypsinized in order to obtain a reference image of the relaxed beads in the gel (Figure 4-7). In Figure 4-8 an example of the stages of boundary formation is shown. These can be described as follows:

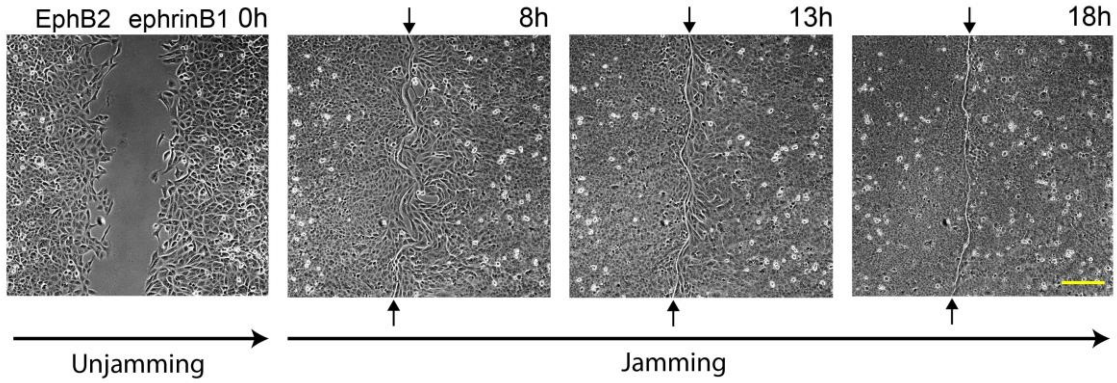

Figure 4-8| Different stages of boundary formation (after release, and after 8, 13 and 18 h of migration). Scale bar is 220 µm.

- A first stage is characterized by polarized migration of the two monolayers approaching each other. Cells at the leading edge extend large lamellipodia exerting high tractions, although these are not restricted to these cells (Trepat, 2009).
- On a second stage, cell monolayers contact each other. Fast lamellipodia extension and ruffling triggers the Eph-ephrin interaction, which promotes inhibition of cadherin clustering at the boundary, preventing formation of adhesive bonds between opposing cells.
- The third stage is the shaping of the boundary. The combination of the contact repulsion and the spatial confinement leads to the construction of actomyosin walls that prevent cell intercalation. During this stage, cells at the boundary elongate parallel to the edge.

- The fourth stage allows the boundary geometry to settle. Curvature is reduced to a certain baseline, probably related to the dimension of the cells and the strength of the repulsive interaction. Boundaries become stabilized and maintained throughout time.

The full process of boundary formation was paralleled by a pronounced increase in cell density throughout the monolayer due to proliferation and migration of cells into the boundary area. The first phase of the experiments, in which monolayers approach each other and cell density decreases, will be hereafter referred to as the unjamming phase. Conversely, the second phase, in which the boundary forms and cell density increases, will be referred to as the jamming phase (NB: This second phase is composed by stages two, three and four of the detailed description).

4.2.2 Structural features of a repulsive boundary

We stained boundaries during the buildup for their most prevalent structures, mainly actin cytoskeleton, E-cadherin adhesions and the nuclei.

Upon contact, opposing epithelia expressing Eph and ephrin failed to create cell-cell junctions. The stainings showed how E-cadherin recruitment is hindered from the boundary cells, whereas cell-cell junctions within each epithelium were built normally (Figure 4-10, a-d, i-l).

Straightening of the boundary was paralleled by the formation of a supracellular actomyosin cable at the edge of each monolayer. Immunostainings also revealed an empty micron-sized band between the two cell populations with the eventual presence of lamellipodia and filopodia that breached the boundary and extended under the opposing

edge. This behavior is unlike the collision between two populations of the same type, which fuse shortly after contact, rapidly creating a cohesive cell monolayer (Liang, 2007) (Figure 4-10, a-d, e-h, q).

The repulsive Eph-ephrin interaction depends on the direct contact between cells to be triggered (Kania & Klein, 2016). Therefore repulsion originates only at contact sites between heterotypic cells, i.e. cells lining the boundary. Interestingly, cells engaged in the first 2-3 rows behind the boundary concomitantly underwent dramatic shape changes during the boundary buildup (Figure 4-10, a-d, m-p).

In addition to the stainings, we segmented boundary cell shapes at different stages of boundary formation and quantified the changes in area, orientation and proliferation (Figure 4-9, a-d). Following the release of the PDMS stencil, cells located at the monolayer edges increased their area and oriented their body and nuclei in the direction of cell motion. Shortly after collision, these cells reversed their orientation and aligned parallel to the boundary. Eventually, oriented cell division restored an isotropic distribution of cell shape by the time the boundary settled. This phenomenon was also fully captured by the nuclei stainings, which deformed with the rest of the cell during time (Figure 4-10, a-d, m-p).

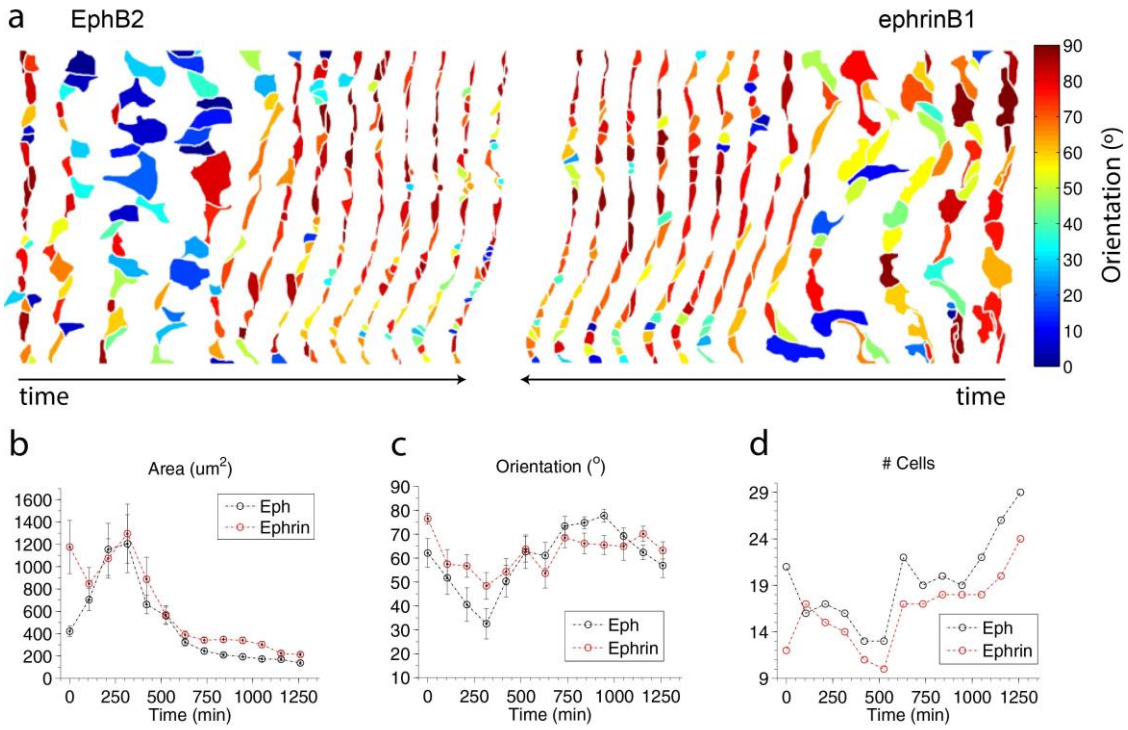

Figure 4-9| a, Time evolution of orientation for cells lining Eph and ephrin epithelia respectively. b, Average area, orientation and number of cells lining Eph and ephrin epithelia during boundary buildup.

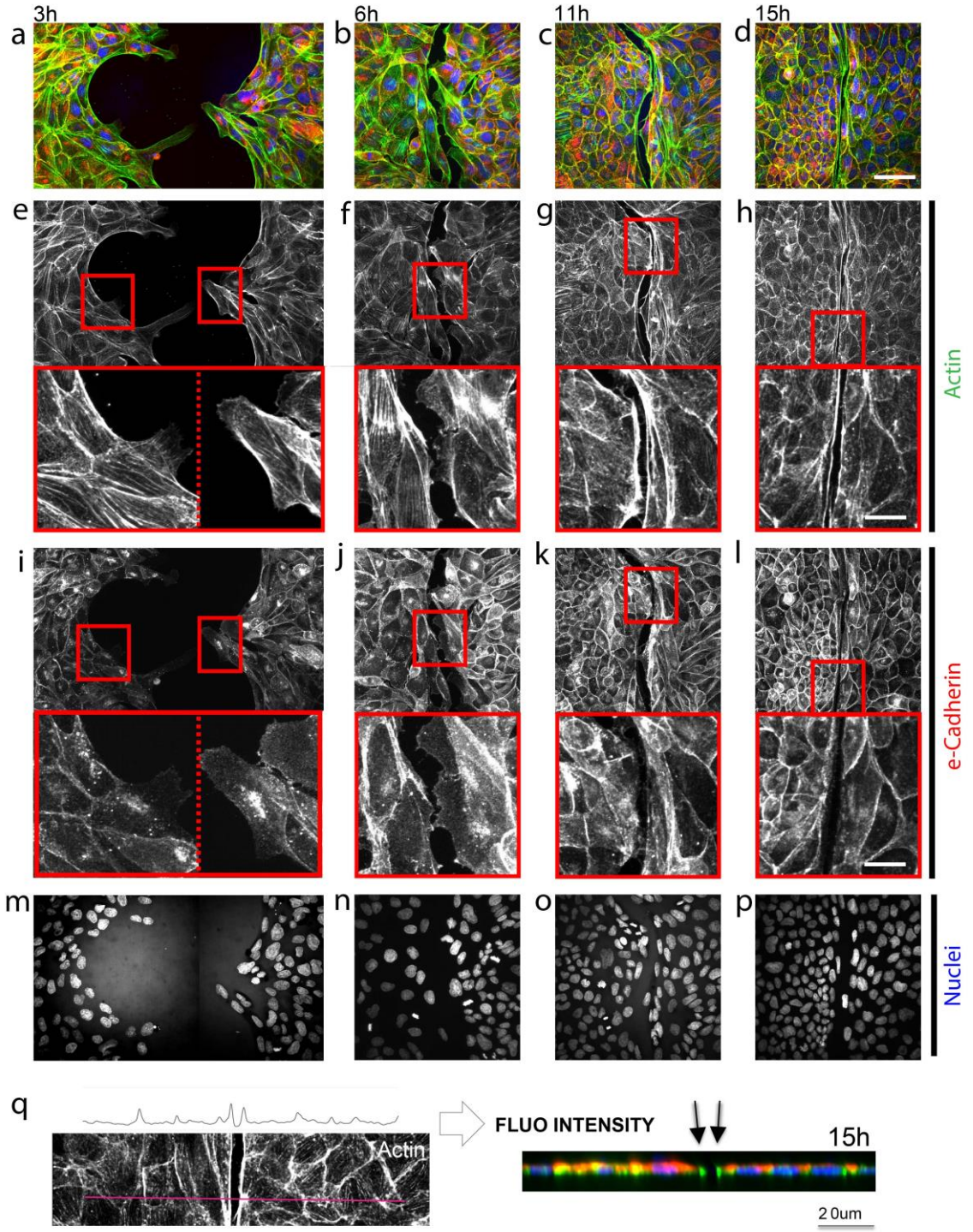

Figure 4-10| a-d, Merged staining of actin (green), E-cadherin (red) and Nuclei (blue) at specified times of boundary formation. Images are maximum projections of spinning disk z-stacks (Scale bar is 55 µm). e-p, Staining of actin (e-h), E-cadherin (i-l) and nuclei (m-p) during boundary formation. Images are maximum projections of spinning disk z-stacks. Zoom scale bar is 18 µm. q, Transversal view of a spinning disk z-stack of a stable boundary (15h after PDMS gasket release).

4.3 Epithelial mechanics during Eph-ephrin boundary buildup

In this section, we provide a study of the cell-matrix tractions, inter- and intra-cellular stresses, velocities and strain rates that epithelial cells undergo or withstand during the process of Eph-ephrin boundary formation. We based our study on the novel assay introduced in the previous section. Our assay allows combining the formation of boundaries with traction force microscopy measurements and bright field/fluorescence imaging of the boundary buildup.

4.3.1 Epithelial forces during Eph-ephrin boundary buildup

To study mechanics of boundary formation, we used traction force microscopy and measured forces at the cell-substrate interface (appendix 7.5).

Throughout the experiments, traction maps exhibited large dynamic fluctuations both at the monolayer edges and behind them (Figure 4-11, a-h). To distinguish fluctuations from systematic traction patterns, we averaged the component normal to the boundary ($T_{\perp}$) over the *y* coordinate, thereby reducing the dimensionality of the system to only one spatial dimension and one temporal dimension. Data were then represented as kymographs (Serra-Picamal, 2012) (Figure 4-11, m). During the unjamming phase, kymographs of $T_{\perp}$ displayed well-known features of monolayer expansion such as a decay of average tractions away from the leading edges (Trepat, 2009). By contrast, during the jamming phase kymographs revealed mechanical patterning characterized by long-lived spatial oscillations of traction forces (Figure 4-11, m). These spatial oscillations did not attenuate or propagate in time.

The autocorrelation function $C_{TT\perp}$ of the traction kymographs during the jamming phase revealed a characteristic spatial period of 52±9 μm, corresponding to ~4 cell diameters (Figure 4-11, o). Traction oscillations were predominantly positive in the EphB2 monolayer, and predominantly negative in the ephrinB1 monolayer. Thus, several rows of cells were found to pull on cell-substrate adhesions away from the boundary, and did so using remarkable oscillatory patterns.

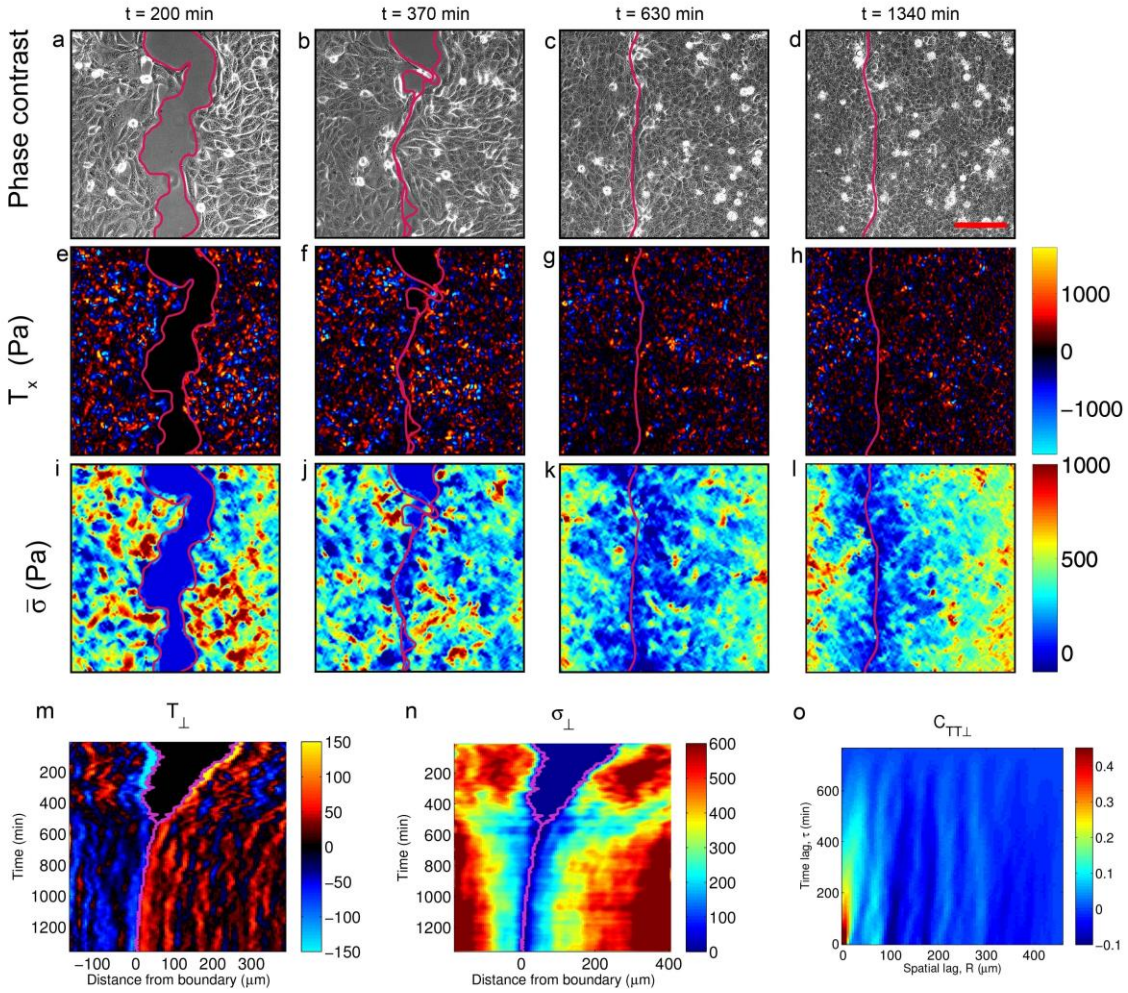

Figure 4-11| a–l, Phase-contrast images (a–d), horizontal traction component T_x (e–h) and average normal stress $\bar{\sigma}$ (i–l) at different times after removing the PDMS stencil. Scale bar, 150 μm. m-n, Kymographs of traction $T_\perp$ (m) and monolayer stress component $\sigma_\perp$ (n). The pink line indicates the average boundary position. o, autocorrelation function $C_{TT\perp}$ of traction kymograph after collision.

4.3.2 Epithelial stresses during Eph-ephrin boundary formation

To assess how these mechanical patterns affected tension within and between cells we computed the 2D stress tensor in the monolayer using monolayer stress microscopy (MSM) (Tambe, 2011), and focused on the projection along the direction normal to the boundary ($\sigma_{\perp}$). To that aim, we imposed mechanical decoupling between the two epithelia. Then we imposed force balance on each epithelium by mirroring each respectively and calculating the stresses for each epithelium with its mirror image (Figure 4-11, a-d; i-l).

In a pseudo-unidimensional cohesive monolayer, $\sigma_{\perp}$ can be approximated by a spatial integral of the traction component $T_{\perp}$ (Trepat, 2009). As such, with each cycle of $T_{\perp}$, $\sigma_{\perp}$ was expected to build up away from the boundary. This was indeed seen to be the case in maps and kymographs of $\sigma_{\perp}$, which showed a systematic increase of monolayer tension with the distance from the boundary (Figure 4-11, n). Together, our force measurements establish that the formation of EphB-ephrinB barriers involves not only local repulsive events at the boundary, but also the mechanical cooperation of many cells located behind it. These rows of cells withstand supracellular mechanical patterns that tend to pull the monolayer away from the boundary.

We quantified σ_{xx} and σ_{yy} for cells lining both sides of the boundary (Figure 4-12). σ_{yy} was gradually released, together with the increase of oriented cell divisions in that direction (Figure 4-12, top) (Figure 4-13, right) (Figure 4-14, a-e). Reversely, σ_{xx} was largely decreased right after both epithelia collided (Figure 4-12, bottom) (Figure 4-13, left). This stress must be transmitted to the neighboring cells and propagated through time. Not

surprisingly, many divisions within each epithelia in the field of view were perpendicularly oriented to the boundary (Figure 4-14, a-e).

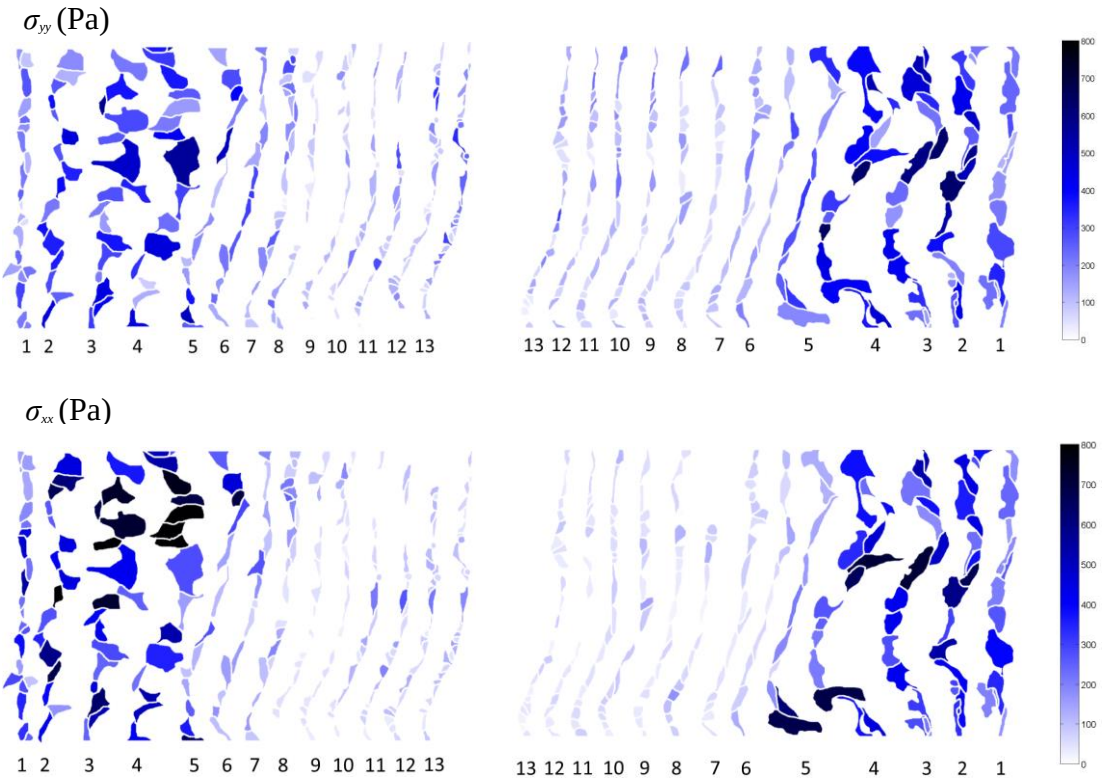

Figure 4-12| σ_{yy} and σ_{xx} time evolution for cells lining both Eph and ephrin epithelia respectively. 105 min between timepoints.

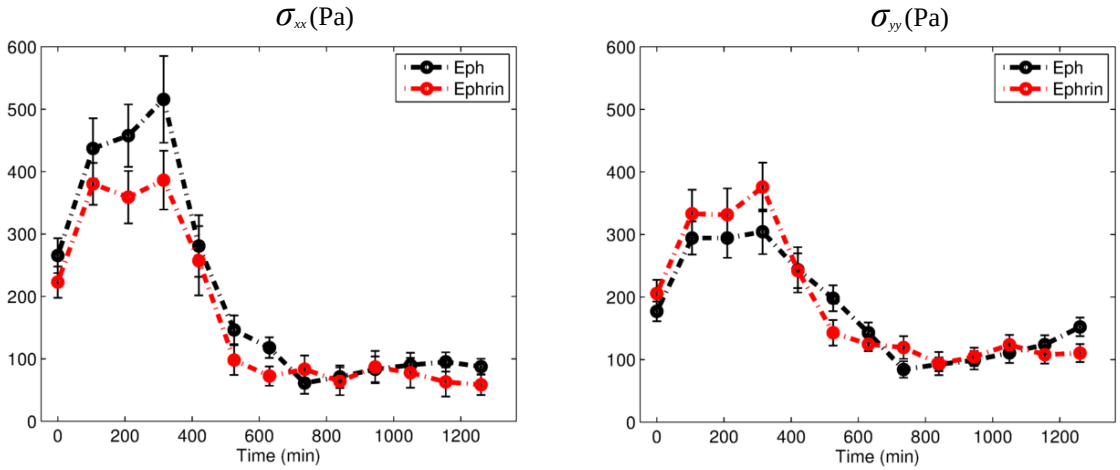

Figure 4-13| Average σ_{yy} and σ_{xx} during boundary buildup for cells lining both epithelia.

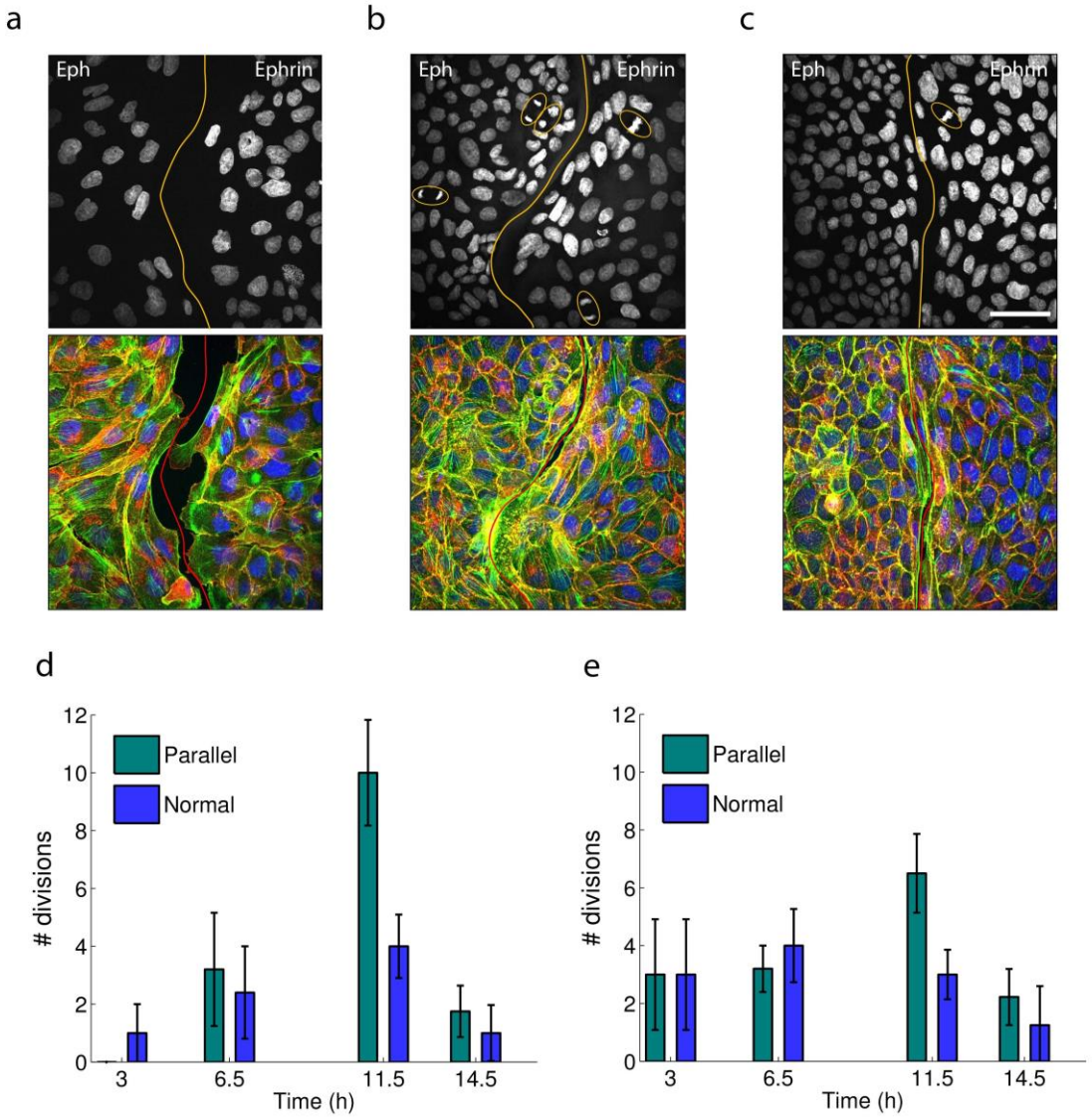

Figure 4-14| a-c, Immunostainings of cell nuclei (top) and merged phalloidin (green), E-cadherin (red) and nuclei (blue) (bottom) at three different time points of boundary formation (6.5h (a), 11.5h (b) and 14.5h (c)). Scale bar is 45 µm. d-e, Total number of divisions in stainings for the Eph (d) and ephrin (e) sides of the monolayer. Divisions were distinguished among parallel (0±10º) or normal (90±10º) to the boundary. During maturation of the boundary (t=11.5h), divisions parallel to the boundary were dominant.

4.3.3 Epithelial velocities during Eph-ephrin boundary formation

We measured cell velocities (V) using particle imaging velocimetry (PIV). Maps of the normal velocity component $V_{\perp}$ revealed a phase of fast cohesive motion during unjamming, followed by a progressive slowing down of monolayer kinematics during jamming (Figure 4-15, a-d; e-h)

(appendix 7.5). Strikingly, the monolayer did not show a full kinetic arrest as had been reported in monolayers of growing density (Angelini, 2011). Instead, soliton-like waves emerged at the monolayer boundary and propagated across the ephrin monolayer. These waves can be clearly discriminated after thresholding velocity maps to separate rapid propagating cells and slow non-propagating cells (Figure 4-15, i-k).

To study these soliton-like waves we computed kymographs of $V_{\perp}$ (Figure 4-15, l). These kymographs showed an unremarkable initial phase of cohesive approach of the two monolayers (~500 min). After monolayer collision, however, kymographs displayed pronounced diagonal bands in the ephrin monolayers, which reveal wave fronts that form at the boundary and propagate until the limits of the field of view without significant attenuation. The kymograph of normal velocities reveals that for some cases the deformation wave propagates through the boundary, despite the lack of mechanical connection between epithelia.

Because of the continuous nature of monolayers, front propagation in the velocity field is indicative of a deformation wave. This was confirmed by kymographs of the strain rate, which showed propagating fronts of cell compression and extension (Figure 4-15, m).

To better characterize deformation waves we computed the autocorrelation function $Cvv_{\perp}$ of the monolayer velocity kymographs $V_{\perp}$ (Figure 4-15, n). $Cvv_{\perp}$ displayed a diagonal band originating at $\tau = 0$ min and $R = 0$ μm and spanning a time interval longer than 100 min and a distance longer than 200 μm. This diagonal band demonstrates the propagation of a deformation wave with a speed corresponding to the inverse of the slope (117±16 μm/h). Besides this dominant band in the correlation function, several parallel secondary bands of similar slope were observed, indicating multiple propagation events of similar velocity.

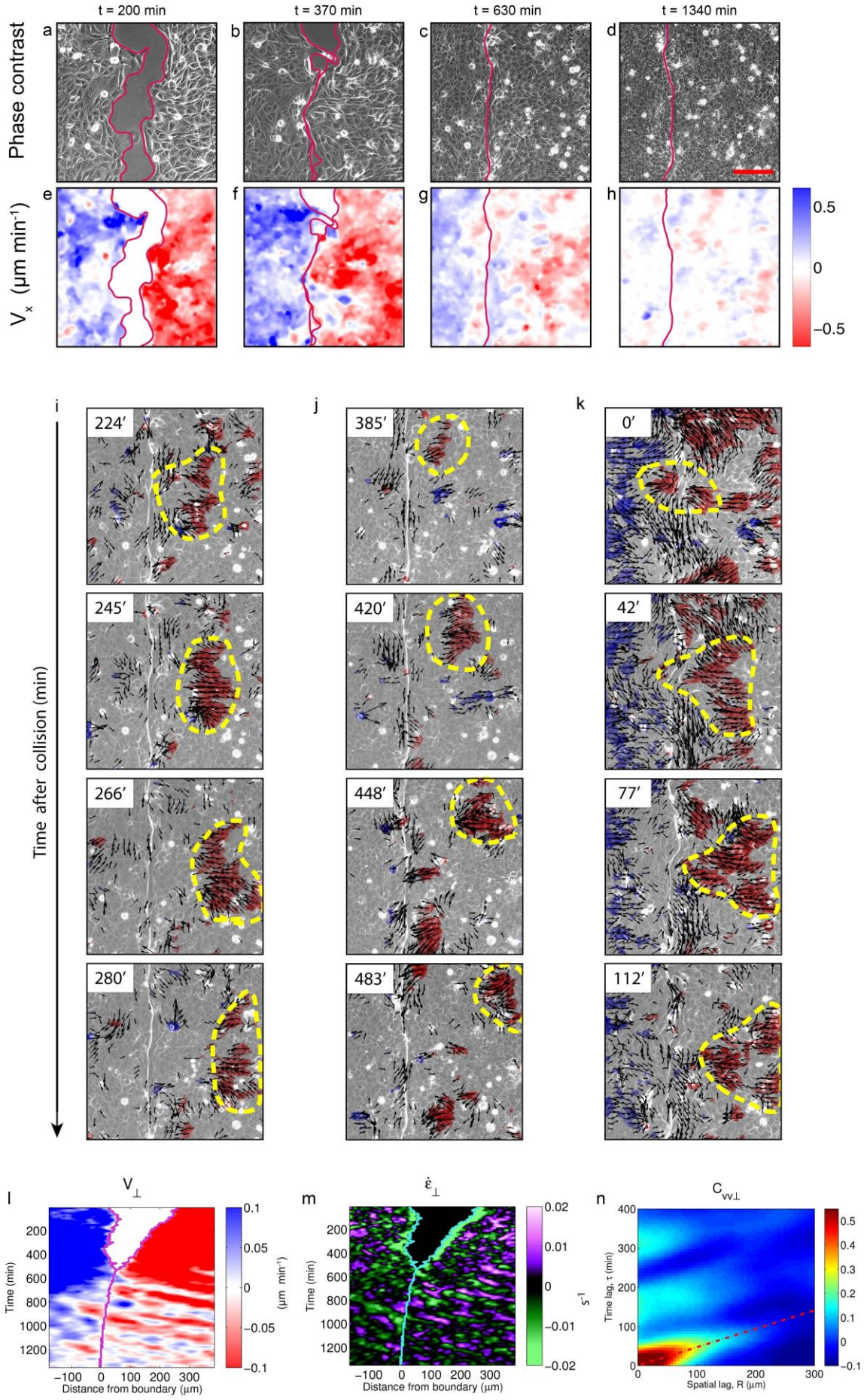
t = 200 min
t = 370 min
t = 630 min
t = 1340 min
Phase contrast
V_x (μm min^{-1})
0.5
0
−0.5
Time after collision (min)
224′
245′
266′
280′
385′
420′
448′
483′
0′
42′
77′
112′
$V_\perp$
$\dot{\varepsilon}_\perp$
$C_{vv\perp}$
Time (min)
Distance from boundary (μm)
Time lag, τ (min)
Spatial lag, R (μm)
(μm min^{-1})
s^{-1}

Figure 4-15| a-h, Phase-contrast images (a–d) and velocity V_x maps (e–h) at different time points after removing the PDMS stencil. Scale bar, 150 μm. i-k, Threshold velocity fields superimposed on phase contrast images for three examples of propagating waves. Dashed yellow lines highlight the propagating pulse. l-m, Kymographs of velocity $V_\perp$ (l) and strain rate $\dot{\varepsilon}_\perp$ (m) during EphB2-ephrinB1 boundary formation. The pink line indicates the boundary position. n, Autocorrelation function $C_{VV_\perp}$ of velocity kymographs for control cells during the jamming phase. Average time between waves was 161±12 min. Average propagation velocity was 117±16 μm/h.

4.4 Exploring the mechanisms of boundary formation and maintenance

Most certainly, collective phenomena observed during Eph-ephrin formation must be paralleled by a sequence of mechanisms acting in tight coordination. We hypothesized that one such mechanism could be cell jamming induced by increased cell density. To test this hypothesis, we carried out boundary formation experiments using cells in which proliferation had been inhibited with thymidine.

We also decided to evaluate the impact that impairing cell-cell contact formation or contractility would have on boundary formation. To do so, we submitted boundaries to different chemical treatments, i.e. EGTA and blebbistatin.

For the sake of clarity, the usual Eph-ephrin repulsive boundary formation will be referred as control case from now on.

4.4.1 Cell proliferation and jamming in boundary buildup

The long-lived nature of traction oscillations after boundary formation prompted us to seek for a mechanism that arrests monolayer dynamics. We hypothesized that one such mechanism could be cell jamming induced by increased cell density (Angelini, 2011; Nnetu, 2012; Pawlizak, 2015; Tambe, 2015; Park, 2015; Garcia, 2015). To test this hypothesis, we carried out boundary formation experiments using cells in which proliferation had been inhibited with thymidine. Like control experiments, non-proliferative monolayers approached each other and formed a stable boundary. Cells did not achieve a high level of compaction at the end of the experiment, which led to high levels of neighbors exchange well after the epithelial contact. Traction kymographs showed oscillatory patterns with a similar period to

controls (51±7 µm, Figure 4-16, a,e,f). However, these patterns were more dynamic and did not become fully arrested with time (Figure 4-16, a). Importantly, compared to control experiments, traction oscillations did not show an offset of opposite sign on each side of the boundary (Figure 4-16, a,c). As such, they had a reduced ability to increase $\sigma_{\perp}$ with distance from the boundary (Figure 4-16, b,d). These experiments support that cell jamming stabilizes supracellular force patterns during Eph-ephrin boundary formation.

To test whether jamming was required for deformation wave propagation we analyzed kymographs of non-proliferative cell monolayers. Kymographs of $V_{\perp}$ showed that propagating fronts were less abundant and less pronounced than in controls (Figure 4-17, a-d, e-h, q), as indicated by a broader diagonal band in $C_{vv\perp}$ (Figure 4-17, r). Jamming thus appears to favor wave propagation. A closer look at the cellular dynamics within each epithelium revealed that clusters of high velocity are larger. Furthermore, high velocity clusters are less evident, given that most cells show a higher level of motility after the collision (Figure 4-17, a-d, e-h).

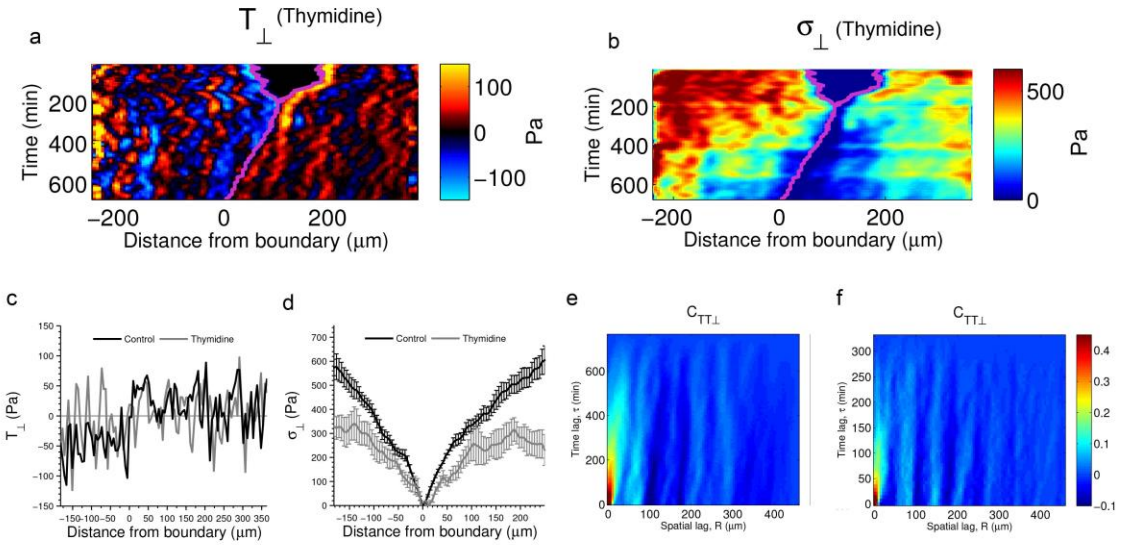

Figure 4-16| a-b, Kymographs of traction $T_{\perp}$ (a) and monolayer stress component $\sigma_{\perp}$ (b) during the formation of an EphB2-ephrinB1 boundary in cells treated with thymidine to inhibit proliferation. The pink line indicates the position of the boundary. c-d, Profile of $T_{\perp}$ (c) and $\langle\sigma_{\perp}\rangle$ (d) 420 minutes after

epithelial collision for untreated monolayers and thymidine treated monolayers. e-f, Autocorrelation function $C_{TT\perp}$ of traction kymographs after collision for untreated cells (e) and thymidine treated cells (f).

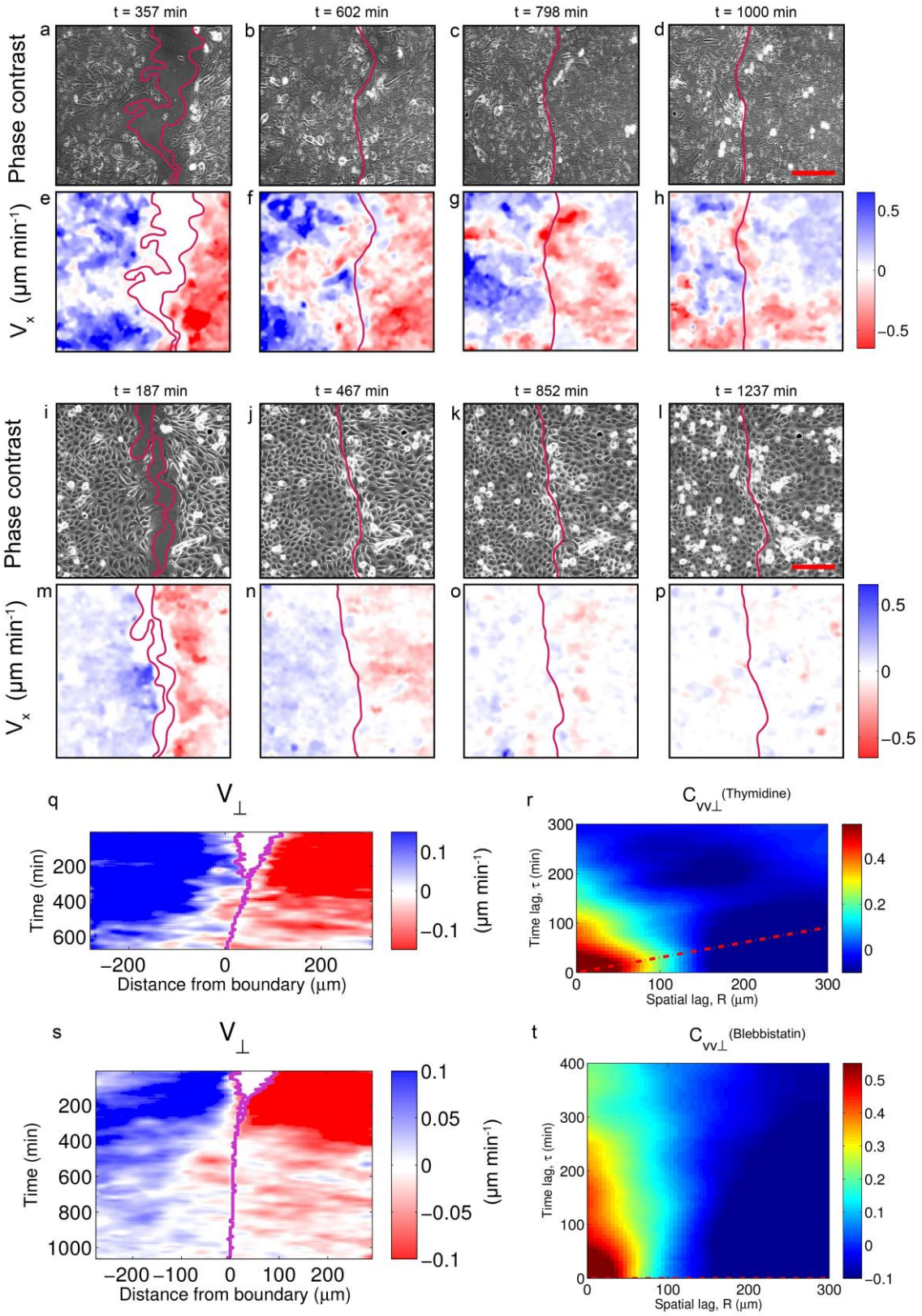

Figure 4-17| a–h, Phase-contrast images (a–d) and velocity V_x (e–h) at different time points after removing the PDMS stencil in cells treated with thymidine to inhibit proliferation. Scale bar, 150 µm. i–p, Phase-contrast images (i–l) and velocity V_x (m–p) at different time points after removing the PDMS stencil in cells treated with blebbistatin to inhibit contractility. Scale bar, 150 µm. q, Kymograph of velocity $V_\perp$ for cells treated with thymidine. r, Autocorrelation function $C_{VV\perp}$ of velocity kymographs for cells treated with thymidine. s, Kymograph of velocity $V_\perp$ for cells treated with blebbistatin. t, Autocorrelation function $C_{VV\perp}$ of velocity kymographs for cells treated with blebbistatin.

4.4.2 Perturbing contractility during repulsive boundary formation

Inhibition of monolayer tension with blebbistatin has also been linked to monolayer jamming through a density independent rigidity transition (Bi, 2015) (Park, 2015). To further study the mechanism underlying deformation propagation, we inhibited myosin activity using blebbistatin (Figure 4-17, i-l, m-p). This treatment largely inhibited traction forces and the formation of actomyosin cables at the boundary, but it did not prevent tissue segregation (Figure 4-18, a-c). Deformation waves were largely absent from kymographs, indicating that their propagation requires monolayer tension (Figure 4-17, s,t).

Furthermore, cells under blebbistatin treatment were unable to properly restructure their cytoskeleton in order to achieve higher levels of jamming. In a control experiment, cells would undergo an average 4-fold compaction in the XY plane, which implies a high level of reorganization in the Z plane. Reversely, for the blebbistatin treated boundaries, cells held an average area of 0.8 times the original area. This went along with the extrusion of approximately 80% of the cell divisions going on in the field of view (appendix 7.8).

Local contractility has also been reported to play a major role in preventing population intermingling in vivo (Calzolari, 2014). Remarkably though, impairing the complete formation of actomyosin cables along the boundary

in our in vitro system did not impair the buildup of stable compartments (Figure 4-18, a-f). These phenomena are fully captured by the stainings of the actin cytoskeleton and the cadherins. Phospho-myosin stainings show a loose distribution about the boundary (Figure 4-18, d-f). This is consistent with the fact that boundaries are unable to correct the original curvature of the epithelial contact under blebbistatin treatment (appendix 7.9).

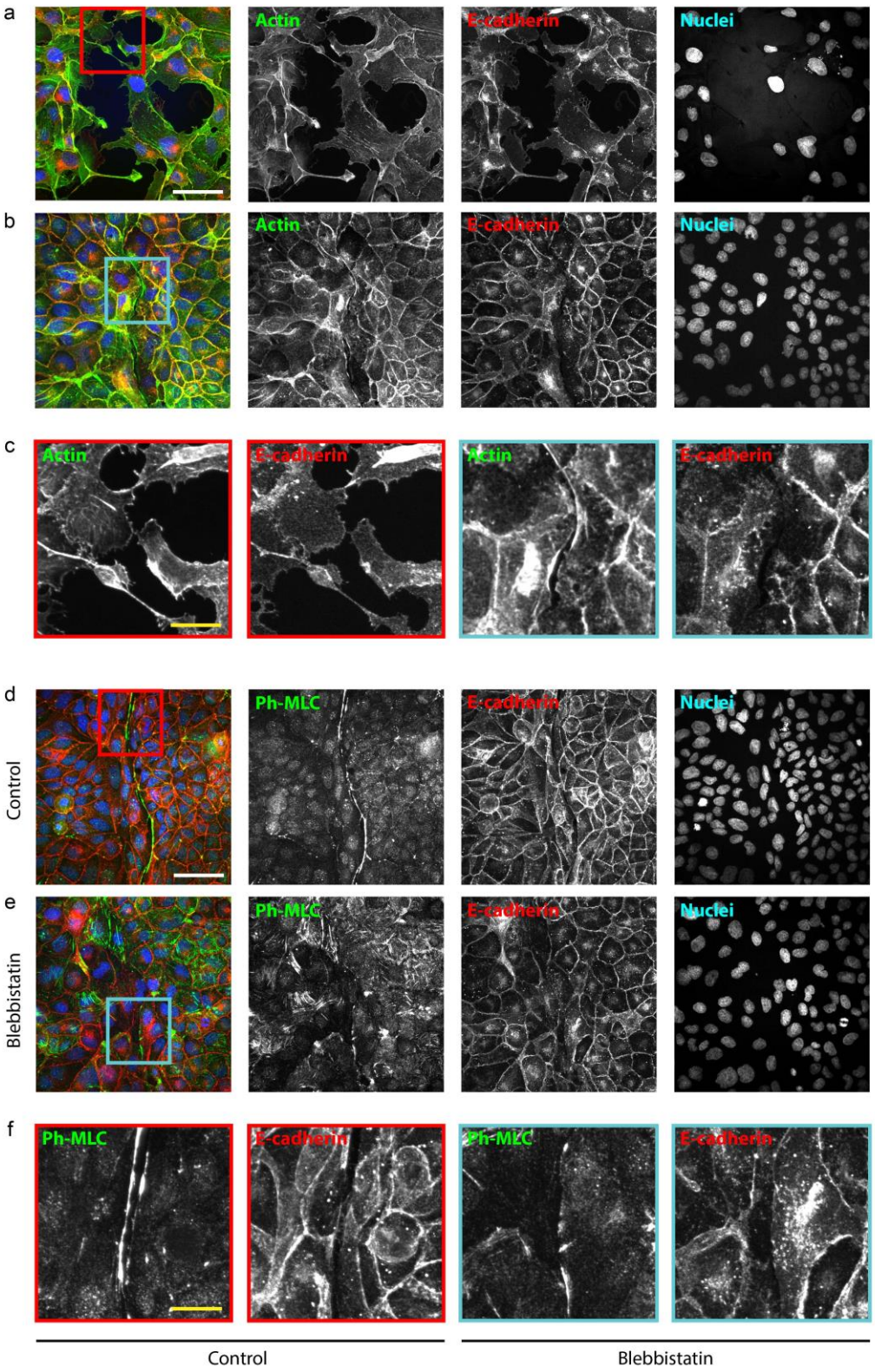

Figure 4-18| a-b, Stainings of phalloidin (green), E-cadherin (red) and nuclei (blue) at 6.5 h (a) and 15 h (b) after PDMS stencil release in blebbistatin treated cells. Images are maximum projections of spinning disk z-stacks. Scale bar is 55 µm. c, Phalloidin and E-cadherin close-ups corresponding to the regions marked in a and b. Scale bar is 20 µm. d-e, Stainings of phospho-MLC (green), E-cadherin (red) and nuclei (blue) 15 h after PDMS stencil release for a control boundary (d) and a boundary under blebbistatin treatment (e). Images are maximum projections of spinning disk z-stacks. Scale bar is 55 µm. f, Phospho-MLC and E-cadherin close-ups of stainings shown in panels d and e. Scale bar is 20 µm.

4.4.3 Cell-cell adherens junctions in segregation

Several biochemical pathways have been uncovered which link Eph–ephrin interactions to a decrease in cadherin-mediated cell adhesion (Cayuso, 2015). Consistent with this, knockdown of E-cadherin decreases Eph–ephrin mediated cell segregation (Cortina, 2007). Furthermore, since the generation of tension in a tissue requires adhesive interactions (Maître, 2012), this may explain the need for cell adhesion in Eph–ephrin mediated cell segregation.

To investigate the role of cadherins in our in vitro assay, we submitted a stable boundary to an EGTA treatment (Figure 4-19, a,b). After 300 minutes, cell-cell junctions were completely disrupted and the boundary was disassembled (Figure 4-19, a,b). After 18 hours, we restored the system with fresh culture medium. In 100 minutes, the boundary was reconstituted (Figure 4-19, a,b). This observation suggests that cadherin-cadherin disruption at the Eph-ephrin contact sites is tightly coupled to the reorganization of the cytoskeleton along the boundary and within epithelia.

We computed the kymographs of $T_{\perp}$ and $V_{\perp}$ for the full process and could observe that $T_{\perp}$ remained unchanged during the EGTA treatment (Figure 4-19, c,e). Concomitantly, velocities were very low and did not show any pattern or soliton-like wave compared with the usual pattern for a control experiment (Figure 4-19, d,f).

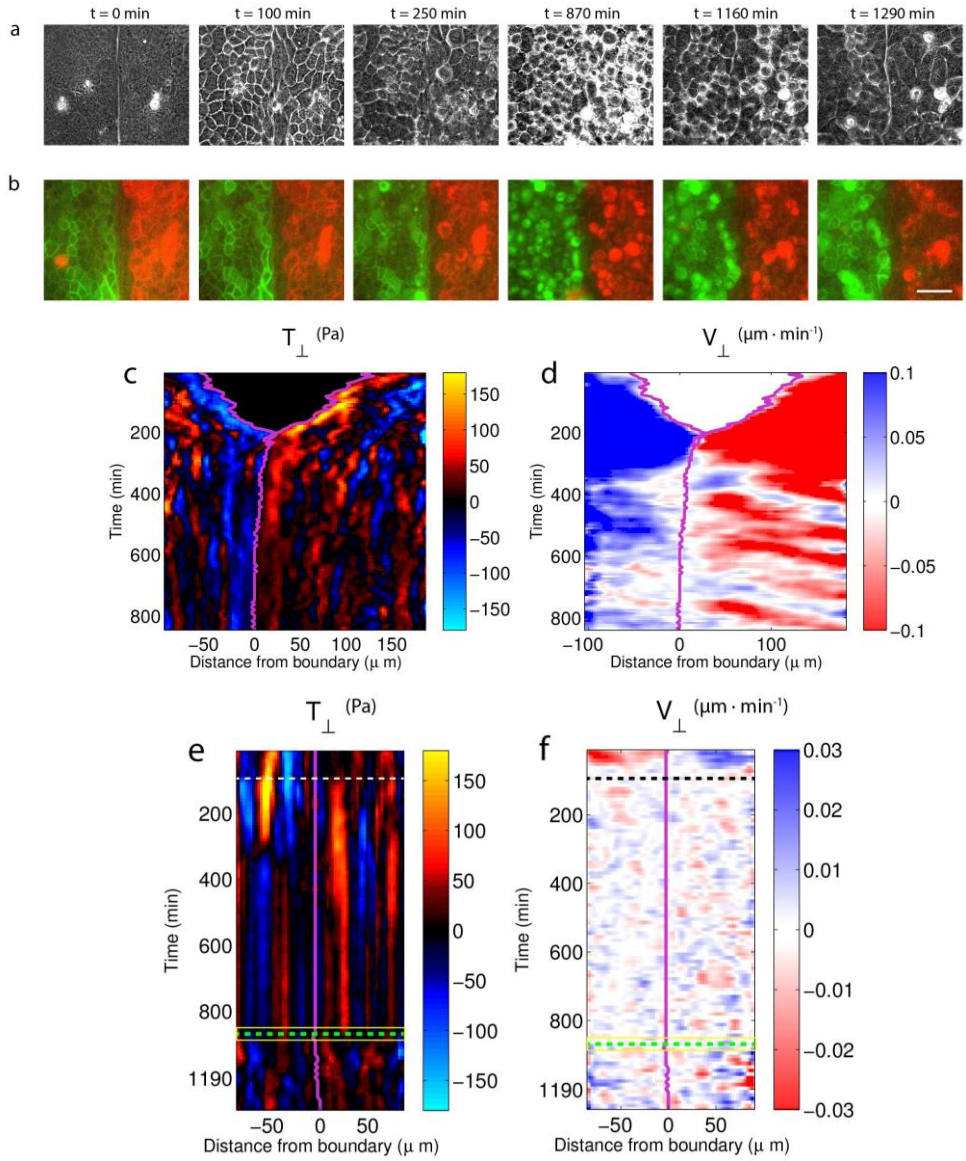

Figure 4-19| a, evolution of stable boundary (24 hours after gasket release) treated with EGTA (t = 100 min) and rescued with normal media (t = 1060 min). b, corresponding fluorescence images of E-cadherin (GFP for Eph cells, RFP for ephrin cells). Bar is 45 μm. c-d, $T_{\perp}$ and $V_{\perp}$ kymographs of control experiment with 40x magnification. e-f, corresponding kymographs of $T_{\perp}$ and $V_{\perp}$ for EGTA treatment. White/black line indicates EGTA treatment application. Green line indicates washing with fresh media. Data from 870 min to 1060 was not taken (prior to EGTA wash up). Yellow box accounts for this discontinuity.

4.5 Boundary formation at high spatial and temporal resolution

Many of the signalling pathways that are downstream of Ephs and ephrins converge to regulate the cytoskeleton. Concomitantly, we took a closer look at the boundary cells by performing high magnification (40x) and high temporal resolution (from 1 to 5 minutes) experiments to be able to capture the fast dynamics of the repulsive phenomenon. In addition, we transfected Eph and Ephrin cell lines with blue (CFP) and red (RFP) lifeact respectively to be able to observe the structural dynamics at each side of the boundary.

One prevalent observation was the cycles of contact-repulsion (Figure 4-20). Eph receptors were locally activated wherever neighbouring ephrin-expressing cells made contact. This triggered dynamic membrane ruffling at the Eph–ephrin contact sites. The contact between Eph-expressing and ephrin-expressing cells was destabilized and, subsequently, the receptor and ligand cells retracted from one another.

Another relevant observation was made during the formation of supracellular actin structures along the boundary (Figure 4-21, c). As both epithelia approached, the cycles of contact of Eph-ephrin happened more often, leading to a higher inhibition of lamellipodia protrusion at the free edge of cells engaged in the boundary. This in turn promoted the stabilization of these edges by fencing the available actin in bundles. Given that all cells at the boundary were exposed to the same repulsive cycles and provided that homotypic cells were mechanically connected through adherens junctions, these actin bundles ended up connecting all cells lining the boundary to create a supra-cellular stabilizing structure. As a consequence, the extension of lamellipodia was diminished, although small ruffling lamellipodia could be observed even after the boundary was created and stabilized (Figure 4-21, a-b).

4.5.1 Boundary displacement in time

During the Eph-ephrin experiments it was observed that the boundary position evolved towards the Eph epithelium (Figure 4-22), suggesting that the ephrin epithelium held a more invasive phenotype. Receptor and ligand could be playing a different role on each side of the boundary, given that the Eph-ephrin interaction is not only a bi-directional signalling pathway, but also an asymmetrical one (Pasquale, 2008; Cowan & Henkemeyer, 2002).

Mainly, Eph cells were prone to retract upon ephrin cell contact and to build strong cell-cell homotypic junctions. Indeed, it was already observed in appendix 7.8 that Eph-expressing cells reach a higher level of packing with respect to ephrin cells. On the other hand, ephrin cells had a looser behavior. They tended to maintain their polarization, and to invade the Eph epithelium.

We wondered if this differential reorganization and compaction was paralleled by any 3D effect, under the assumption that cell volume must be preserved over time. For that, we developed an assay on glass to avoid the poroelastic effects of PA gels (Casares, 2015). In agreement with the previous observation, the strong Eph epithelium compaction in XY was paralleled by an expansion in Z (Figure 4-23). 19 hours after stencil release, the focal plane of the Eph epithelium was 7.7 μm higher that the ephrin focal plane.

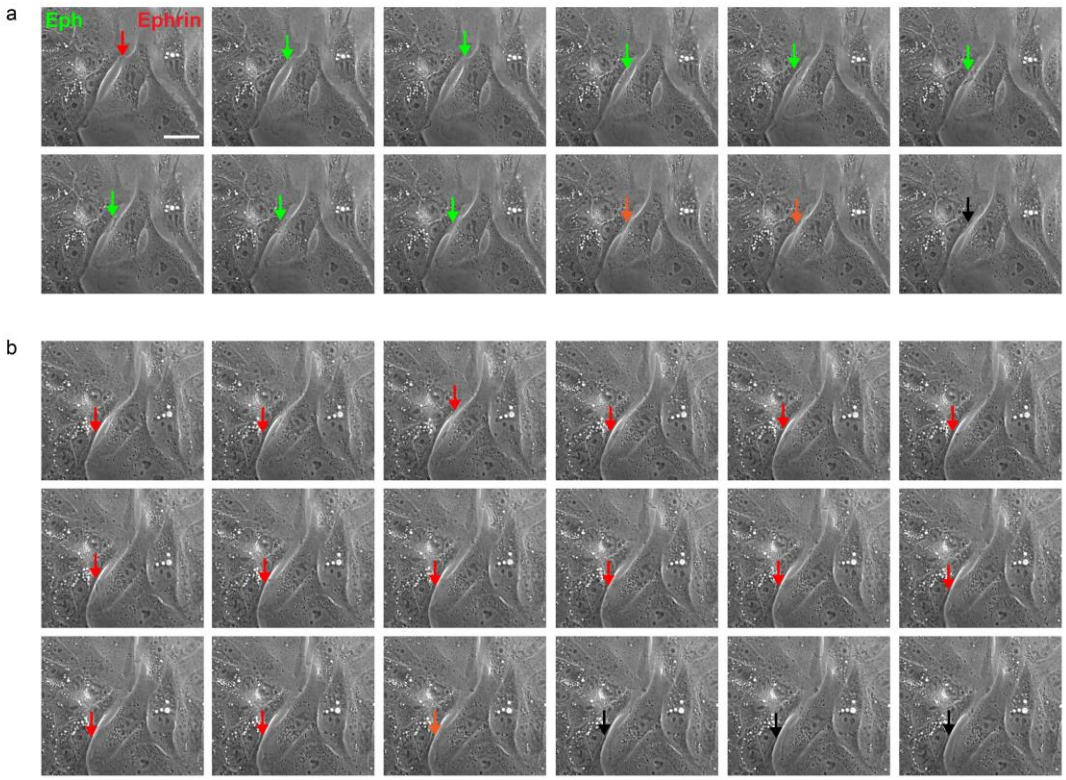

Figure 4-20| a, Evolution of an extending lamellipodia. Red arrow stands for Eph-cell extension; green arrow stands for ephrin-cell extension. Orange arrow stands for destabilization of contact. Black arrow stands for cellular retraction. b, another example of ruffling lamellipodia. Colorcode of arrows is maintained. Images were acquired at 1 frame/min. Bar is 42 µm.

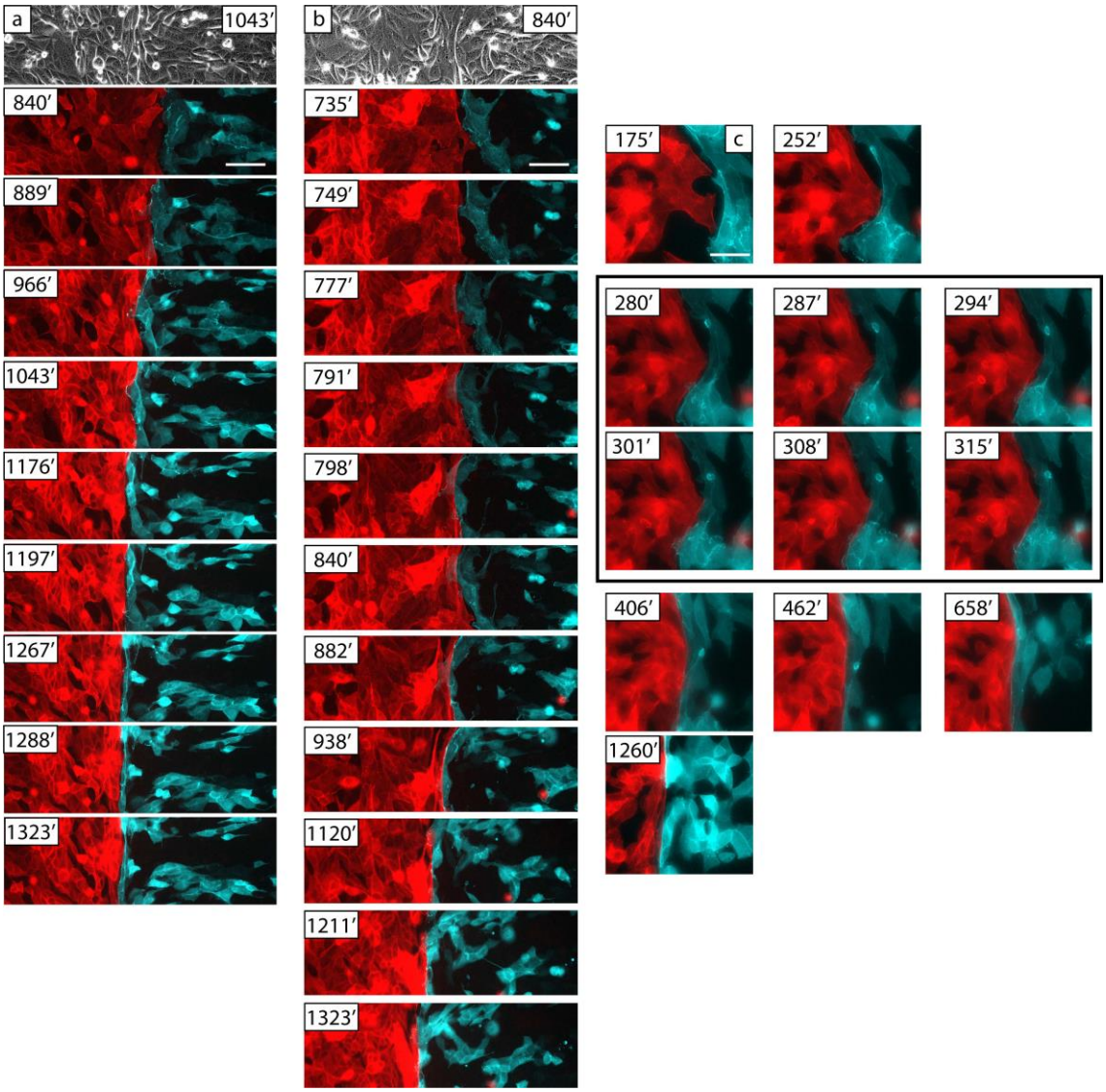

Figure 4-21| a-b, Sequences of lamellipodia extension well after the boundary is completely built up. Eph cells carry a RFP-lifeact construct. Ephrin cells carry a CFP-lifeact construct. Scale bar is 100 µm. c, Detail of a lamellipodia extension cycle followed by an actin bundle recruitment afterwards during boundary buildup. Scale bar is 34 µm.

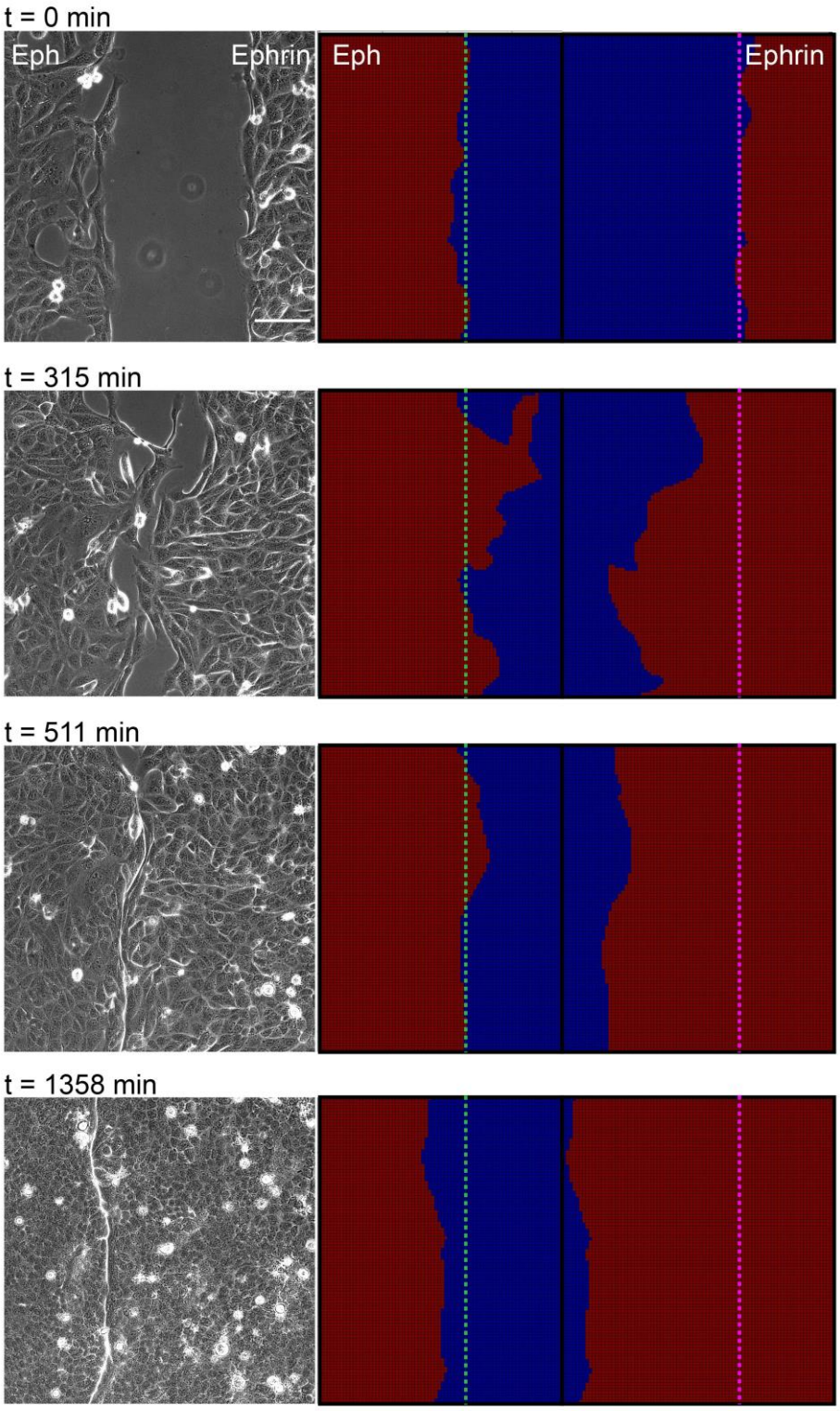

Figure 4-22| Masks corresponding to the migrating epithelia during boundary buildup. Scale bar is 150 µm.

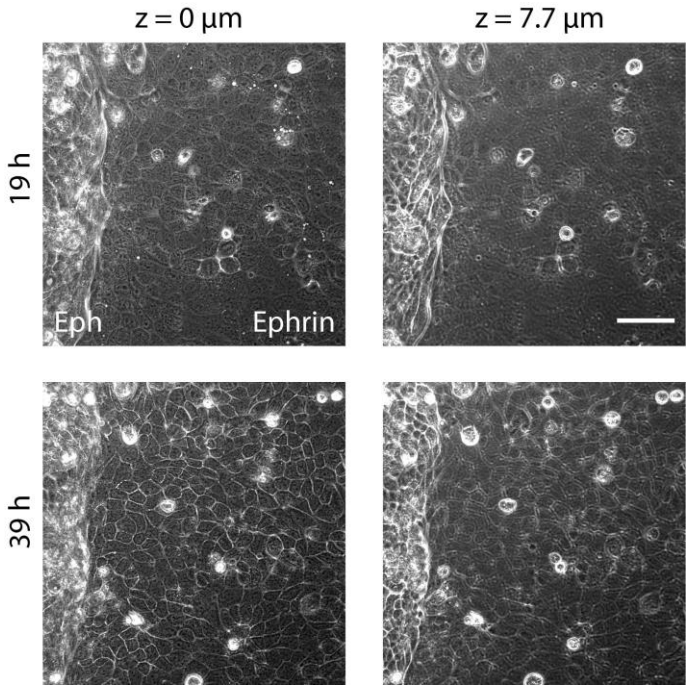

Figure 4-23| Boundary buildup on glass depicting the differential 3-dimensional behavior of Eph-expressing and ephrin-expressing populations. Bar is 72 µm.

4.6 Comparing Eph-ephrin boundaries to other boundary-like mechanisms of segregation

Aside from the Eph-ephrin boundary formation, there are other contexts in which cells migrate against a border. Consequently, we wondered if deformation waves were specific to the Eph-ephrin interaction, or whether they were a general feature of epithelial interfaces instead. To that end, we compared the formation of epithelial boundaries driven by Eph-ephrin repulsive interactions with those driven by volume exclusion against an obstacle. We also compared the repulsive boundary situation to the attractive boundary formation, which consisted of two homotypic epithelia colliding (wound healing). For the sake of clarity, we begin by summarizing the characteristic features of the control case: boundary formation driven by Eph-ephrin repulsion.

4.6.1 Summary of characteristic features for the repulsive boundary formation

We could summarize the most remarkable traits observed during the Eph-ephrin repulsive boundary formation (control) as follows:

- Elongation of cells and acto-myosin contraction of cables at the boundary.

Supracellular cable formation was always observed, with the exception of the blebbistatin treated cells and the EGTA treated cells. EGTA treated cells could not build cell-cell junctions, which led to the disruption of the

actomyosin cable, which is a downstream effect of the cell-cell contact repulsion between Eph and ephrin expressing cells.

- Fluidization of cells engaged in the repulsive interaction.

Cells lining the boundary were highly motile in the direction parallel to it. This fluidization ceased after tangential stress was released by oriented cell divisions. Cell proliferation at the boundary also promoted jamming of cells involved therein. Boundary cells of thymidine treated assays also showed high levels of motility. Reversely, blebbistatin treated boundaries did not show any reorganization of the marginal cells.

- Tight organization of normal forces beyond the boundary.

Cells withstood a stable pattern of forces, fingerprint of the high level of coordination required for cells engaged in the boundary to build up. The autocorrelation function of the kymograph of normal tractions $C_{TT\perp}$ revealed that tractions held a period of 52 μm after the epithelial contact. The pattern was also observed, to a lower extend, in the thymidine assays. Results for the blebbistatin treatment have not been shown given that forces observed were very low.

- Buildup of tensile stress within each epithelium and about the boundary.

Strong tensile stress was built up along with boundary formation. However, the stress pattern was less pronounced when cells were unable to jam after the epithelial collision.

- Soliton –like waves propagation.

Deformation waves traveled with a speed of 117 μm/h from the boundary to the end of the field of view without significant attenuation. Waves were propagated with a period of 160 min. Blebbistatin boundary $C_{vv\perp}$ showed absent temporal propagation of waves. Kymograph of $V_{\perp}$ for thymidine treated boundaries showed less propagation fronts and less pronounced than in controls.

4.6.2 Frustrated migration by volume extrusion

To study the mechanics of a migrating epithelium stopped by a physical wall, we replaced the ephrinB monolayer with a PDMS slab (Figure 4-24, a-d, e-h, i) and analyzed dynamics after the collision between the EphB monolayer and the wall (Figure 4-24, a-d). We observed that several wave fronts emerged at the EphB/PDMS boundary and propagated for tens of cell diameters, like in the case of the EphB-ephrinB boundary (Figure 4-24, j). The strong fronts of deformation travelling from the boundary inwards had an average constant period of 85±9 min and travelled at a speed of 171±2 μm/h (Figure 4-24, k).

These experiments establish that mechanical waves are not triggered by a specific chemical interaction at the boundary. Rather, they appear to be a generic feature of repulsive epithelial interfaces during jamming.

NB: In this assay we did not have access to the traction forces because of technical limitations. These experiments were performed on glass.

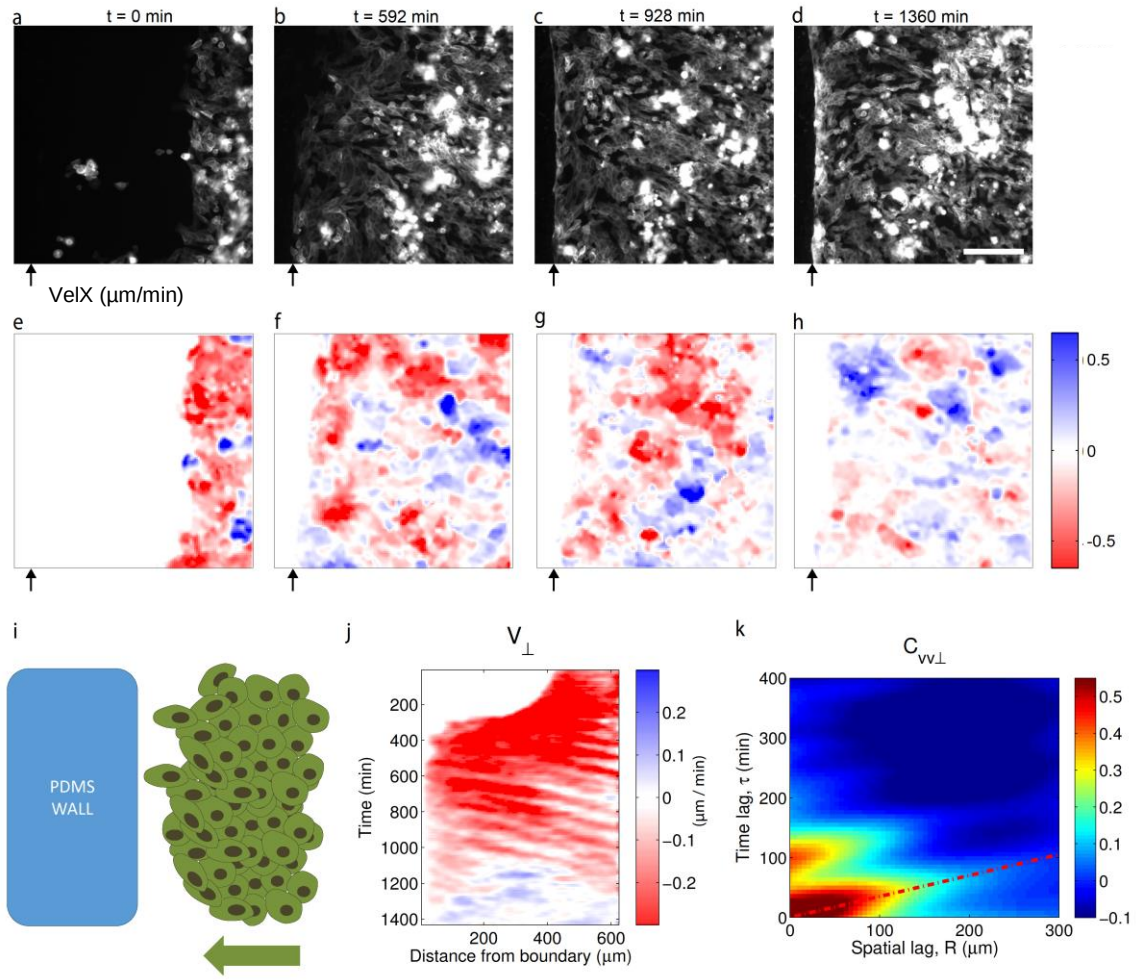

Figure 4-24| a–d, Fluorescence images of MDCK cells expressing EphB2 and lifeact-CFP during collision against a PDMS wall. e-h, Velocity component V_x corresponding to the time points indicated in a-d. Black arrows indicate the position of the wall. Scale bar, 150 µm. i, Scheme of the experimental design. j, Kymograph of velocity $V_\perp$. k, Autocorrelation function of $V_\perp$. Average period between propagation events was 85±9 min. Average propagation velocity was 171±2 µm/h.

4.6.3 Buildup of attractive boundaries

We wanted to study other kind of boundaries to unravel the particular traits of epithelia interfaces. Because of its implications in wound healing (Anon, 2012; Brugués, 2014), we thought that an encounter between homotypic cells would be of great interest. Thus, we seeded MDCK cells expressing the Eph construct at both cavities (Figure 4-25, a).

Much as in the previously observed interfaces, Eph-Eph interfaces showed clear patterns of forces very similar to the ones observed in the Eph-ephrin scenario (Figure 4-25, b). Stripes of traction had an average period of 58±8 µm (Figure 4-25, d). After epithelia collided, cells at the vicinity of the boundary exerted high forces. However, as both epithelia fused together by creating cadherin-cadherin junctions at their contact sites, forces at the boundary finally vanished.

Strikingly, we observed that waves of deformation also originated at the fusing boundary and spread symmetrically into both epithelia (Figure 4-25, c). The wave fronts travelled periodically each 150 min in average with a speed of 85±18 µm/h and they lasted until the boundary was completely healed (Figure 4-25, e). Our results suggest that the system has mechanical memory with regards to the boundary location, by undergoing the same mechanical patterns as other interfaces. The time window for these mechanisms to take place fit the time span that epithelia need to seal the wound.

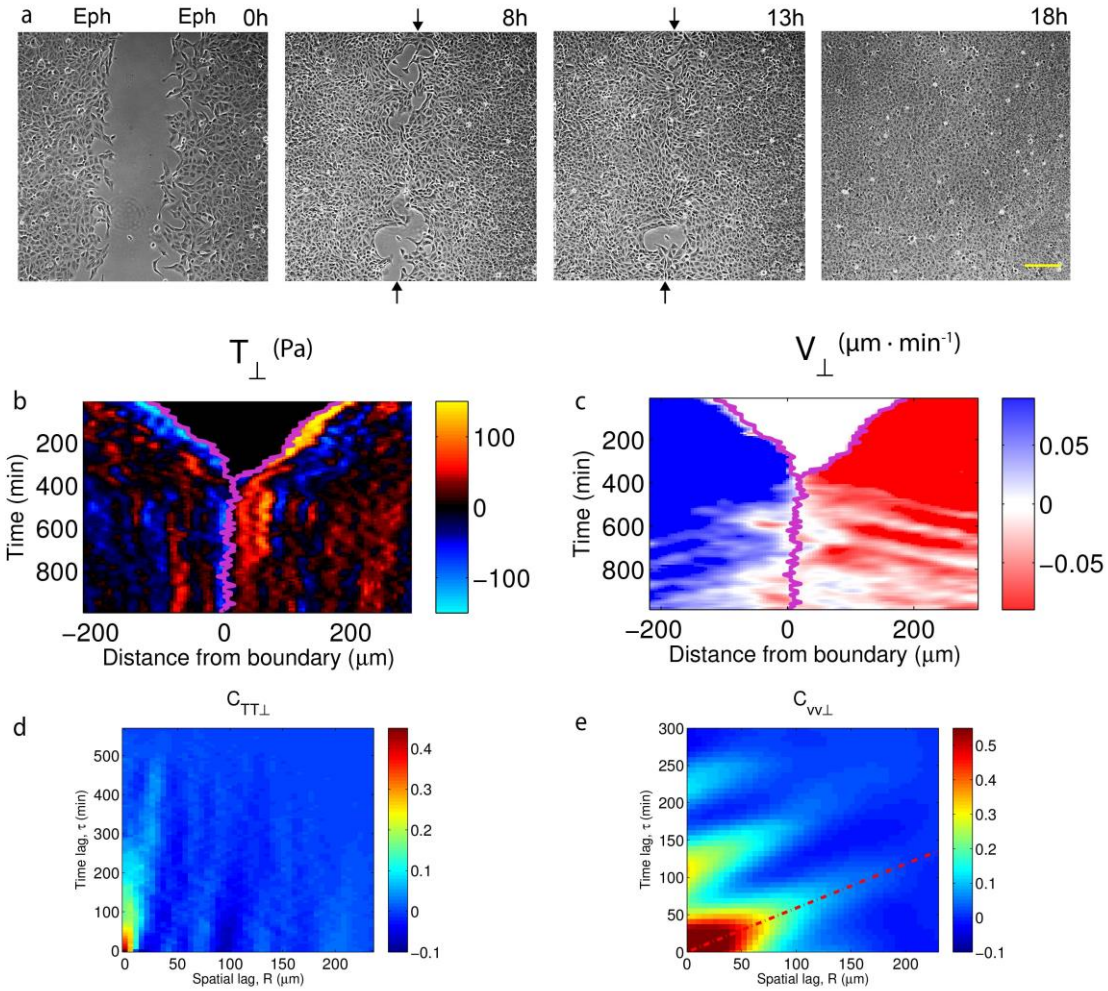

Figure 4-25| a, Phase-contrast images at different times during boundary healing for MDCK EphB-positive cells. Scale bar, 150 μm. b, Kymograph of traction $T_\perp$. c, Kymograph of velocity $V_\perp$. The pink line indicates the position of the boundary. d, Autocorrelation function $C_{TT\perp}$ of traction kymographs after collision of both Eph epithelia. e, Autocorrelation function $C_{VV\perp}$ of velocity kymographs for wound healing during the jamming phase.

5 DISCUSSION

5.1 Motivation: forces in physiology and pathology

Physical forces at the cellular level have been recognized as being fundamental to biological form and function, but until recently these forces have remained out of reach.

Over the last 10 years, studies have shown that virtually all cells can respond to applied or cell-generated mechanical forces by the complex process of biological mechanotransduction (Bradamante, 2014; DuFort, 2011; Hoffman, 2011; Jaalouk, 2009). Accordingly, it is widely recognized that defects in mechanotransduction can contribute to human diseases and atypical mechanical stresses (Bradamante, 2014; Jaalouk, 2009; Janmey, 2011).

In addition, cells are not usually found in isolation, but they rather tend to migrate collectively in sheets, strands and clusters (Friedl & Alexander, 2011; Friedl & Gilmour, 2009; Weber, 2012). Metastasis and invasion, as well as development, remodelling and wound repair are examples in which collective cellular migration plays a central role. However, collective cellular migration is poorly understood, being highlighted as one of the greatest unsolved mysteries in all of biology (Editors, 2011).

Formation and stabilization of boundaries in tissue have been studied from a physical perspective during the last decades. The correct positioning and collective migration of cells is crucial at the first stages of vertebrate development. Vertebral defects arise from defects in embryonic elongation and segmentation (McMillen & Holley, 2015 (Current Opinion in Genetics & Development)), which must be addressed from the level of gene networks to a cross-scale physical model incorporating cellular mechanics, the extracellular matrix, and tissue fluidity.

The Eph-ephrin juxtacrine interaction has been spotted as a fundamental interaction in the creation of epithelial boundaries (Miao & Wang, 2009). Furthermore, it bears importance during directed migration of neural crest cells (Haeger, 2015; Krull, 1997), and it is also an anti-carcinogenic signalling pathway in the context of intestinal lining (Herath, 2010).

Although these processes are beginning to be deciphered, there is not a consensus about the mechanism of segregation to date. In this dissertation we aimed at understanding better the mechanics of repulsive boundary buildup by studying the system at the mesoscale, i.e. the scale at which mechanics of collective cell migration are broadly captured.

5.2 Limitations of the study

5.2.1 Experimental limitations

In this work we have provided a study of the forces and morphological changes that epithelial cells undergo during the process of Eph-ephrin boundary formation. To do so, we developed a novel assay that allowed the formation of boundaries together with the measurement of traction forces exerted by cells and the imaging of the boundary buildup.

We had to come up with design solutions to overcome a number of limitations, mainly: (i) the co-culture of different cell populations seeded in close vicinity (300-400 μm of interdistance); (ii) the creation of a physical barrier that could be attached to PA gels without damaging them during hours of incubation.

Advances in 3D printing allowed us to print a master that enabled stencil replication in PDMS over bench. In this way, we could overcome the usual clean room procedure to pattern the stencil by photolithography. We used magnetic PDMS for this assay. Thus stencils were made of a mixture of PDMS and magnetite. A magnet underneath the sample secured the magnetic PDMS stencil on the wet polyacrylamide gel while preserving the gel protein coating.

Although this assay proved robust enough to provide compelling results, it carried some drawbacks. When using gels of 1-6 kPa of stiffness, z-deformations at the vicinity of the boundary could not be ignored and provoked that the sample went out of focus after 12-13 hours of seeding. Technically, this issue was amended by working on stiffer gels (15 kPa) and by imaging with lower magnification (20x), less sensitive to small changes in focus. Conceptually, we also recovered a 2-dimensional

problem and minimized the presumable poroelastic effects along the boundary as well (Casares, 2015).

Arguably, 15kPa comprises a stiff substrate to epithelial cells. Although it falls within the physiological range, results produced cannot be generalized to soft tissues and low rigidities thus limiting the impact of the observations. Still, working on PA gels rather than on glass provides with a more physiological environment to cells, being also a tunable one. Traction force microscopy code extended to 3 dimensions would allow studying the system at lower rigidities, including the z deformations as a quasi-3D system. Regarding the poroelastic effects, they could be prevented by performing the assay on soft PDMS.

5.2.2 Analytical limitations

Most of the experiments were performed on cells with an Eph or ephrin construct transfection and an E-cadherin fluorescent marker at a very low concentration – which did not allow for imaging during long periods. Concomitantly, most of our structural observations come from stainings, which give an overview of the boundary buildup major changes, but cannot tackle with the dynamics of the segregation. At the last stage of the project we could access viral transfection and generate new cell lines containing GFP or CFP actin respectively. Based on these cell lines, we did some high resolution experiments that confirmed our prior observations (results 4.5). We also developed a possible hypothesis for the formation of the actomyosin fence in view of these experiments (appendix 7.10). Still, we did not couple these last observations with high resolution tractions.

5.2.3 Conceptual limitations

Although jamming is appointed as a possible theoretical framework to unify the observations of this study, there is not a jamming model that describes our model system to date. Therefore, we believe that such theoretical body should be developed and tested against our experimental observations. The starting point could be the work of Blanch et. al. (Blanch, 2015), which predicts the appearance of soliton-like migrating patterns in their study of collective cell migration. Also work by J. H. Kim describing kenotaxis should be considered (Kim, 2013), in which intracellular stresses pulling cell-matrix adhesions away from a boundary were already observed.

5.3 Summary of results

5.3.1 Cells engaged in the formation of repulsive boundaries undergo dramatic structural and shape changes

In our model experiments, we could identify different stages of the boundary formation:

A first stage was characterized by polarized migration of the two monolayers approaching against each other. Cells at the leading edge extended large lamellipodia exerting large forces, although forces were not restricted to these cells.

In a second stage, cell monolayers contacted each other. Fast lamellipodia extension and ruffling triggered the Eph-ephrin interaction, which promoted inhibition of cadherin clustering at the boundary, preventing formation of adhesive bonds between opposing cells.

The third stage was the shaping of the boundary. The combination of the contact repulsion and the spatial confinement led to the construction of acto-myosin walls that prevented cell intercalation. During this stage, cells at the boundary elongated parallel to the edge.

The fourth stage allowed the boundary geometry to settle. Curvature was reduced to a certain baseline, probably related to the dimension of the cells, the strength of the repulsive interaction, cell density and tension at the acto-myosin cable. In this stage, jamming, cell proliferation and differential adhesion could be contributing to the stabilization of the boundary and to its maintenance.

We found that, upon contact, marginal and submarginal cells drastically elongated parallel to the boundary. This morphological change was paralleled by relaxation of forces normal to the boundary. Transient changes in cell shape were relaxed by oriented cell division to yield

isotropic cell packing at the end of the process. Shape relaxation owing to cell division was accompanied by a decrease in σ_{xx} and σ_{yy}.

After the contact, many cells became static. Still, some cells remained highly motile. We observed that the dynamics of these groups of cells accounted for the strong pattern of deformation waves observed at the kymographs of $V_{\perp}$.

5.3.2 Collective traction patterns promote the segregation of cell populations during Eph-ephrin repulsive boundary formation

Traction kymographs revealed normal static traction patterns after the epithelial collision. The mechanical patterns accounted for the tight mechanical coordination of cells beyond the boundary.

Normal forces involved in the boundary formation showed a dramatic decrease in magnitude right after the crash. Tangential forces, in turn, showed a subtler decrease in magnitude after the contact.

During the unjamming phase, $\sigma_{\perp}$ built up quickly within the first few cell rows and reached a plateau thereafter. Upon contact, $\sigma_{\perp}$ decayed sharply and then exhibited progressive buildup that was stabilized in time as monolayers jammed.

Impairing cellular proliferation during boundary buildup led to revealing results. Forces maintained the pattern previously described, but traction oscillations did not show an offset of opposite sign on each side of the boundary. Concomitantly, the increase in $\sigma_{\perp}$ was reduced, in agreement with the thesis that jamming stabilizes supracellular force patterns during Eph-ephrin boundary formation.

In agreement with the previous observation, we also studied cells treated with blebbistatin to find out that opposing epithelia did not fuse by the end of the experiment under such condition. Boundaries with impaired contractility remained unchanged in shape during buildup, though, and actomyosin supracellular structures did not line each side of the boundary.

These observations establish that formation of repulsive boundaries involves not only local repulsive events at the boundary, but also the mechanical cooperation of many cells located behind it. This cooperation leads to supracellular mechanical patterning that pulls cell-substrate adhesions away from the boundary (appendix 7.6).

5.3.3 Epithelial jamming and cell contractility are sufficient to sustain deformation waves during the buildup of repulsive boundaries

The formation of traction patterns was paralleled by the generation of soliton-like deformation waves that propagated away from the boundary across tens of cells. These waves could be clearly discriminated after thresholding velocity maps to separate rapid propagating cells from slow non-propagating cells. A kymograph of normal velocities revealed that some deformation waves propagated even through the boundary, despite the lack of mechanical connection between them.

For cells under a thymidine treatment, kymographs of $V_{\perp}$ showed that propagating fronts were less abundant and less pronounced than in control experiments. We concluded that jamming plays an essential role in boundary formation, both by stabilizing supracellular force patterns and by fostering the creation of deformation waves, which may be related with the settling of boundaries to their final conformation.

For cells under a blebbistatin treatment, kymographs of $V_{\perp}$ showed that waves of deformation were largely prevented. After a detailed look, it was observed that both epithelia underwent a large number of cell extrusions during cell divisions after boundary contact. We concluded that contractility in the context of boundary formation is necessary not only for the correct buildup of supracellular structures along the boundary, but also to provide the necessary tension that deformation waves require to arise and further to ensure the correct cell packing of both tissues.

5.3.4 Deformation waves appear in a wide range of repulsive and attractive interfaces

To further investigate the characteristics of boundary formation, we studied frustrated migration against a physical barrier (passivated PDMS barrier). We observed that cells from the leading edge aligned with the boundary, elongating by their principal axis. In addition, cells buried within epithelia underwent the pattern of deformation waves previously described. Therefore, we inferred that frustration of migration is enough to create highly correlated fronts of deformation that travel through the epithelium.

Surprisingly, an encounter between two monolayers of homotypic cells caused travelling deformation waves as well. In this situation, though, symmetric waves arose from the contact position. Much as the two epithelia would end up fusing by building homotypic cell-cell junctions, the system showed memory by holding these travelling deformation waves during the process of fusion. In conclusion, mechanics of attractive boundaries - while both tissues are not completely sealed - behave as repulsive boundaries for a timespan of hours.

5.4 Boundary formation and jamming: exploring the connection

Besides the local role of Eph-ephrin interactions at the boundary, our findings establish the emergence of supracellular mechanical structures that contribute to sustain epithelial segregation by engaging cells far behind the boundary. Further, we show that soliton-like deformation waves are triggered at the epithelial interface and propagate across the monolayer. These waves are not specific to a chemical interaction at the boundary but rather appear to be a generic feature of repulsive epithelial interfaces. Propagation of mechanical waves in epithelial monolayers has been previously reported (Serra-Picamal, 2012) (Matsubayashi, 2011) but, in every case, these waves were associated with cellular motion. By contrast, deformation waves identified here emerge at repulsive interfaces during jamming. It is thus unclear how these waves can be accounted for by previously proposed mechanisms based on cycles of stiffening and fluidization (Serra-Picamal, 2012) or feedback between strain, polarization and contractility (Banerjee, 2015).

The connection between boundary formation and cell proliferation has been recently explored, leading to some unexpected revelations. In their work, Willecke et. al. found that boundaries of Dachsous cadherin activity modulate the hippo signaling pathway to induce cell proliferation, thereby contributing to the control of organ size (Willecke, 2008). In turn, Jeffrey O. Bush and Philippe Soriano found the ephrinB1 forward signaling to regulate craniofacial morphogenesis by controlling cell proliferation across Eph-ephrin boundaries (Bush, 2010). Still, they claimed that the underlying mechanisms are unresolved. In contrast, anti-proliferative activities have been reported for Eph-ephrin signalling in neural progenitor cells, the epidermis, and breast cancer cells (Holmberg, 2005; Noren, 2006; Ricard, 2006; Genander, 2010). Another unexpected connection was found by

Delarue et. al. when studying a different collectivity, namely a population of microbes. They revealed a collective mechanism of confinement, which they called self-driven jamming, that promotes the buildup of large mechanical pressures in microbial populations (Delarue, 2016). Microfluidic experiments on budding yeast populations in space-limited environments showed that self-driven jamming arises from the gradual formation and sudden collapse of force chains driven by microbial proliferation, extending the framework of driven granular matter (Radjai, 1996; Majmudar, 2005; Bi, 2011; Heussinger & Barrat, 2009).

Although jamming remains contentious, the concept has become prominent because it could well unify the understanding of a remarkably wide range of soft materials, including foams, colloids, suspensions and granular matter. The dynamics of the cellular collective comprising a monolayer are reminiscent of all these same hallmarks (Sadati, 2013). Indeed, in both inert and living condensed systems, dynamics are constrained by many of the same physical factors. For example, concerning the basic unit, whether a living cell, a foam bubble or a colloidal particle these factors include volume exclusion, size (Zhou, 2009), deformability (Mattsson, 2009), mutual crowding and caging (Schall, 2007; Segre, 2001), mutual adhesion/repulsion (Trappe, 2001) and imposed mechanical deformation (stretch or shear) (Trepat, 2007; Krishnan, 2009; Oliver, 2010; Wyss, 2007). Consequently, cell jamming is increasingly becoming a reasonable model to explain epithelial mechanics of migration and confinement. In the context of boundary formation, we hypothesize that jamming would be a solid theoretical body to start modeling epithelial segregation from a new perspective.

5.5 Outlook

In view of the results of this work, we propose a series of future experiments which would lead to a higher understanding of the phenomenon captured with our assay. Mainly, they are the following:

- Given the importance of contractility and actin bundling during the buildup of repulsive boundaries, it would be advisable to develop a new cell line carrying both a myosin and actin fluorescent construct. Furthermore, visualizing E-cadherin junction dynamics together with actin or myosin could help in deciphering the apparent disjointed relationship between tractions and velocities. Also by studying other elements of cytoskeleton, like the intermediate filaments, we could also evaluate the impact of CIL in the cycles of Eph-ephrin contact-repulsion (Theveneau, 2010).

- Considering the tight interplay among Rho GTPases both at the cycles of repulsion and during the assembly of the actin supracellular structure, interrogating Rho GTPases signalling could help identifying the Eph-ephrin interaction downstream effectors. These dynamics could be coupled to the already known mechanics. We suggest using FRET technique to that aim.

- Lastly, visualizing the actomyosin cable would allow for its perturbation with ease, for example by laser ablating it locally. This would help in deciphering which the role of the actomyosin cable is and if it is related to the generation of

deformation waves or the traction patterns observed. Also transfecting Eph-ephrin cells with a photoactivatable RhoA construct to create local contractility at the boundary would allow studying its propagation from the boundary inwards the epithelia.

Developing a model that would jointly account for our *T-V* observations would be the natural next step in this project. As mentioned before, first we would address the question of whether the deformation waves observed are of a soliton-like nature or not. To that purpose, we would develop an assay that would allow demonstrating the necessary conditions for a wave to be a soliton: maintaining their shape while propagating at constant velocity, remaining localized to a region and being able to interact with other solitons emerging from the collision unchanged, except for a phase shift. Ideally, we would develop an assay based on a collectively migrating epithelium frustrated at both sides. Arising from frustrated migration, we should observe the interaction between solitons generated at the opposed edges.

Putting the work in perspective, we could also extend the 1-dimensional boundary buildup observations to a 2-dimensional sorting process. We developed a first sorting assay, in which preliminary observations were in agreement with previous results in boundaries (Appendix 7.7). Still a rigorous analysis should be implemented in order to come up with further conclusions.

In this line of reasoning, extending the model system to study 3D sorting would be of great relevance in physiology. In development, it has been observed that the germ layer arrangement in vitro does not reproduce the in

vivo positioning (Ninomiya, 2011; Schötz, 2008). Therefore, studying 3D sorting in vivo should be pursued (Poh, 2014; Sasai, 2013). With regard to the theoretical model, parameter dependencies established with 2D models should be reviewed in light of the 3D experimental results (Hutson, 2008).

5.6 State of the art and perspectives

Cell mechanosensing, as well as adhesion and migration, begin at the scale of the molecule. Events at this scale are seen most often as the most upstream and, therefore, the most fundamental. In collective systems, however, events at many scales of length make contributions of equal importance, and even interact directly and strongly across scales (Pegoraro, 2016).

Nowadays, Physics at some scale bigger than the cell but smaller than the tissue – the mesoscale – remains the missing link that is required to tie together findings that might otherwise seem counterintuitive (Pegoraro, 2016). One of these key encounters at the mesoscale involves boundary formation, cell sorting and the differential adhesion hypothesis (DAH) (Foty, 2005; Amack, 2012). To our mind, there is a great deal of understanding missing on this matter. For that, we have studied boundary formation using tools at the mesoscale, being able to interrogate forces, velocities and stresses within this subtle but still enlightening scope.

Adhesion, contractility and proliferation, to name a few, might not be able to describe a collective phenomenon that includes a wide palette of physical and molecular interactions independently. To bridge this gap, we shifted the spotlight to the emerging concept of cell jamming, which points to only a small set of parameters that govern when a cellular collective might jam and rigidify like a solid, or instead unjam and flow like a fluid (Park, 2016). Further work and the development of a model able to predict our observations will shed light on the matter, disclosing the staples of the mechanical phenomena therein.

Investigation of cell jamming in certain diseases, including cancer (Haeger, 2014; Pawlizak, 2015) and asthma (Park, 2015), are just now beginning to appear in the literature (Pegoraro, 2016).

Recent findings by Park et. al. suggest that cell jamming may play a central role in the homeostasis of airway epithelium (Park, 2015). When airway epithelial cells from healthy human donors are cultured in an air-liquid interface, they are initially unjammed, but as they mature and differentiate over 14 days they eventually jam. This transition to the jammed state can be disturbed, however, by external stimuli or disease conditions. They have observed that compressive stresses that mimic the effects of bronchoconstriction provoke the transition of the mature epithelial layer from the jammed state back to the unjammed state. Furthermore, when cells are cultured from asthmatic donors, the transition to jamming is significantly delayed. A causal and mechanistic role for rejamming in the recovery process, or for unjamming or delayed jamming as precipitating factors in an asthmatic exacerbation, remain matters of speculation - it could well be just a consequence -, but point nevertheless to open fundamental questions.

In cancer, the conversion to collective invasion with increasing ECM confinement supports the concept of cell jamming as a guiding principle for melanoma and fibrosarcoma cells into dense tissue (Haeger, 2014). What is more, Pawlizak et.al. show at their work that dynamical effects such as directional motility, friction and jamming may play an important role in tissue compartmentalization across the epithelial−mesenchymal transition, associated with processes such as metastasis (Pawlizak, 2015).

All in all, the fields of boundary formation, epithelial confinement and sorting seem to be intimately related. The relationships among them are far from being fully understood, but there may be lots of light shed on that subject in the near future. Jamming, differential adhesion and contact-repulsion are different shades of the physics behind the formation of repulsive and attractive boundaries. Next steps in their modeling across scales, linking genes, interactions and mechanics, may be crucial for the detailed understanding of the role of these interplaying mechanisms.

6 CONCLUSIONS

1) We developed an in vitro assay to study cellular forces, deformations, and structure during the formation of distinct types of epithelial boundaries.

2) Boundary formation between cell populations expressing Eph and ephrin involves the assembly of a supracellular acto-myosin cable, the abrogation of E-cadherin adhesion at the Eph-ephrin epithelial contact sites, and oriented cell division to relax cell shape.

3) Cells behind the boundary exhibit long-lived oscillatory traction patterns that tend to pull cell-substrate adhesions away from repulsive interfaces. These patterns have a characteristic length scale of several cell diameters and give rise to a gradient of intercellular stress. Thus, a supracellular mechanical organization contributes to sustain epithelial segregation by engaging cells far behind the boundary.

4) Mechanical waves are triggered at the epithelial interface and propagate across the monolayer. These waves are reminiscent of solitons in the sense that they comprise solitary pulses and that they roughly maintain shape and speed.

5) Propagation of mechanical waves requires the action of myosin motors and cell jamming.

6) Mechanical waves are not specific to the Eph-ephrin interaction at the boundary but rather appear to be a generic feature of atttractive and repulsive epithelial interfaces.

7 APPENDICES

7.1 Publications and conferences

Pilar Rodríguez-Franco, Agustí Brugués, Raimon Sunyer, Vito Conte, Pere Roca-Cusachs, Xavier Trepat; Long-lived force patterns and deformation waves at repulsive epithelial boundaries, September 2016 (under review).

Rodríguez-Franco, P., Brugués A.,Güell G., Sunyer R., Conte, V., Forces driving epithelial boundary formation by Eph/Ephrin interactions, December 2015. American Society for Cell Biology Meeting. San Diego (USA). Poster communication.

'Long-ranged force patterns and waves during the formation and maintenance of repulsive epithelial barriers', May 2016. PhD Discussion Session, IBEC. Oral communication.

Pilar Rodríguez-Franco, Agustí Brugués, Vito Conte, Raimon Sunyer, Pere Roca-Cusachs, Xavier Trepat, Long-ranged force patterns and waves during the formation and maintenance of repulsive epithelial barriers, June 2016. 9th IBEC Symposium on Bioengineering for Active Ageing. Barcelona (Spain). Poster communication.

Rodríguez-Franco, P., Brugués A.,Güell G., Sunyer R., Conte, V., Forces driving epithelial boundary formation by Eph/Ephrin interactions, September 2015. 8th IBEC Symposium on Bioengineering for Regenerative Medicine; Barcelona (Spain). Poster communication.

Rodríguez-Franco, P.; Zalvidea, D.; Castaño, O.; Planell, J.; Noally, J.; Engel, E.; Trepat, X., ; How do cells behave in 3 dimensions? Measuring forces within scaffolds. 6th IBEC Symposium on Bioengineering and Nanomedicine; Barcelona 2013. Poster communication.

7.2 Workshops and conference attendance

6th European Cell Mechanics Meeting. Barcelona, May 2015. Organizer: IBEC, UB, QuanTissue, The Company of Biologists, JPK. Conference attendance.

Campus Gutenberg: Comunicación y cultura científica. Barcelona, September 2014. Organizer: UPF, OCC, Obra Social La Caixa. Conference attendance.

International Symposium: Visualizing signalling nanoplatforms at a higher spatiotemporal resolution; Castelldefels (Barcelona), May 2013. Organizer: ICREA. Symposium attendance.

Campus Gutenberg: Comunicación y cultura científica. Barcelona, September 2013. Organizer: UPF, OCC, Obra Social La Caixa. Conference attendance.

Quantissue meeting 2013: Computational approaches to networks, cells and tissues. Barcelona, April 2013. Organizer: CRG, PRBB. Meeting attendance.

LightSheet microscopy workshop; Barcelona, February 2013. Organizer: IRBB, CRG, ICFO. Workshop attendance.

7.3 Outreach activities

‘Cells exert Forces’ – Workshop for all ages (2014/15)

In collaboration with PhD. Laura Casares

Workshop for families on cell mechanics, showing the physics behind cell biology. In roughly 12 minutes and by means of easy experiments, participants understand the basics of cell mechanics and the fact that cells can exert forces. Despite being an original content for Secondary Education for ‘Fira Recerca en directe 2014’, we adapted the contents to different audiences. This allowed us to bring the workshop to ‘Festival de Ciència, Tecnologia i Innovació NOVUM’ in 2014 and also this 2015 spring.

http://festivalcti.bcn.cat/festa_post/les-cel%C2%B7lules-fan-forca/

http://www.pcb.ub.edu/portal/noticies/-/noticia/not_el-pcb-participa-a-novum-la-novena-edicio-del-festival-de-ciencia-tecnologia-i-innovacio

3RD JIPI Conference – Organising Committee Member (2015)

The JIPI is an interdisciplinary meeting for and from PhD Students from Catalunya. It has become an opportunity to meet PhD students, share experience and research, envision different problems and explore different professional areas. This year I have contributed to its design and management, especially on the ‘Scientific Transparency’ debate.

http://www.ub.edu/jipi/

‘Descobreix els patrons de la natura’ – Workshop for PCB educational programme (2014/2016)

In collaboration with PhD. Student Marina Uroz

We have developed a 2 hour workshop for Secondary Education / High School introducing the reaction-diffusion math, which predicts a variety of animal coats; zebra stripes, leopard spots,... In two years, we have thought that content to 12 different groups of students, from professional training students to secondary and A-levels students. The experience has been utterly satisfying and, what is more, the workshop will continue being though in the PCB program for years.

As an example, students from School Apeles Mestre created a blog content out of what they learned during the activity.

http://apellesmesciencies.blogspot.com.es/2015/02/taller-descobreix-els-patrons-de-la.html

7.4 Cell sorting protocol

1. Trypsinize the cells as usual.
2. Resuspend them in DMEM with 10%FBS.
3. Leave at 37ºC for 30 min.
4. Count the cells.
5. Centrifuge the cells.
6. Resuspend in blocking Buffer (read below) in such a volume that you have a suspension of $4 \cdot 10^6$ cells/ml.
7. Prepare 8 tubes with 5ml of cells at $4 \cdot 10^6$ cells/ml. In total you prepare 40 million of cells. Leave for 15 minutes.
8. Add anti-ephrin-B1 antibody (R&D AF473) to 1:100 dilution if you want to sort the ephrin-B1-E-cadherin-Cherry cells (10 ul in 1 ml // 50 ul in 5 ml).
9. Add ephrin-B1-Fc recombinant protein (sigma E0653) to 1:200 dilution if you want to sort the EphB2-E-cadherin-GFP cells (1ul in 200 ul // 25ul in 5ml).
10. Leave for 20-25 min on ice.
11. Wash twice with staining buffer (washes consist on centrifuging the cells, removing supernatant, adding staining buffer, centrifuging, removing supernatant, adding staining buffer, centrifuging and removing supernatant).
12. Add staining buffer with the secondary antibody diluted 1:400 (donkey anti goat-labeled with a far red fluorochrom for ephrin-B1 antibody and donkey anti human-labeled with a far red fluorochrom for ephrin-B1-Fc) (1ul in 400ul // 12.5ul in 5ml).
13. Leave for 20-25 min on ice.
14. Wash twice with staining buffer.
15. Resuspend in staining buffer.

16. Go to the FACS. There you have to sort the population of cells double positive for GFP and far red (in EphB2-E-cadherin-GFP) or the double positive for cherry and far red (for ephrin-B1-E-cadherin-Cherry cells).

Staining buffer: PBS + 5% FBS +Penicillin/Strep at the same concentration as in culture media.

Blocking buffer: Staining buffer + 1% donkey serum.

NB: We choose far red for the staining because the cells already have green and red labeling.

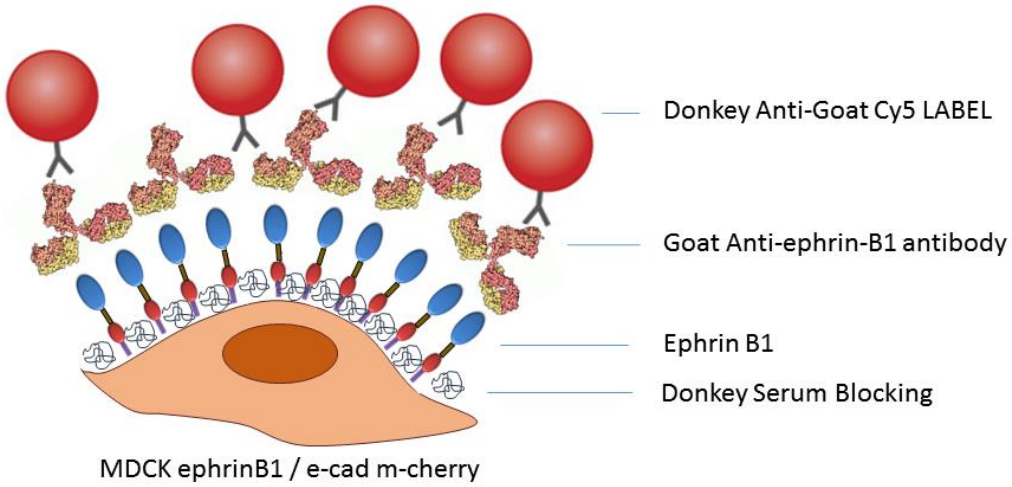

Figure 7-1| Scheme of chemistry applied to ephrinB1 cells prior to their sorting.

7.4.1 Example of FACS sorting sequence: ephrinB1 cells

1) A sample of wild type MDCK cells is characterized. First, we chose a population which showed a homogeneous granularity (Side Light Scatter, SSC) and a homogeneous cell size (Forward Light Scatter, FSC-A). From that first population P1, we run doublet

discrimination by detecting disproportions between cell size vs. cell width (homogeneous cell area (FSC-A) vs. width (FSC-W)).

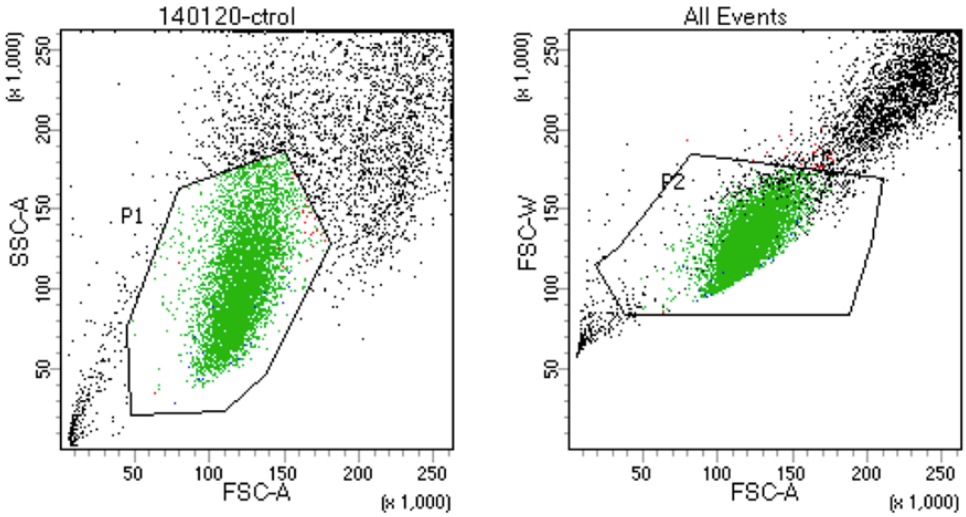

2) We set a threshold for both channels of interest: red (to detect m-cherry) and far red (to detect CY5). This threshold defined darkness.

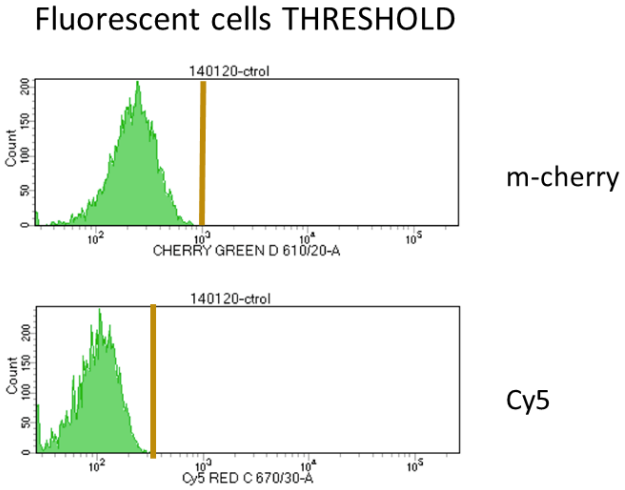

3) We run the same procedure as for the MDCK cells, but now with the cells of interest (ephrin-B1-E-cadherin-Cherry cells). We selected cells falling within the previously set areas, P1 and P2 respectively.

4) We visualized the signal in a far red vs. red chart. From this population (P3), we selected cells which brightness was above the threshold for darkness (P6). In this way, we had all the co-bright cells selected.

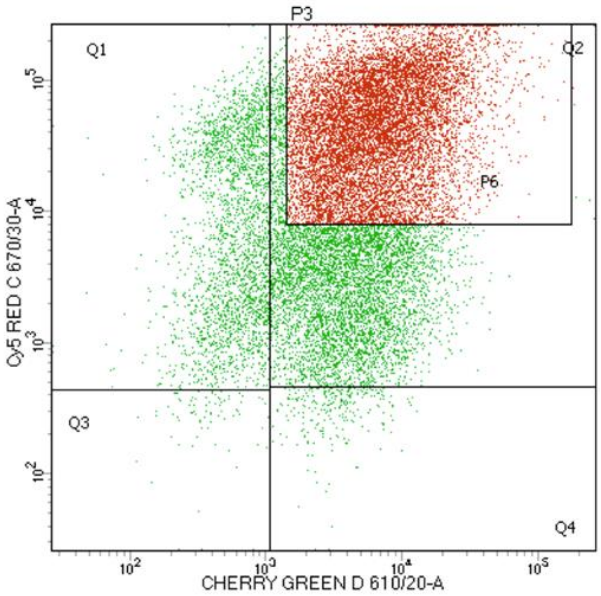

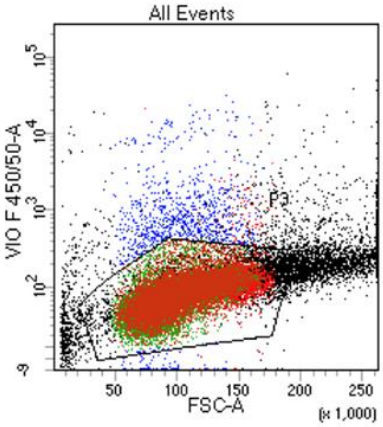

Population	#Events	%Parent	%Total
All Events	28,831	####	100.0
P1	22,982	79.7	79.7
P2	21,024	91.5	72.9
P3	20,175	96.0	70.0
Q1	2,723	13.5	9.4
Q2	17,097	84.7	59.3
P6	11,281	66.0	39.1
Q3	82	0.4	0.3

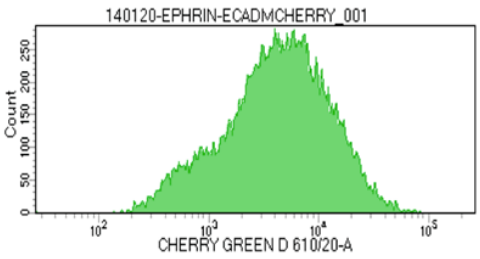

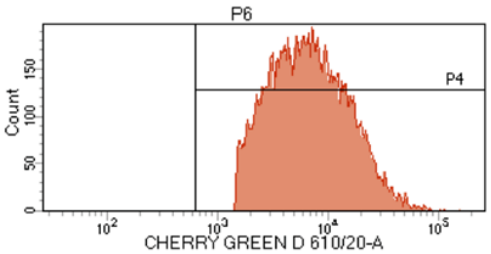

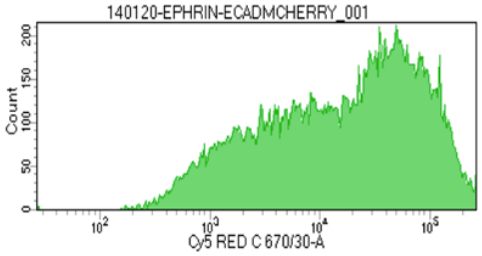

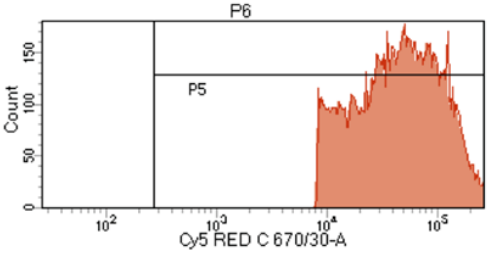

5) We resorted a limited amount of the sorted cells, following the same sequence of sorting. The result was very consistent with the first sorting.

Final re-sorting

Mostly within
the selected region

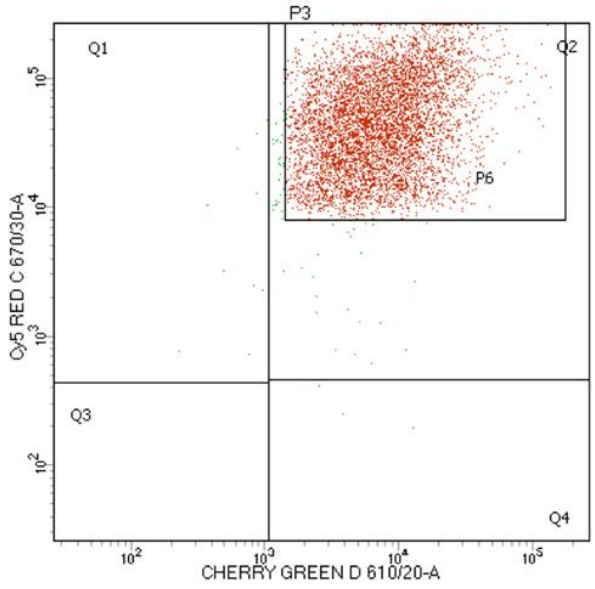

7.5 Average Traction and Velocities during boundary formation

We computed the average traction during time for both Cartesian components.

Normal forces involved in the boundary formation show a dramatic decrease in magnitude right after the crash. Tangential forces show a subtle decrease in magnitude after the crash.

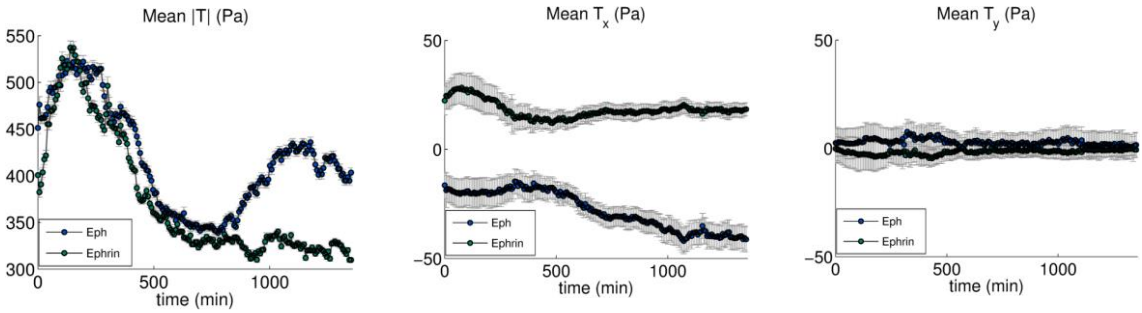

Figure 7-2| Time evolution of forces during boundary buildup.

We also computed the average velocity during time for both components. In average, velocities show a fast decrease in magnitude right after the epithelial collision.

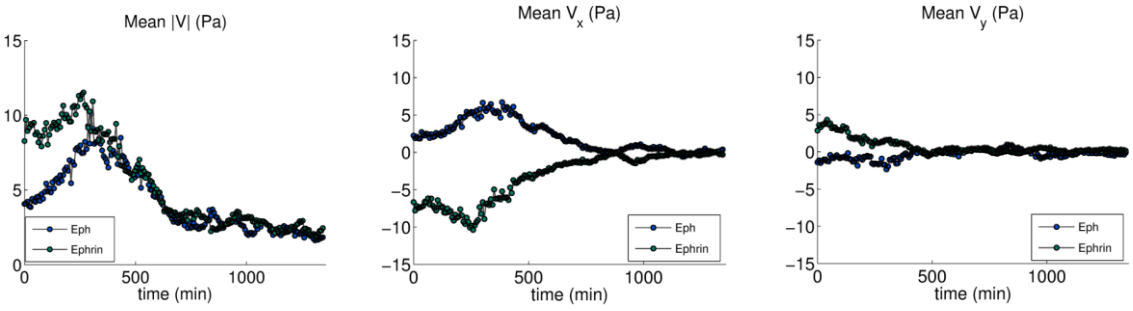

Figure 7-3| Time evolution of velocities during boundary buildup.

7.6 Z-deformations during Eph-ephrin boundary buildup

We studied the deformations in the Z dimension to corroborate the tensile state of the epithelia. To that aim, we took z-stacks of a complete boundary from end to end of the gel in 150 µm steps at the vicinity of the boundary. Beyond the center of the gel, the stacks were acquired every 2000 µm. In this way, we could have a general view of the collective deformations that both epithelia produced to the gel in the third dimension, Z (Figure 7-4,a). The profiles obtained for an Eph-ephrin epithelium along time are shown in Figure 7-4,b. The profiles obtained for an Eph-Eph epithelium along time are shown in Figure 7-4,c. Even if the trend was the same at the outer corners (tensile effect of an expanding monolayer), differences aroused as we approached to the boundary. At the very center, an edgy tip could be observed for the Eph-ephrin boundary intermediate space. We conclude that this is a treadmill of each independent epithelium pinching and stretching the gel towards the interior of the epithelium. Only that we are seeing the same effect face to face and in close vicinity. Furthermore, there may be some poroelastic effects due to the fact that a blank space is left between epithelia and in direct contact with the medium (Casares, 2015). Although we did not investigate this further, we foresee that there may be an interest in conveying a clearer experiment to disentangle the deformations caused by the boundary build up itself and the presumable poroelastic effect that goes along.

a)

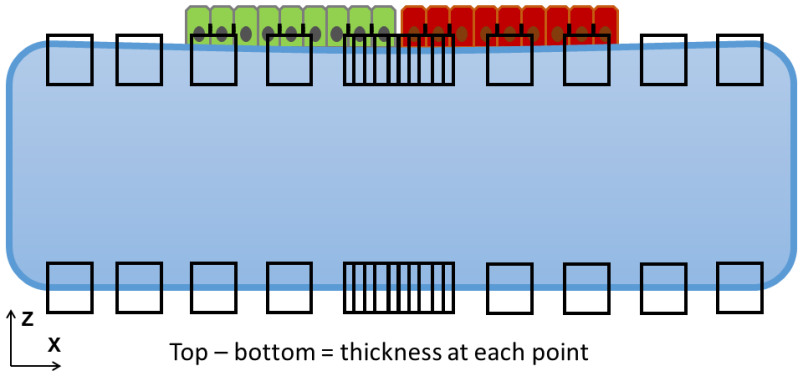

b)

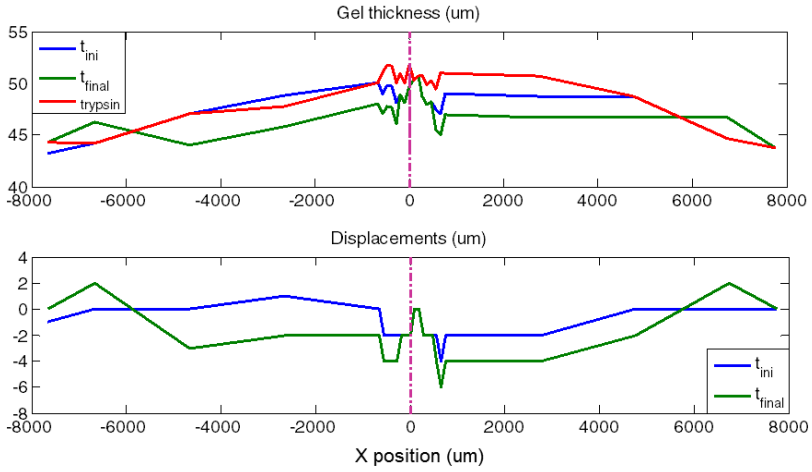

c)

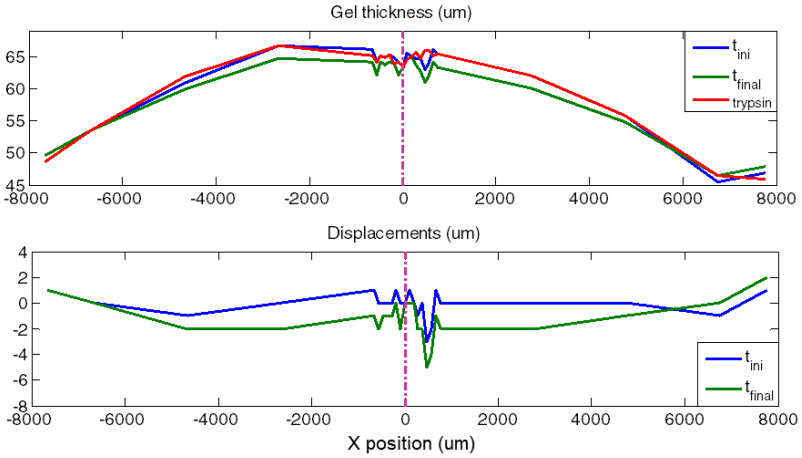

Figure 7-4| a, Scheme of the sequence of z-stacks that covered the boundary buildup evolution. Each box stands for one z-stack. b, gel thickness and concomitant deformations for Eph-ephrin boundary buildup. c, gel thickness and concomitant deformations for Eph-Eph wound healing.

7.7 Co-culture sorting experiments

We developed a co-culture assay to extend our observations to a two dimensional scenario. We seeded an even mixture of Eph and ephrin expressing cells in a 1/3 ratio and observed the sorting of the two populations. We observed that Eph-cells clusters were always the most frequent outcome, and decided to observe their peculiarities for the different treatments applied.

For the control assay, 2-dimensional sorting assays fully captured the same traits observed in the boundary buildup formation experiments. Clusters of Eph-cells were surrounded and isolated by ephrin cells (Figure 7-5). Clusters stabilized in time to their final shape.

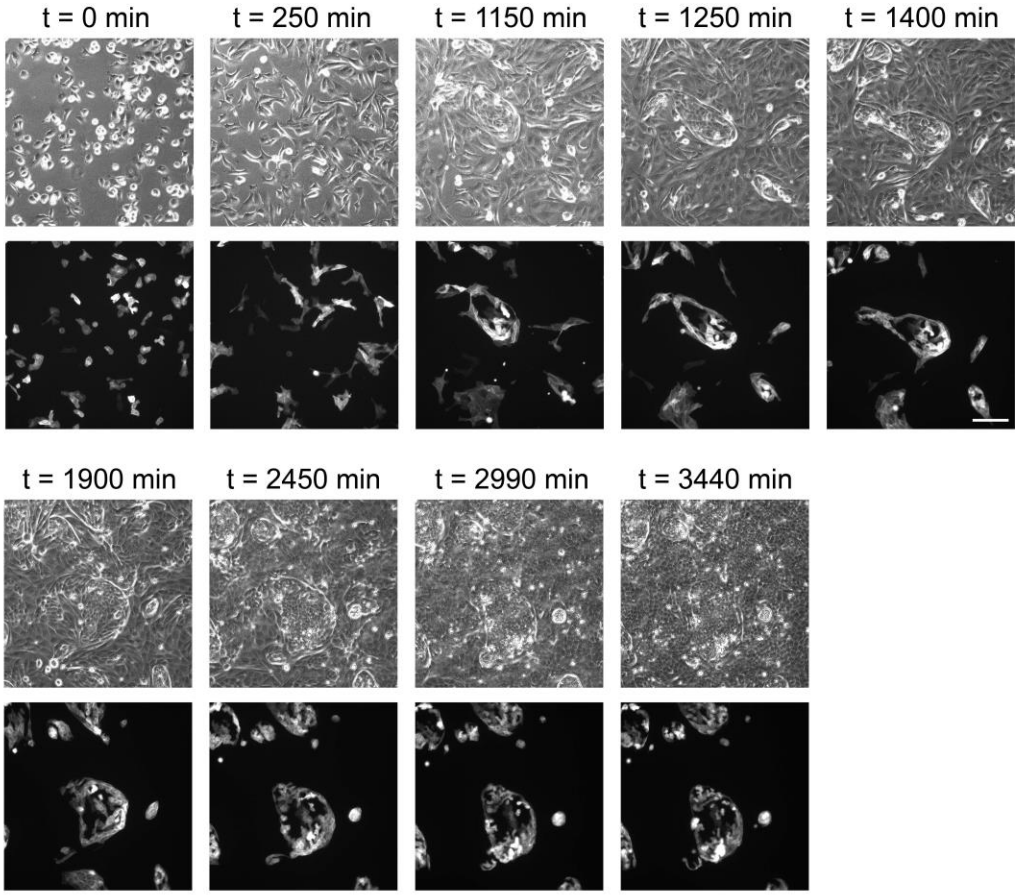

Figure 7-5| Time evolution of a control co-culture assay for Eph-ephrin cells. Top view: Bright field; Bottom view: lifeact fluorescence (Eph-cells).

Co-culture experiments showed that for thymidine treated cells the segregation does not reach stabilization after 57 hours (Figure 7-6), whereas for the control case sorted clusters became stable and large due to jamming and cell proliferation. In particular, control cluster size remained mostly unchanged after 30 hours for the average Eph-ephrin sorting assay (Figure 7-5).

Under a blebbistatin + thymidine treatment, the co-culture sorting assay fully captured the same traits observed in the boundary build up formation experiments. Mainly, Eph clusters were sorted out by ephrin cells correctly although cell jamming was prevented (Figure 7-7).

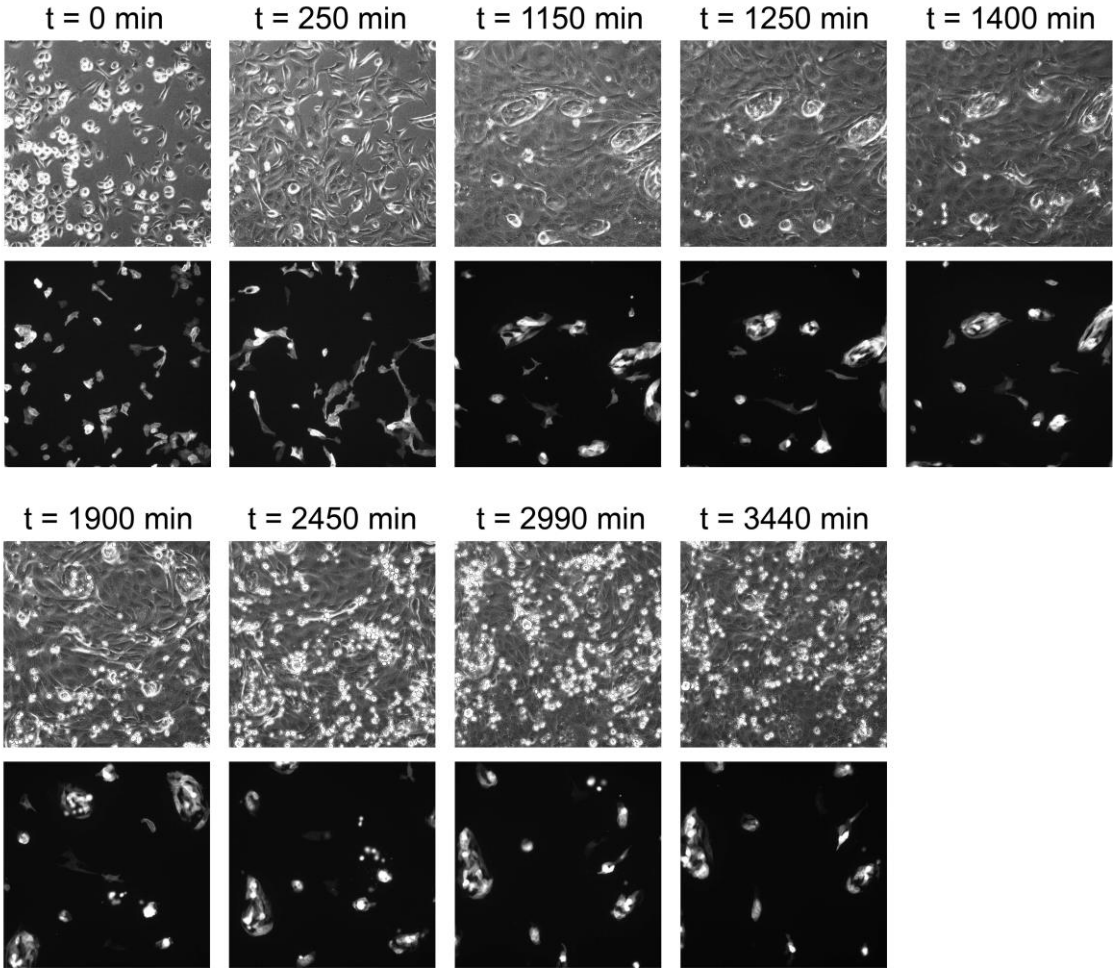

Figure 7-6| Time evolution of a co-culture assay for Eph-ephrin cells under a thymidine treatment.

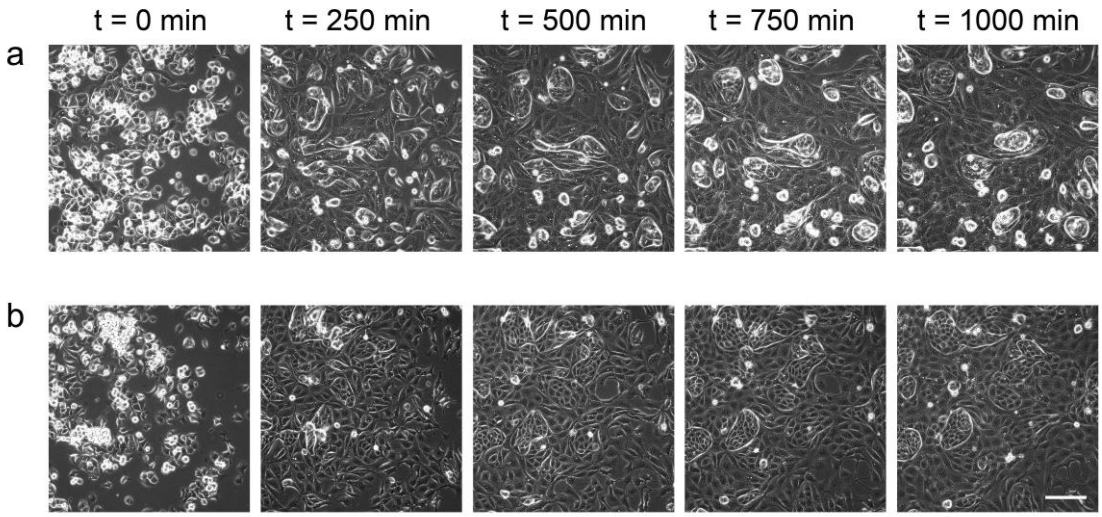

Figure 7-7| Time evolution of a co-culture assay for Eph-ephrin cells under a blebbistastin + thymidine treatment (bottom) against an assay of thymidine treated cells (top).

7.8 Segmentation of control vs. blebbistatin treated boundaries

We wanted to quantify the jamming between a control boundary and a boundary under blebbistatin treatment in which deformation waves did not arise. For that, we did a population study by segmenting all cells on each epithelium for different phases of the boundary formation.

We segmented cells following a custom-made software after applying the method described in Materials and Methods, 3.2.7, to boundary-engaged epithelia. The software was based on a sequence of feature recognition commands (Figure 7-8).

To asses if the segmentation was accurate, we did a semi-manual segmentation of one experiment as a training set. We compared the distribution histograms for the different parameters of interest on the training and the automatic databases. Results are shown in Figure 7-9. It can be seen that small cell areas are overestimated with the automatic method. We decided to discard area values under 30 μm^2, which mostly corresponded to segmentation of small features of the images rather than cells and were biasing the statistics.

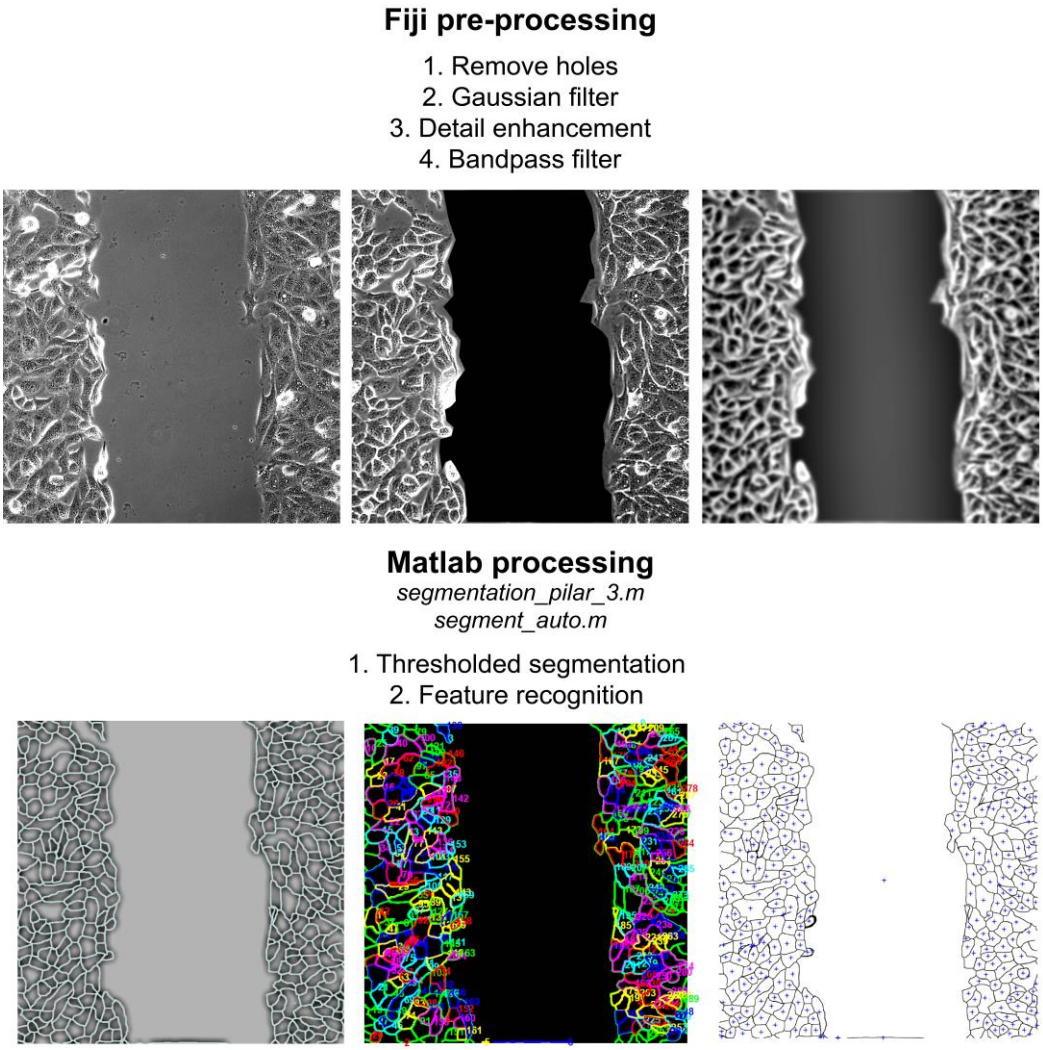

Figure 7-8| Sequence of segmentation-aimed processing of the boundary buildup.

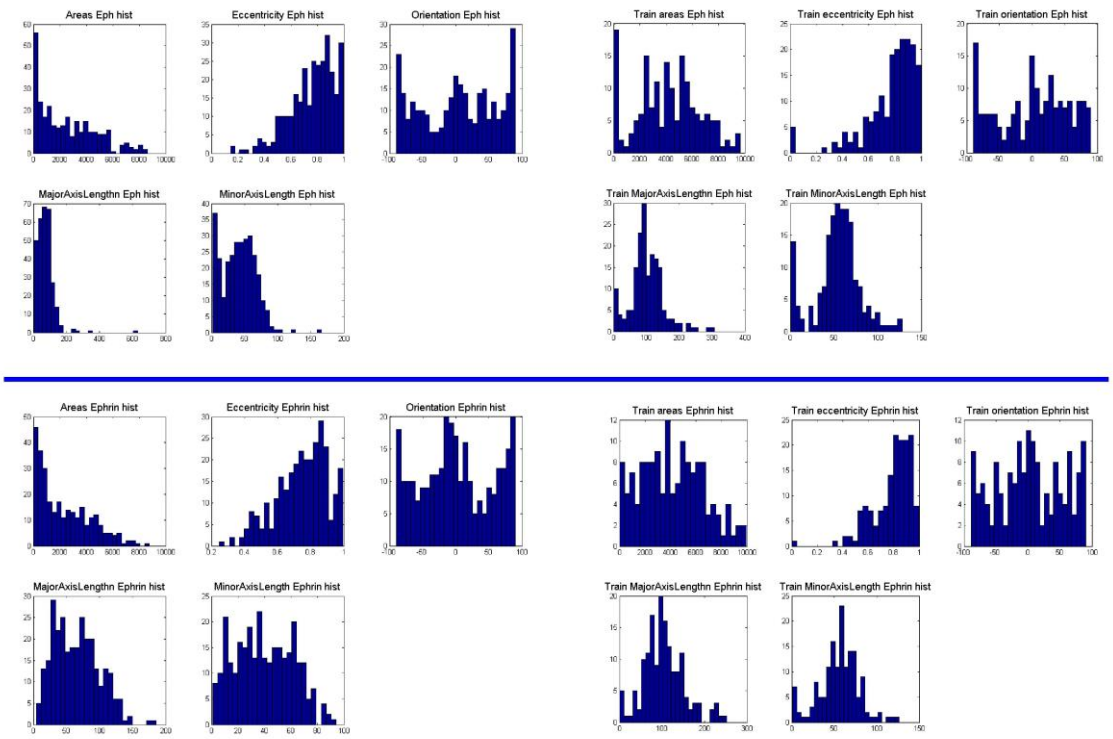

Figure 7-9| Upper side: statistics for an automatically segmented image with our custom software. Lower side: statistics for a semi-manually segmented image as a test.

We found out that for the control case cell area was decreased from an average of 317±9 μm^2 to 175±3 μm^2 for Eph cells and from an average of 286±5 μm^2 to 248±5 μm^2 for ephrin cells. The eccentricity, major axis and minor axis length concomitantly decreased. Orientation, though, remained barely unchanged in average throughout time. Further, the number of cells was increased to a three-fold for Eph cells, and doubled for ephrin cells (Figure 7-10).

Reversely, under a blebbistatin treatment none of the parameters (i.e. Area, eccentricity, orientation, major axis length, minor axis length, number of cells) underwent a significant change during time (Figure 7-11).

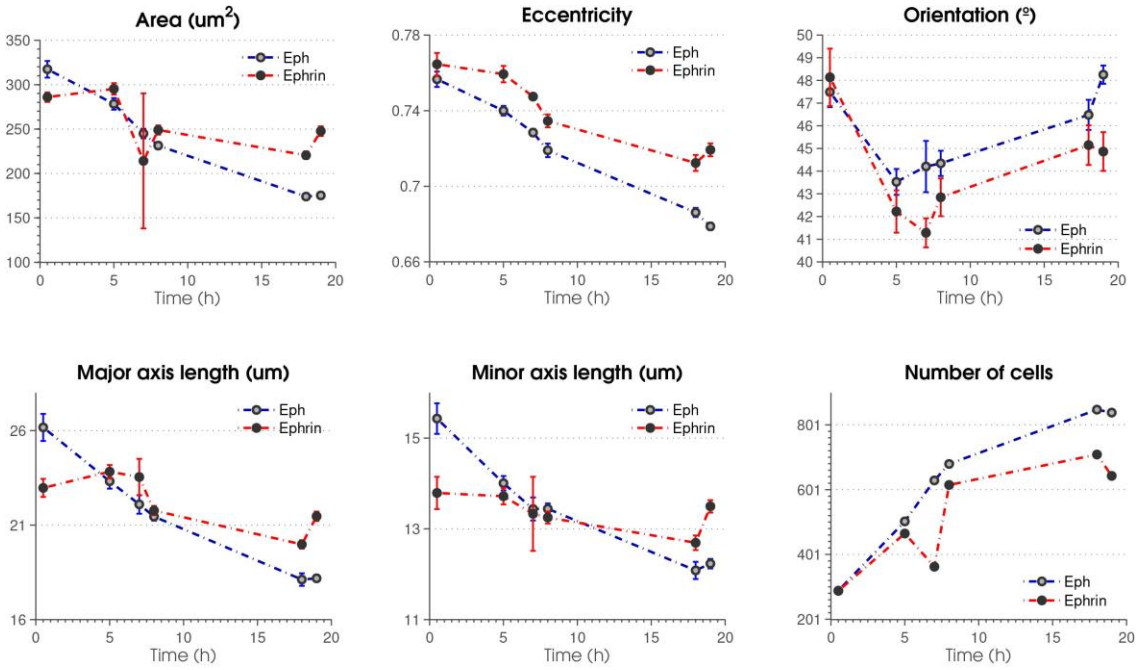

Figure 7-10| Time evolution of Area, Eccentricity, Orientation, Major axis length, Minor axis length and Number of cells for Eph and ephrin population during boundary buildup.

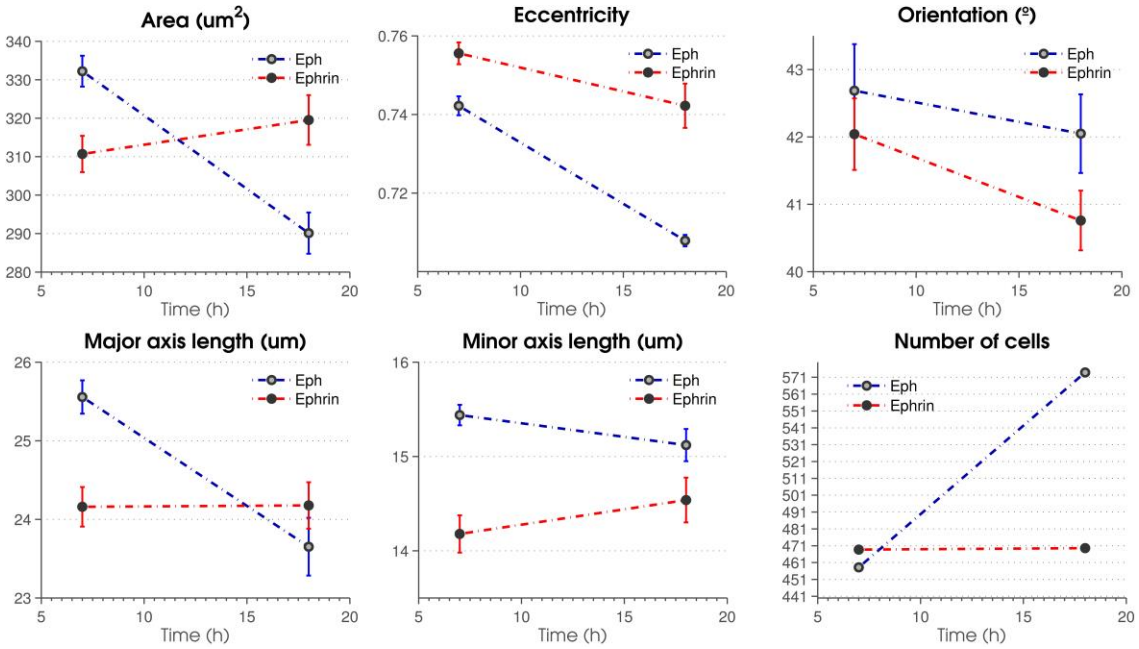

Figure 7-11| Time evolution of Area, Eccentricity, Orientation, Major axis length, Minor axis length and Number of cells for blebbistatin treated Eph and ephrin population during boundary buildup.

7.9 Boundary curvature evolution

We tracked the curvature evolution of Eph and ephrin side of the boundary with time during boundary formation. The initial curvature was corrected in time, during the interplay of Eph and ephrin populations before the boundary stabilized (Figure 7-12, Figure 7-13). Reversibly, we observed that under blebbistatin treatment the curvature was not corrected and remained unchanged over the experiment (Figure 7-14, Figure 7-15).

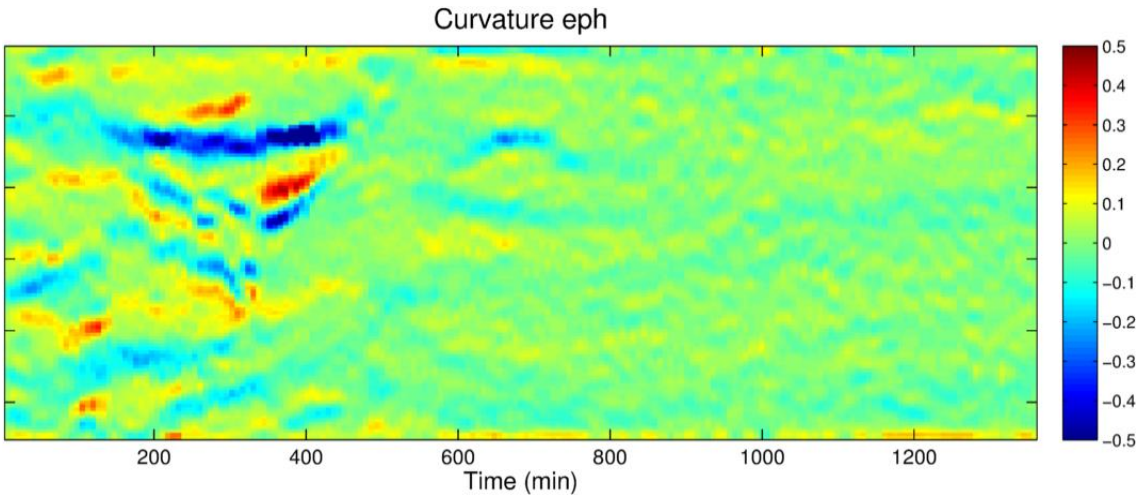

Figure 7-12| Curvaturfe evolution of Eph epithelium during control boundary formation (left to right).

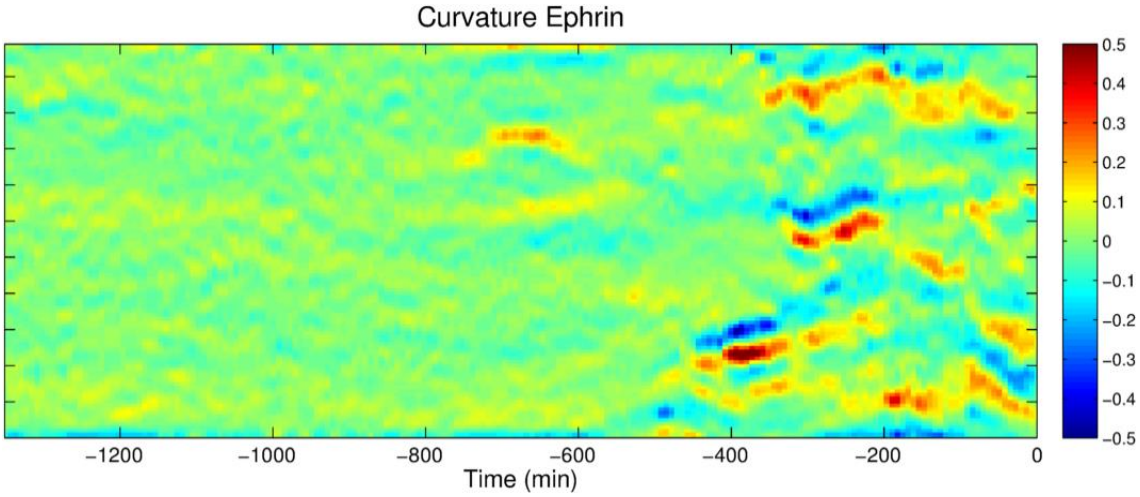

Figure 7-13| Curvature evolution of ephrin epithelium during control boundary formation (right to left).

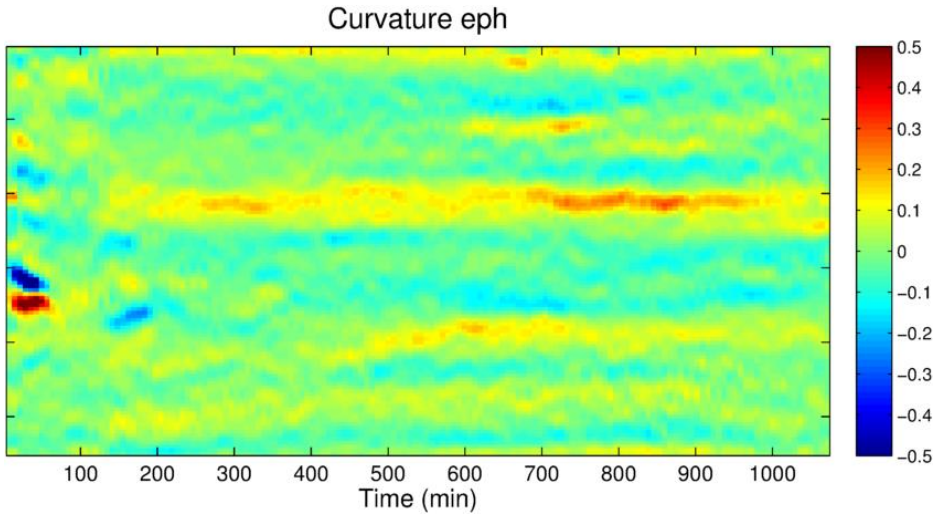

Figure 7-14| Curvature evolution of Eph epithelium during boundary formation under blebbistatin treatment (left to right).

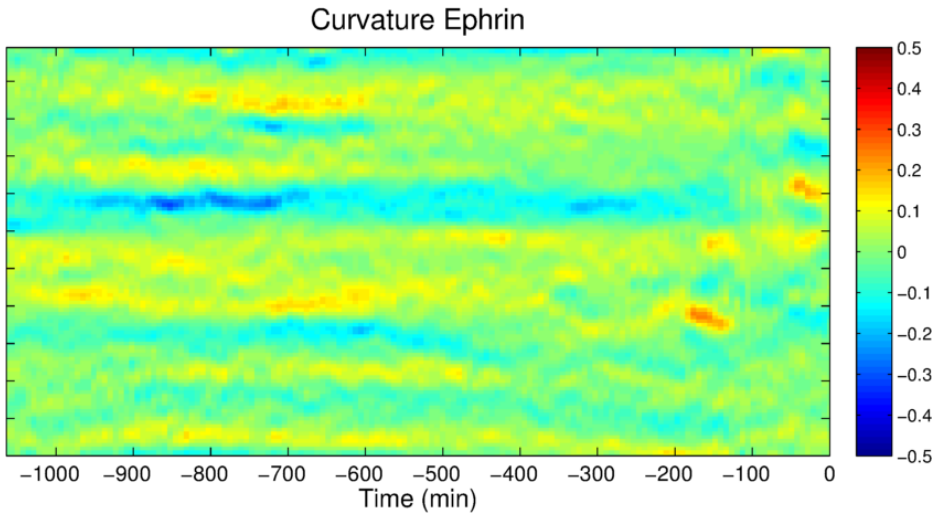

Figure 7-15| Curvature evolution of ephrin epithelium during boundary formation under blebbistatin treatment (right to left).

7.10 Eph-ephrin local mechanism discussion

7.10.1 Boundary formation at high spatial and temporal resolution

We aimed at studying the dynamics of boundary buildup at short temporal and spatial scales, in order to better understand the local mechanics behind the collective phenomenon.

One prevalent observation was the cycles of contact-repulsion. Eph receptors are locally activated wherever neighboring ephrin-expressing cells make contact. This triggers dynamic membrane ruffling at the Eph–ephrin contact sites, which are known to be Rac-regulated (Marston, 2003). The contact between Eph-expressing and ephrin-expressing cells is destabilized by different proposed mechanisms (Introduction,1.2). Subsequently, the receptor and ligand cells retract from one another. The following cell retraction events are dependent on actin polymerization (Marston, 2003), which in turn is dependent on Rac signalling within the receptor-expressing cells.

This course of action is reminiscent of the CIL (contact inhibition of locomotion) sequence, which occurs when a cell stops migrating in a particular direction upon contact with another cell (Batson, 2013). In the context of CIL, activation of RhoA at the cell contact site could lead to the collapse of membrane protrusions and a change in cell polarity, thereby directing migration away from the cell contact (Batson, 2013). Recent work has shown that RhoA/ROCK signalling is required for CIL in chick heart fibroblasts (Kadir, 2011), which is known to mediate actin contractility. However, these cells exhibited almost normal CIL properties following inhibition of myosin contractility by treatment with blebbistatin, in agreement with what we observed in our assay. Instead, it was found that the RhoA/ROCK pathway mediates CIL by regulating the microtubule

cytoskeleton (Kadir, 2011). This observation could inspire future experiments. They would include further studying the role of microtubules stabilization in the formation of Eph-ephrin epithelial boundaries.

CIL is a very well-known mechanism at the single cell-cell level, but it is still poorly understood in the context of directional collective migration. In the context of chemotactic mesenchymal-like cells, Theveneau et. al. (Theveneau, 2010) have observed that CIL mediated by inhibition of protrusion and Rac1 at the leader cells in turn promotes protrusion and activation of Rac1 at the free edge, creating cycles of directional collective cell migration (run) and timely tumbling.

In the context of epithelial boundaries, homotypic junctions between neighboring cells would impede to a great extend Rac1 repolarization of cells in the opposite direction. Instead, we hypothesize that cycles of Rac1 recruitment are needed for the extension of lamellipodia promoting contact among Eph- and ephrin-expressing cells at the free edge. As both epithelia approach, the cycles of contact of Eph-ephrin happen more often, leading to a higher inhibition of Rac1 at the free edge of cells engaged in the boundary. This could in turn promote the recruitment of Rock/RhoA at these edges, stabilizing them by fencing the available actin in bundles. Given that all cells at the boundary are exposed to the same repulsive cycles and provided that homotypic cells are mechanically connected through adherens junctions, these actin bundles end up connecting all cells lining the boundary to create a supra-cellular stabilizing structure. As a consequence, the extension of lamellipodia is diminished.

7.10.2 Boundary displacement in time

During the Eph-ephrin experiments it was observed that the boundary position evolved towards the Eph epithelium, suggesting that the ephrin

epithelium held a more invasive phenotype. Receptor and ligand playing a different role on each side of the boundary was no surprise, given that the Eph-ephrin interaction is not only a bi-directional signalling pathway, but also an asymmetrical one (Pasquale, 2008; Cowan & Henkemeyer, 2002).

Mainly, Eph cells were prone to retract upon ephrin cell contact and to build strong cell-cell homotypic junctions. On the other hand, ephrin cells had a looser behavior. They tended to maintain their polarization, and to invade the Eph epithelium.

We wondered if this differential reorganization and compaction was paralleled by any 3D effect. In agreement with the previous observation, the strong Eph epithelium compaction in XY was paralleled by an expansion in Z. Surprisingly, 19 hours after stencil release the focal plane of the Eph epithelium was 7.7 µm higher than the ephrin focal plane.

These observations are in line with what Barrios et. al. observed in their study of somite morphogenesis (Barrios, 2003). In their study, the activation of EphA4 led to the cell-autonomous acquisition of a columnar morphology and apical redistribution of beta-catenin, aspects of epithelialization characteristic of cells at somite boundaries. They also observed that activation of EphA4 leads to the non-autonomous acquisition of columnar morphology and polarized relocalization of the centrosome and nucleus in cells on the opposite side of the forming boundary.

Our analysis highlights the importance of the Eph-ephrin contact in the formation of a fully functional boundary, but also points at the differential role of each of the moieties. In the context of our study, it would be interesting to develop further experiments to disentangle the specific role of EphB2 and ephrinB1 in order to fully explain the displacement of the boundary in time.

8 BIBLIOGRAPHY

Adams R. H., F. Diella, S. Hennig, F. Helmbacher, U. Deutsch, R. Klein (2001). The Cytoplasmic Domain of the Ligand EphrinB2 Is Required for Vascular Morphogenesis but Not Cranial Neural Crest Migration, Cell 104(1): 57-69.

Alberts B., A. Johnson, J. Lewis, D. Morgan, M. Raff, K. Roberts, P. Walter (2002). Molecular Biology of the cell, Garland Science.

Amack J. D., M.L. Manning (2012). Knowing the boundaries: extending the differential adhesion hypothesis in embryonic cell sorting, Science 338: 212–215.

Angelini, T.E. et al. (2011). Glass-like dynamics of collective cell migration. Proceedings of the National Academy of Sciences, 108(12): 4714–4719.

Anon E., Serra-Picamal X., Hersen P., Gaurhier N. C., Sheetz M. P., Trepat X., Ladoux B., (2012). Cell crawling mediates collective cell migration to close undamaged epithelial gaps. PNAS 109:27.

Arvanitis D., A. Davy (2008). Eph/ephrin signaling: networks, Genes & Dev 22: 416-429.

Baker M. (2012). Direct protein control, Nature Methods (Technology Feature) 9(5): 443-445.

Banerjee S., Utuje K. J. C., Marchetti M. C. (2015). Propagating Stress Waves During Epithelial Expansion. Physical Review Letters 114: 228101.

Barrios A., Poole R. J., Durbin L., Brennan C., Holder N., Wilson S. W.(2003). Eph/Ephrin Signaling Regulates the Mesenchymalto-Epithelial Transition of the Paraxial Mesoderm during Somite Morphogenesis. Current Biology, 13: 1571-1582.

Bartley, T.D., Hunt, R.W., Welcher, A.A., Boyle, W.J., Parker, V.P., Lindberg, R.A., Lu, H.S., Colombero, A.M., Elliott, R.L., Guthrie, B.A., et al. (1994). B61 is a ligand for the ECK receptor protein-tyrosine kinase, Nature 368: 558-560.

Batlle E., D. G. Wilkinson (2012). Molecular Mechanisms of Cell Segregation and Boundary Formation in Development and Tumorigenesis, Cold Spring Harbor Perspectives in Biology 4(1): a008227.

Batson J., Astin J.W., Nobes C.D. (2013). Regulation of contact inhibition of locomotion by Eph–ephrin signalling, Journal of Microscopy 251,3: 232-241.

Bazellieres E., V. Conte, A. Elosegui-Artola, X. Serra-Picamal, M. Bintanel-Morcillo, P. Roca-Cusachs, J. J. Muñoz, M. Sales-Pardo, R. Guimerà, X. Trepat (2015). Control of cell–cell forces and collective cell dynamics by the intercellular adhesome, Nature Cell Biology 17: 409-420.

Beckmann, M.P., Cerretti, D.P., Baum, P., Vanden Bos, T., James, L., Farrah, T., Kozlosky, C., Hollingsworth, T., Shilling, H., Maraskovsky, E., et al. (1994). Molecular characterization of a family of ligands for eph-related tyrosine kinase receptors, EMBO J. 13: 3757-3762.

Bergert M., A. Erzberger, R. A. Desai, I. M. Aspalter, A. C. Oates, G. Charras, G. Salbreux, E. k. Paluch (2015). Force transmission during adhesion-independent migration, Nature Cell Biology, Letter 17: 524-529.

Bi D., Lopez J. H., Schwarz J. M., Manning M. L. (2015). A density-independent rigidity transition in biological tissues. Nature Physics 11: 1074–1079.

Bi, D., J. Zhang, B. Chakraborty & R. P. Behringer (2011). Jamming by shear, Nature 480: 335–358.

Blanch C. (2015). Mechanical instabilities and dynamics of living matter, Doctorate Dissertation (UB), chapter 4.

Bradamante S., L. Barenghi, J. A. M. Maier (2014). Stem Cells toward the Future: The Space Challenge, Life (Review) 4: 267-280.

Brodland GW. (2002). The Differential Interfacial Tension Hypothesis (DITH): a comprehensive theory for the self-rearrangement of embryonic cells and tissues, Journal of Biomechanical Engineering 124(2): 188-197.

Brugués A., E. Anon, V. Conte, J. H. Veldhuis, M. Gupta, J. Colombelli, J. J. Muñoz, G. W. Brodland, B. Ladoux, X. Trepat (2014). Forces driving epitelial wound healing, Nature Physics 10: 683-690.

Bush J. O., P. Soriano (2010). Ephrin-B1 forward signaling regulates craniofacial morphogenesis by controlling cell proliferation across Eph–ephrin boundaries, GENES & DEVELOPMENT (Cold Spring Harbor Laboratory Press) 24:2068–2080.

Calzolari S., Terriente J., Pujades C. (2014). Cell segregation in the vertebrate hindbrain relies on actomyosin cables located at the interhombomeric boundaries. The EMBO Journal 33:686-701.

Casares L., R. Vincent, D. Zalvidea, N. Campillo, D. Navajas, M. Arroyo, X. Trepat (2015). Hydraulic fracture during epitelial stretching, Nature Materials 14: 343-351.

Cayuso J., Xu Q., Wilkinson D. G. (2015). Mechanisms of boundary formation by Eph receptor and ephrin signaling. Developmental Biology: Cell Adhesion in Development (review), 401 (1): 122-131.

Cheng, H.J. Flanagan, J.G. (1994). Identification and cloning of ELF-1, a developmentally expressed ligand for the Mek4 and Sek receptor tyrosine kinases, Cell 79: 157-168.

Colombelli J., A. Besser, H. Kress, E. G. Reynaud, P. Girard, E. Caussinus, U. Haselmann, J. V. Small, U. S. Schwarz, E. H. K. Stelzer (2009). Mechanosensing in actin stress fibers revealed by a close correlation between force and protein localization, Journal of Cell Science 122: 1665-1679.

Cortina C., Palomo-Ponce S., Iglesias M., Fernández-Masip J. L., Vivancos A., Whissell G., Mireia Humà M., Peiró N., Gallego L., Jonkheer S., Davy A., Lloreta J., Sancho E., Batlle E. (2007). EphB-ephrin-B interactions suppress colorectal cancer progression by compartmentalizing tumor cells. Nature Genetics, 39: 1376 – 1383.

Cost A. L., P. Ringer, A. Chrostek-Grashoff, C. Grashoff (2015). How to Measure Molecular Forces in Cells: A Guide to Evaluating Genetically-Encoded FRET-Based Tension Sensors, Cellular and Molecular Bioengineering 8(1): 96-105.

Cowan C. A., Henkemeyer M. (2002). Ephrins in reverse, park and drive. Trends in Cell Biology (review), 12(7): 339-346.

Dahmann C., A. C. Oates, M. Brand (2011). Boundary formation and maintenance in tissue development, Nature Reviews Genetics 12: 43-55.

Delarue M., J. Hartung, C. Schreck, P. Gniewek, L. Hu, S. Herminghaus, O. Hallatschek (2016). Self-driven jamming in growing microbial populations, Nature Physics 12: 762–766.

DuFort C. C., M. J. Paszek, V. M. Weaver (2011). Balancing forces: architectural control of mechanotransduction, Nature Reviews Molecular Cell Biology 12: 308-319.

Duguay D., R. A. Foty, M. S. Steinberg (2003). Cadherin-mediated cell adhesion and tissue segregation: qualitative and quantitative determinants, Developmental Biology 253(2): 309-323.

Dupont S., L. Morsut, M. Aragona, E. Enzo, S. Giulitti, M. Cordenonsi , F. Zanconato, J. L. Digabel, M. Forcato , S. Bicciato, N. Elvassore & S. Piccolo (2011). Role of YAP/TAZ in mechanotransduction, Nature 474: 179-183.

Editors, 2011. News focus: mysteries of the cell, Science 334: 1046-1051.

Egea J., R. Klein (2007). Bidirectional Eph–ephrin signaling during axon guidance, Trends in Cell Biology, Cell Review 17(5): 230-238.

Fagotto F., N. Rohani, A-S. Touret, R. Li (2013). A Molecular Base for Cell Sorting at Embryonic Boundaries: Contact Inhibition of Cadherin Adhesion by Ephrin/Eph-Dependent Contractility, Developmental Cell 27(1): 72-87.

Fagotto, F. (2014). The cellular basis of tissue separation, Development (review) 141: 3303-3318.

Fink J, N. Carpi, T. Betz, A. Bétard, M. Chebah, A. Azioune, M. Bornens, C. Sykes, L. Fetler, D. Cuvelier, M. Piel (2011). External forces control mitotic spindle positioning, Nature Cell Biology 13: 771–778.

Foty R. A., C. M. Pfleger, G. Forgacs, M. S. Steinberg (1996). Surface tensions of embryonic tissues predict their mutual envelopment behavior, Development 122: 1611-1620.

Foty R. A., M. S. Steinberg (2004). Cadherin-mediated cell-cell adhesion and tissue segregation in relation to malignancy, int J Dev Biol 48(5-6): 397-409.

Foty R. A., M. S. Steinberg (2005). The differential adhesion hypothesis: a direct evaluation, Developmental Biology 278(1): 255-263.

Friedl, P., D. Gilmour (2009). Collective cell migration in morphogenesis, regeneration and cancer, Nature Reviews Molecular Cell Biology 10: 445–457.

Friedl, P., S. Alexander (2011). Cancer invasion and the microenvironment: plasticity and reciprocity, Cell 147: 992–1009.

Galizia, C.G., P. M. Lledo (2013). Mechanosensation, Neurosciences - From Molecule to Behavior: A University Textbook; Springer-Verlag.

Garcia S., E. Hannezo, J. Elgeti, J-F. Joanny, P. Silberzan, N. S. Gov (2015). Physics of active jamming during collective cellular motion in a monolayer, PNAS 112(50): 15314-15319.

Genander M., J. Holmberg, J. Frisen (2010). Ephrins negatively regulate cell proliferation in the epidermis and hair follicle, Stem Cells 28: 1196–1205.

Getsios S., A. C. Huen, K. J. Green (2004). Working out the strength and flexibility of desmosomes, Nature Reviews Molecular Cell Biology 5, 271-281.

Gibson M. C., A. B. Patel, R. Nagpal, N. Perrimon (2006). The emergence of geometric order in proliferating metazoan epithelia, Nature Letter 442: 1038-1041.

Grashoff C., B. D. Hoffman, M. D. Brenner, R. Zhou, M. Parsons, M. T. Yang, M. A. McLean, S. G. Sligar, C. S. Chen, T. Ha, M. A. Schwartz (2010). Measuring mechanical tension across vinculin reveals regulation of focal adhesion dynamics, Nature 466: 263-266.

Green J. B. A. (2008). Sophistication of cell sorting, Nature Cell Biology 10 (news and views): 375-377.

Guillot C., T. Lecuit (2013). Mechanics of epithelial tissue homeostasis and morphogenesis, Science 340(6137): 1185-1189.

Gumbiner B. M. (1996). Cell Adhesion: The Molecular Basis of Tissue Architecture and Morphogenesis, Cell Review 84(3): 345-357.

Haeger A., K. Wolf, M. M. Zegers, P. Friedl (2015). Collective cell migration: guidance principles and hierarchies, Trends in Cell Biology 25(9): 556-566.

Haeger A., M. Krause, K. Wolf, P. Friedl (2014). Cell jamming: Collective invasion of mesenchymal tumor cells imposed by tissue confinement, Biochimica et Biophysica Acta 1840: 2386–2395.

Harburger D. S., D. A. Calderwood (2009), Integrin signalling at a glance, Journal of Cell Science 122: 159-163.

Herath N. I., Boyd A. W. (2010). The role of Eph receptors and ephrin ligands in colorectal cancer, Int. J. Cancer 126 (9): 2003-2011.

Heussinger, C. & Barrat, J. L. (2009). Jamming transition as probed by quasistatic shear flow, Phys. Rev. Lett. 102: 218303.

Himanen J. P., D. B. Nikolov (2003). Eph signaling: a structural view, Trends Neurosci. 26(1): 46-51.

Himanen J.P., N. Saha, D.B. Nikolov (2007). Cell-cell signaling via Eph receptors and ephrins, Curr. Opin. Cell Biol., 19: 534-542.

Hirai H., Maru Y., Hagiwara K., Nishida J., Takaku F. (1987). A novel putative tyrosine kinase receptor encoded by the *Eph* gene, Science 238: 1717-1720.

Hirata E., D. Park, E. Sahai (2014). Retrograde flow of cadherins in collective cell migration, Nature Cell Biology 16: 621-623.

Hoffman, B.D., C. Grashoff, M.A. Schwartz (2011). Dynamic molecular processes mediate cellular mechanotransduction, Nature 475: 316–323.

Holmberg J., A. Armulik, K.A. Senti, K. Edoff, K. Spalding, S. Momma, R. Cassidy, J. G. Flanagan, J. Frisen (2005). Ephrin-A2 reverse signaling negatively regulates neural progenitor proliferation and neurogenesis, Genes Dev 19: 462–471.

Hutson M. S., G. W. Brodland, J. Yang, D. Viens (2008). Cell Sorting in Three Dimensions: Topology, Fluctuations, and Fluidlike Instabilities, PRL 101: 148105.

Iskratsch, T., H. Wolfenson, M.P. Sheetz (2014). Appreciating force and shape - the rise of mechanotransduction in cell biology, Nature Reviews Molecular Cell Biology 15(12): 825-833.

Jaalouk, D.E., J. Lammerding (2009). Mechanotransduction gone awry, Nat. Rev. Mol. Cell Biol. 10: 63–73.

Janmey P. A., C. A. McCulloch (2007). Cell Mechanics: Integrating Cell Responses to Mechanical Stimuli, Annu. Rev. Biomed. Eng. 9:1–34.

Janmey, P.A., R.T.Miller (2011). Mechanisms of mechanical signaling in development and disease, J. Cell Sci. 124: 9–18.

Jülich D, A.P. Mould, E. Koper, S.A. Holley (2009). Control of extracellular matrix assembly along tissue boundaries via Integrin and Eph/Ephrin signaling, Development 136(17): 2913-21.

Kadir, S., Astin, J.W., Tahtamouni, L., Martin, P., Nobes, C.D. (2011) Microtubule remodelling is required for the front-rear polarity switchduring contact inhibition of locomotion. J. Cell Sci. 124: 2642–2653.

Kaminski A., G. R. Fedorchak, J. Lammerding (2014). The Cellular Mastermind (?) - Mechanotransduction and the Nucleus, Progress in Molecular Biology and Translational Science: Mechanotransduction 126:157–203.

Kandow C. E., P. C. Georges, P. A. Janmey, K. A. Beningo (2007). Polyacrylamide Hydrogels for Cell Mechanics: Steps Towards Optimization and Alternative Uses, Methods in Cell Biology 83: 29–46.

Kania A., Klein R. (2016). Mechanisms of ephrin–Eph signalling in development, physiology and disease. Nature Reviews Molecular Cell Biology, 17: 240–256.

Kiehart, D.P., C.G. Galbraith, K.A. Edwards, W.L. Rickoll, R.A. Montague (2000). Multiple forces contribute to cell sheet morphogenesis for dorsal closure in Drosophila, J. Cell Biol. 149:471–490.

Kim D., P. K. Wong, J.Park, A. Levchenko, Y. Sun (2009). Microengineered Platforms for Cell Mechanobiology, Annual Review of Biomedical Engineering 11: 203-233.

Kim J. H., X. Serra-Picamal, D. T. Tambe, E. H. Zhou, C. Y. Park, M. Sadati, J-A. Park, R. Krishnan, B. Gweon, E. Millet, J. P. Butler, X. Trepat, J. J. Fredberg (2013). Propulsion and navigation within the advancing monolayer sheet, Nature Materials 12: 856-863.

Kleinman H. K., D. Philp, M. P. Hoffman (2003). Role of the extracellular matrix in morphogenesis, Current Opinion in Biotechnology 14(5): 526-532.

Krieg M., Y. Arboleda-Estudillo, P.-H. Puech, J. Käfer, F. Graner, D. J. Müller, C. P. Heisenberg (2008). Tensile forces govern germ-layer organization in zebrafish, Nature Cell Biology 10: 429-436.

Krishnan, R., C. Y. Park, Y. C. Lin, J. Mead, R. T. Jaspers, X. Trepat, G. Lenormand, D. Tambe, A. V. Smolensky, A. H. Knoll, J. P. Butler, J. J. Fredberg (2009). Reinforcement versus fluidization in cytoskeletal mechanoresponsiveness, PLoS ONE 4: e5486.

Krull C. E., R. Lansford, N. W. Gale, A. Collazo, C. Marcelle, G. D. Yancopoulos, S. E. Fraser and M. Bronner-Fraser (1997). Interactions of Eph-related receptors and ligands confer rostrocaudal pattern to trunk neural crest migration, Current Biology 7(8): 571–580.

Landsberg K. P., R. Farhadifar, J. Ranft, D. Umetsu, T. J. Widmann, T. Bittig, A. Said, F. Jülicher, C. Dahmann (2009). Increased Cell Bond Tension Governs Cell Sorting at the Drosophila Anteroposterior Compartment Boundary, Cell 19(22):1950-1955.

Laussu J., A. Khuong, J. Gautrais, A. Davy (2014). Beyond boundaries - Eph:ephrin signaling in neurogenesis, SPECIAL FOCUS: EPHRIN SIGNALING: REVIEWS; Cell Adhesion & Migration 8(4).

Lecuit T., P-F. Lenne (2007). Cell surface mechanics and the control of cell shape, tissue patterns and morphogenesis, Nature Reviews Molecular Cell Biology 8: 633-644.

Legant W. R., C. K. Choi, J. S. Miller, L. Shao, L. Gao, E. Betzig, C. S. Chen (2013). Multidimensional traction force microscopy reveals out-of-plane rotational moments about focal adhesions, PNAS 110(3): 881-886.

Lemmon C. A., N. J. Sniadecki, S. A. Ruiz, J. L. Tan, L. H. Romer, C. S. Chen (2005). Shear Force at the Cell-Matrix Interface: Enhanced Analysis for Microfabricated Post Array Detectors, Mechanics & chemistry of biosystems : MCB. 2(1):1-16.

Levental I., Georges P.C., Janmey P.A. (2007). Soft biological materials and their impact on cell function, Soft Matter 3: 299-306.

Liang, C.C., Park, A.Y., Guan, J.-L. (2007). In vitro scratch assay: a convenient and inexpensive method for analysis of cell migration in vitro. Nature Protocols, 2(2): 329–333.

Lin S., B. Wang, S. Getsios (2012). Eph/ephrin signaling in epidermal differentiation and disease, Semin Cell Dev Biol. 23(1): 92-101.

Lisabeth E. M., G. Falivelli, E. B. Pasquale (2013). Eph Receptor Signaling and Ephrins, Cold Spring Harb Perspect Biol; 5:a009159.

Lodish, H., A. Berk, S. L. Zipursky, P. Matsudaira, D. Baltimore, J. Darnell, W.H. Freeman (2000). Molecular Cell Biology, 4th edition.

Maitre J. L., , H. Berthoumieux, S.F. Krens, G. Salbreux, F. Julicher, E. Paluch, C.P. Heisenberg (2012). Adhesion functions in cell sorting by mechanically coupling the cortices of adhering cells. Science, 338: 253–256.

Maître J. L., C. P. Heisenberg (2013). Three Functions of Cadherins in Cell Adhesion, Current Biology 23(14): R626-R633.

Majmudar, T. S. & Behringer, R. P. (2005). Contact force measurement and stress-induced anisotropy in granular materials, Nature 435: 1079–1082.

Marston D. J., S. Dickinson, C. D. Nobes (2003). Rac-dependent trans-endocytosis of ephrinBs regulates Eph–ephrin contact repulsion, Nature Cell Biology 5: 879-888.

Matsubayashi, Y., Razzell, W. & Martin, P. (2011). 'White wave' analysis of epithelial scratch wound healing reveals how cells mobilise back from the leading edge in a myosin-II-dependent fashion. Journal of Cell Science. 124: 1017–1021.

Mattsson, J., H. M. Wyss, A. Fernandez-Nieves, K. Miyazaki, Z. Hu, D. R. Reichman, D. A. Weitz (2009). Soft colloids make strong glasses, Nature 462: 83–86.

McMillen P., S. A. Holley (2015). Integration of cell–cell and cell–ECM adhesion in vertebrate morphogenesis, Current Opinion in Cell Biology: cell adhesion and migration 36: 48-53.

McMillen P., Holley S. A. (2015). The tissue mechanics of vertebrate body elongation and segmentation, Current Opinion in Genetics & Development 32:106–111.

Mellitzer G., Q. Xu, D. G. Wilkinson (1999). Eph receptors and ephrins restrict cell intermingling and communication, Nature 400: 77-81.

Mese G., G. Richard, T. W. White (2007). Gap Junctions: Basic Structure and Function, Journal of Investigative Dermatology 127: 2516–2524.

Miao H. and B. Wang (2009). Eph/ephrin signaling in epithelial development and homeostasis, Int J Biochem Cell Biol. 41(4): 762–770.

Millán, J., R. J. Cain, N. Reglero-Real, C. Bigarella, B. Marcos-Ramiro, L. Fernández-Martín, I. Correas, A. J. Ridley (2010). Adherens junctions connect stress fibres between adjacent endothelial cells, BMC Biology 8:11.

Monier, B., A. Pélissier-Monier, A. H. Brand, B. Sanson (2010). An actomyosin-based barrier inhibits cell mixing at compartmental boundaries in Drosophila embryos, Nature Cell Biology Letters, 12(1): 60-65.

Nagafuchi A. (2001). Molecular architecture of adherens junctions, current opinion in cell biology 13(5): 600-603.

Niessen C. M., B. M. Gumbiner (2002). Cadherin-mediated cell sorting not determined by binding or adhesion specificity, JCB 156(2): 389-400.

Nievergall E., M. Lackmann, P. W. Janes (2011). Eph-dependent cell-cell adhesion and segregation in development and cancer. Cell Mol Life Sci 69:1813-42.

Ninomiya H., R. David, E. W. Damm, F. Fagotto, C. M. Niessen, R. Winklbauer (2011). Cadherin-dependent differential cell adhesion in Xenopus causes cell sorting in vitro but not in the embryo , Journal of Cell Science 125: 1877–1883.

Nirmitha I., H. and A. W. Boyd (2009). The role of Eph receptors and ephrin ligands in colorectal cancer, International Journal of Cancer 126(9): 2003-11.

Nnetu, K.D., Knorr, M., Strehle, D. (2012). Directed persistent motion maintains sheet integrity during multi-cellular spreading and migration. Soft Matter 8(26): 6913-6921.

Noren N.K., G. Foos, C.A. Hauser, E.B. Pasquale (2006). The EphB4 receptor suppresses breast cancer cell tumorigenicity through an Abl–Crk pathway, Nat Cell Biol 8: 815–825.

Nose A., A. Nagafuchi, M. Takeichi (1988). Expressed recombinant cadherins mediate cell sorting in model systems, Cell 54(7): 993-1001.

Oliver, M., T. Kova´ts, S. Mijailovich, J. Butler, J. Fredberg, G. Lenormand (2010). Remodeling of integrated contractile tissues and its dependence on strain-rate amplitude, Physical Review Letters 105: 158102.

Palmer A., R. Klein (2003). Multiple roles of ephrins in morphogenesis, neuronal networking, and brain function, Genes & Dev. 17:1429-1450.

Park J-A., J.H. Kim, D. Bi (2015). Unjamming and cell shape in the asthmatic airway epithelium, Nat. Mater. 14: 1040–1048.

Park J-A., L. Atia, J. A. Mitchel, J. J. Fredberg, J. P. Butler (2016). Collective migration and cell jamming in asthma, cancer and development, Journal of Cell Science (commentary) 0: 1-9.

Partridge M.A., E. E. Marcantonio (2006). Initiation of Attachment and Generation of Mature Focal Adhesions by Integrin-containing Filopodia in Cell Spreading, Molecular Biology of the Cell 17(10): 4237–4248.

Pasquale E. B. (2010). Eph receptors and ephrins in cancer: bidirectional signalling and beyond. Nature Reviews Cancer 10: 165-180.

Pasquale E.B. (2005). Eph receptor signalling casts a wide net on cell behavior, Nat Rev Mol Cell Biol. 6(6):462-75.

Pasquale, E. B. (2008). Eph-Ephrin Bidirectional Signaling in Physiology and Disease, Cell Review 133(1): 38-52.

Pawlizak S., A.W. Fritsch, S. Grosser D. Ahrens, T. Thalheim, S. Riedel, T. R. Kießling, L. Oswald, M. Zink, M. L. Manning, J. A. Käs (2015). Testing the differential adhesion hypothesis across the epithelial-mesenchymal transition, New. J. Phys. 17: 083049.

Pegoraro A. F., J. J. Fredberg, J-A. Park (2016). Review Article Problems in biology with many scales of length: Cell–cell adhesion and cell jamming in collective cellular migration, Experimental Cell Research 343: 54–59.

Poh Y-C., J. Chen, Y. Hong, H. Yi, S. Zhang, J. Chen, D. C. Wu, L. Wang, Q. Jia, R. Singh, W. Yao, Y. Tan, A. Tajik, T. S. Tanaka, N. Wang (2014). Generation of organized germ layers from a single mouse embryonic stem cell, Nature Communications 5:4000.

Radjai, F., M. Jean, J. J. Moreau & S. Roux (1996). Force distribution in dense two-dimensional granular systems, Phys. Rev. Lett. 77: 274–277.

Rauzi M., P. F. Lenne (2015). Probing Cell Mechanics with Subcellular Laser Dissection of Actomyosin Networks in the Early Developing Drosophila Embryo, Tissue Morphogenesis; Methods in Molecular Biology 1189: 209-218.

Ravasio A., I. Cheddadi, T. Chen, T. Pereira, H. Ting Ong, C. Bertocchi, A. Brugues, A. Jacinto, A. J. Kabla, Y. Toyama, X. Trepat, N. Gov, L. Neves de Almeida, B. Ladoux (2015). Gap geometry dictates epithelial closure efficiency, Nature Communications 6: 7683.

Redies C., M. Takeichi (1996). Cadherins in the developing central nervous system: an adhesive code for segmental and functional subdivisions, Developmental Biology 180(2): 413-423.

Reffay M., M. C. Parrini, O. Cochet-Escartin, B. Ladoux, A. Buguin, S. Coscoy, F. Amblard, J. Camonis, P. Silberzan (2014). Interplay of RhoA and mechanical forces in collective cell migration driven by leader cells, Nature cell biology 16: 3.

Reintsch, W.E., Habring-Mueller, A., Wang, R.W., Schohl, A., and Fagotto, F. (2005). Beta-Catenin controls cell sorting at the notochord-somite boundary independently of cadherin-mediated adhesion, J. Cell Biol. 170: 675–686.

Ricard J., J. Salinas, L. Garcia, D. J. Liebl (2006). EphrinB3 regulates cell proliferation and survival in adult neurogenesis, Mol Cell Neurosci 31: 713–722.

Rohani, N., Canty, L., Luu, O., Fagotto, F., Winklbauer, R. (2011). EphrinB/ EphB signaling controls embryonic germ layer separation by contact-induced cell detachment, PLoS Biol. 9: e1000597.

Röper K. (2013). Supracellular actomyosin assemblies during development, Bioarchitecture 3(2): 45-49.

Sadati M., N. T. Qazvini, R. Krishnan, C. Y. Park, J. J. Fredberg (2013). Collective migration and cell jamming, Differentiation 86: 121–125.

Saha N., J. P. Himanen, D. B. Nikolov (2007). Cell-Cell Signaling via Eph Receptors and Ephrins, Curr Opin Cell Biol. 19(5): 534-542.

Sasai Y. (2013). Next-Generation Regenerative Medicine: Organogenesis from Stem Cells in 3D Culture, cell stem cell (perspective) 12(5): 520-530.

Schall, P., D. A. Weitz, F. Spaepen (2007). Structural rearrangements that govern flow in colloidal glasses, Science 318: 1895–1899.

Schötz, E-M., R. D. Burdine, F. Jülicher, M. S. Steinberg, C-P. Heisenberg, R. A. Foty (2008). Quantitative differences in tissue surface tension influence zebrafish germ layer positioning, HFSP Journal 2(1): 42–56.

Segre, P.N., V. Prasad, A. B. Schofield, D. A. Weitz (2001). Glasslike kinetic arrest at the colloidal-gelation transition, Physical Review Letters 86: 6042–6045.

Serra-Picamal X., Conte V., Sunyer R., Muñoz J.J., Trepat X. (2015). Methods in Cell Biology 25:309-330. Biophysical Methods in Cell Biology: chapter 17.

Serra-Picamal, X., Conte V., Vincent R., Anon E., Tambe D. T., Bazellieres E., Butler J. P., Fredberg J. J., Trepat X. (2012). Mechanical waves during tissue expansion. Nature Physics 8: 628–634.

Solanas G., C. Cortina, M. Sevillano, E. Batlle (2011). Cleavage of E-cadherin by ADAM10 mediates epithelial cell sorting downstream of EphB signaling, Nature Cell Biology 13: 1100-1107.

Souza N. (2014). Tiny tools to measure force, Nature Methods 11(1): Methods to Watch (Special Feature).

Steinberg M. S. (1963). Reconstruction of Tissues by Dissociated Cells, Science 141 (3579): 401-408.

Style R. W., R. Boltyanskiy, G. K. German, C. Hyland, C. W. MacMinn, A. F. Mertz, L. A. Wilen, Y. Xuc, E. R. Dufresne (2014). Traction force microscopy in physics and biology, Soft Matter 10: 4047-4055.

Sugimura K., S. Ishihara (2013). The mechanical anisotropy in a tissue promotes ordering in hexagonal packing, Development 140: 4091-4101.

Takeichi M. (2014). Dynamic contacts: rearranging adherens junctions to drive epithelial remodeling, Nature Reviews Molecular Cell Biology 15: 397–410.

Tambe D. T., C. C. Hardin, T. E. Angelini, K. Rajendran, C. Y. Park, X. Serra-Picamal, E. H. Zhou, M. H. Zaman, J. P. Butler, D. A. Weitz, J. J. Fredberg, X. Trepat (2011). Collective cell guidance by cooperative intercellular forces, Nature Materials 10: 469-475.

Tambe D. T., Fredberg J. J. (2015). And I hope you like jamming too. New Journal of Physics, 17: 091001.

Tan J. L., J. Tien, D. M. Pirone, D. S. Gray, K. Bhadriraju, C. S. Chen (2003). Cells lying on a bed of microneedles: An approach to isolate mechanical force, PNAS 100(4): 1484-1489.

Tepass U., D. Godt, R. Winklbauer (2002). Cell sorting in animal development: signalling and adhesive mechanisms in the formation of tissue boundaries, Current Opinion in Genetics & Development 12: 572-582.

Theveneau E., Marchant L., Kuriyama S., Gull M., Moepps B., Parsons M., Mayor R. (2010). Collective Chemotaxis Requires Contact-Dependent Cell Polarity; Developmental Cell, 19:39-53.

Trappe, V., V. Prasad, L. Cipelletti, P. N. Segre, D. A. Weitz (2001). Jamming phase diagram for attractive particles, Nature 411: 772–775.

Trepat X., M. R. Wasserman, T. E. Angelini, E. Millet, D. A. Weitz, J. P. Butler, J. J. Fredberg (2009). Physical forces during collective cell migration, Nature Physics 5: 426-430.

Trepat, X., L. Deng, S. An, D. Navajas, D. Tschumperlin, W. Gerthoffer, J. Butler, J. Fredberg (2007). Universal physical responses to stretch in the living cell, Nature 447: 592–595.

Trichet L., J. L. Digabel, R. J. Hawkins, S. R. K. Vedula, M. Gupta, C. Ribrault, P. Hersen, R. Voituriez, B. Ladoux (2012). Evidence of a large scale mechanosensing mechanism for cellular adaptation to substrate stiffness, PNAS 109(18): 6933-6938.

Van Roy F., G. Berx (2008). The cell-cell adhesion molecule E-cadherin, Cellular and Molecular Life Sciences (Review) 65: 3756-3788.

Vasioukhin V., C. Bauer, M. Yin, E. Fuchs (2000). Directed Actin Polymerization Is the Driving Force for Epithelial Cell–Cell Adhesion, Cell 100 (2): 209-219.

Vogel V., M. Sheetz (2006). Local force and geometry sensing regulate cell functions, Nature Reviews Molecular Cell Biology 7: 265-275.

Wang J. H-C., J-S Lin (2007). Cell traction force and measurement methods, Biomechanics and Modeling in Mechanobiology, Review 6(6): 361-371.

Wang X., L. He, Y. I. Wu, K. M. Hahn, D. J. Montell (2010). Light-mediated activation reveals a key role for Rac in collective guidance of cell movement in vivo, Nature Cell Biology 12: 591-597.

Weber, G.F., M.A. Bjerke, D.W. DeSimone (2012). A mechanoresponsive cadherin-keratin complex directs polarized protrusive behavior and collective cell migration, Developmental Cell 22: 104–115.

Willecke M., F. Hamaratoglu, L. Sansores-Garcia, C. Tao, G. Halder (2008). Boundaries of Dachsous Cadherin activity modulate the Hippo signaling pathway to induce cell proliferation, PNAS 105(39): 14897–14902.

Wu Y., D. Frey, O. I. Lungu, A. Jaehrig, I. Schlichting, B. Kuhlman, K. M. Hahn (2009). A genetically encoded photoactivatable Rac controls the motility of living cells, Nature 461: 104-108.

Wu Y., Wang X, He L, Montell D, Hahn KM. (2011). Spatiotemporal Control of Small GTPases with Light Using the LOV Domain, Methods in enzymology 497:393-407.

Wyss, H.M., K. Miyazaki, J. Mattsson, Z. Hu, D. R. Reichman, D. A. Weitz (2007). Strain-rate frequency superposition: a rheological probe of structural relaxation in soft materials, Physical Review Letters 98: 238303.

Xi H-Q., X-S. Wu, B. Wei, L. Chen (2012). Eph receptors and ephrins as targets for cancer therapy, J. Cell. Mol. Med. 16 (12): 2894-2909.

Xu Q., G. Mellitzer, V. Robinson, D. G. Wilkinson (1999). In vivo cell sorting in complementary segmental domains mediated by Eph receptors and ephrins, Nature 399: 267-271.

Zhou, E.H., X. Trepat, C. Y. Park, G. Lenormand, M. N. Oliver, S. M. Mijailovich, C. Hardin, D. A. Weitz, J. P. Butler, J. J. Fredberg (2009). Universal behavior of the osmotically compressed cell and its analogy to the colloidal glass transition. Proceedings of the National Academy of Sciences of the United States of America 106: 10632–10637.